Peer Reviewed

Title:
Spurious Tone Mitigation in Fractional-N Phase-Locked Loops

Author:
Familier, Eythan

Acceptance Date:
2016

Series:
UC San Diego Electronic Theses and Dissertations

Degree:
Ph.D., Electrical Engineering (Electronic Circuits and Systems)UC San Diego

Advisor(s):
Galton, Ian A

Committee:
Buckwalter, James F, Cauwenberghs, Gert, Hodgkiss, William S, Milstein, Laurence B

Permalink:
http://escholarship.org/uc/item/8kk1812j

Abstract:

UNIVERSITY OF CALIFORNIA, SAN DIEGO

Spurious Tone Mitigation in Fractional-*N* Phase-Locked Loops

A dissertation submitted in partial satisfaction of the requirements for the degree

Doctor of Philosophy

in

Electrical Engineering (Electronic Circuits and Systems)

by

Eythan Familier

Committee in charge:

Professor Ian A. Galton, Chair
Professor James F. Buckwalter
Professor Gert Cauwenberghs
Professor William S. Hodgkiss
Professor Laurence B. Milstein

2016

The dissertation of Eythan Familier is approved, and it is acceptable in quality and form for publication on microfilm and electronically:

_____

_____

_____

_____

_____

Chair

University of California, San Diego

2016

DEDICATION

To my parents.

TABLE OF CONTENTS

LIST OF FIGURES

LIST OF TABLES

ACKNOWLEDGEMENTS

I would like to thank my advisor, Professor Ian Galton, for his invaluable support and advice throughout my time here. His passion for engineering, his relentless search for the truth, and his dedication to his students are admirable, and his role in my development as an engineer cannot be overstated.

I would also like to thank my lab mates, friends, and family for their constant support.

Chapter 1, in full, has been published in the IEEE Transactions on Signal Processing, volume 61, number 16, pages 4172-4180, August 2013. E. Familier, I. Galton, 2013. The dissertation author is the primary investigator and author of this paper. Professor Ian Galton supervised the research which forms the basis for this paper.

Chapter 2, in full, has been published in the IEEE Transactions on Signal Processing, volume 61, number 17, pages 4270-4283, September 2013. E. Familier, C. Venerus, I. Galton, 2013. The dissertation author is the primary investigator and author of this paper. Professor Ian Galton supervised the research which forms the basis for this paper.

Chapter 3, in full, has been submitted for publication to the IEEE Transactions on Circuits and Systems I: Regular Papers. E. Familier, I. Galton, 2016. The dissertation author is the primary investigator and author of this paper. Professor Ian Galton supervised the research which forms the basis for this paper.

Chapter 4, in full, is currently being prepared for submission for publication of the material. E. Familier, I. Galton. The dissertation author is the primary investigator and

author of this material. Professor Ian Galton supervised the research which forms the basis for this material.

VITA

2016	Doctor of Philosophy in Electrical Engineering (Electronic Circuits and Systems), University of California, San Diego
2012	Master of Science in Electrical Engineering (Electronic Circuits and Systems), University of California, San Diego
2010	Bachelor of Science in Electrical Engineering, California Institute of Technology

PUBLICATIONS

E. Familier, I. Galton, "Second and Third-Order Noise Shaping Digital Quantizers for Low Phase Noise and Nonlinearity-Induced Spurious Tones in Fractional-*N* PLLs," *IEEE Trans. Circuits Syst. I*, accepted for publication.

C. Weltin-Wu, E. Familier, I. Galton, "A Linearized Model for the Design of Fractional-*N* Digital PLLs Based on Dual-Mode Ring Oscillator FDCs," *IEEE Trans. Circuits Syst. I*, vol. 62, no. 8, 2015.

E. Familier, C. Venerus, I. Galton, "A Class of Quantizers with DC-Free Quantization Noise and Optimal Immunity to Nonlinearity-Induced Spurious Tones," *IEEE Trans. Signal Process.*, vol. 61, no. 17, 2013.

E. Familier, I. Galton, "A Fundamental Limitation of DC- Free Quantization Noise with respect to Nonlinearity-Induced Spurious Tones," *IEEE Trans. Signal Process.*, vol. 61, no. 16, 2013.

A. Vakili, E. Familier, B. Hassibi, "On the Eigendistribution of the Steady-State Error Covariance Matrix for the Extended RLS Algorithm", *IEEE ICASSP*, 2009.

ABSTRACT OF THE DISSERTATION

Spurious Tone Mitigation in Fractional-*N* Phase-Locked Loops

by

Eythan Familier

Doctor of Philosophy in Electrical Engineering (Electronic Circuits and Systems)

University of California, San Diego, 2016

Professor Ian A. Galton, Chair

Fractional-*N* phase-locked loops (PLLs) are widely used to synthesize local oscillator signals for modulation and demodulation in communication systems. Their phase error inevitably consists of both a periodic component made up of spurious tones and a random component called phase noise. Spurious tones are particularly harmful to the performance of typical communication systems, so most communication standards stipulate stringent limits on their maximum power in relevant frequency bands.

High-performance PLLs generally contain noise-shaping coarse quantizers to control their output frequency. Such quantizers are a fundamental source of spurious

tones in the PLL's phase error. This is because spurious tones are inevitably induced when the quantizer's quantization noise is subjected to nonlinear distortion from analog circuit imperfections. This dissertation presents a rigorous analysis of this effect and a way to mitigate it through the use of a class of digital quantizers with first and higher-order highpass shaped quantization noise which are optimized for spurious tone and phase noise mitigation.

The first chapter of this dissertation presents a mathematical analysis of spurious tone generation via nonlinear distortion of quantization noise. It proves that subjecting the quantization noise running sum of a digital quantizer to a nonlinearity of a certain order will inevitably induce spurious tones, and shows the relation between such nonlinearity order and the range of values the quantization noise running sum takes. The results are general and apply to any digital quantizer.

The second chapter of this dissertation presents a class of digital quantizers with optimal immunity to nonlinearity-induced spurious tones and with first-order highpass shaped quantization noise. It presents design solutions for digital quantizers with quantization noise that can be subjected to nonlinear distortion of a given order without inducing spurious tones, and relies on the results from the first chapter to prove that the presented solutions are optimal in terms of spurious tone generation.

The third chapter of this dissertation presents digital quantizers with second and third-order highpass shaped quantization noise which can be optimized for either spurious tone or phase noise mitigation. These quantizers can replace the often-used delta-sigma

modulators in high-performance PLLs to either improve spurious-tone performance at the expense of slightly higher PLL phase noise or lower PLL phase noise.

The fourth chapter of this dissertation present an integrated circuit PLL which implements the second and third-order digital quantizers presented in the third chapter. It demonstrates record-setting spurious tone performance due to the use of these digital quantizers and to a new linearity-enhancement PLL timing scheme.

CHAPTER 1

A FUNDAMENTAL LIMITATION OF DC-FREE QUANTIZATION NOISE WITH RESPECT TO NONLINEARITY-INDUCED SPURIOUS TONES

Abstract—Fractional-*N* phase-locked loops (PLLs) are widely used to synthesize local oscillator signals for modulation and demodulation in communication systems. Such PLLs generate and subsequently lowpass filter DC-free quantization noise as part of their normal operation. Unfortunately, the quantization noise and its running sum inevitably are subjected to nonlinear distortion from analog circuit imperfections which causes spurious tones in the PLL output signal that can degrade communication system performance. This paper presents the first general mathematical analysis of this phenomenon. It proves that if the running sum of the quantization noise, $t[n]$, satisfies $t_{low} < t[n] \leq t_{high}$ for all n, where t_{low} and t_{high} are integers, then subjecting $t[n]$ to kth-order distortion for at least one $k \in \{1, 2, 3, \ldots, t_{high} - t_{low}\}$ will result in spurious tones for most fractional-*N* PLL output frequencies regardless of how the quantization is performed. It also shows that quantizers exist which are optimal in the sense that subjecting the running

Manuscript received January 25, 2013; revised April 26, 2013; accepted May 07, 2013. Date of publication May 16, 2013; date of current version July 22, 2013. The associate editor coordinating the review of this manuscript and approving it for publication was Prof. Ljubisa Stankovic. This work was supported by the National Science Foundation under Award 0914748.
The authors are with the Department of Electrical and Computer Engineering, University of California at San Diego, La Jolla, CA 92093-0407 USA (e-mail: galton@ucsd.edu).
Color versions of one or more of the figures in this paper are available online at http://ieeexplore.ieee.org.
Digital Object Identifier 10.1109/TSP.2013.2263504

sum of their quantization noise to kth-order distortion for any $k \in \{1, 2, 3, \ldots, t_{high} - t_{low} - 1\}$ does not result in any spurious tones. In a typical fractional-*N* PLL, the larger the range of $t[n]$ the greater the power of the PLL's phase noise, so these results imply a fundamental tradeoff between phase noise power and spurious tones in PLLs.

I. INTRODUCTION

Fractional-*N* phase-locked loops (PLLs) are widely used to synthesize local oscillator signals for modulation and demodulation in communication systems, as they can provide fine frequency tuning resolution with relatively low power consumption and integrated circuit area [1], [2]. Ideally, a fractional-*N* PLL's output signal is perfectly periodic, so its phase increases linearly with time. Unfortunately, non-ideal circuit behavior causes the actual phase of the output signal to deviate from its ideal phase, where the deviation is referred to as *phase noise*. The phase noise inevitably consists of both periodic components called spurious tones and random components. Spurious tones are particularly harmful to the performance of typical communication systems, so most communication standards directly or indirectly stipulate stringent limits on the maximum power of the spurious tones in addition to specifying the maximum tolerable power of the overall phase noise in relevant frequency bands [3].

Fractional-*N* PLLs generally contain noise-shaping coarse quantizers, most commonly implemented as digital delta-sigma (ΔΣ) modulators, which have recently been shown to be a significant, albeit indirect, source of phase noise spurious tones [4]–

[10]. The output frequency of a fractional-*N* PLL is controlled by a digital codeword that represents a rational number, α, between 0 and 1. The coarse quantizer operates on α and generates a digital sequence that can be viewed as the sum of α and DC-free *quantization noise* [11]–[13][2]. The quantization noise is converted into analog form, integrated, and lowpass filtered within the PLL, and the resulting waveform directly adds to the PLL phase noise [1]. Unfortunately, the quantization noise and its running sum are subjected to nonlinear distortion from inevitable analog circuit imperfections, and this can induce spurious tones even when the quantization noise itself is free of spurious tones.

This problem is mitigated in the fractional-*N* PLL presented in [7] wherein the *successive requantizer* proposed in [6] is used in place of a ΔΣ modulator. The successive requantizer offers the advantage that its quantization noise and the running sum of its quantization noise remain free of spurious tones even when subjected to the type of nonlinear distortion commonly imposed by non-ideal circuit behavior in PLLs. This enables the PLL presented in [7] to achieve state-of-the-art spurious tone performance, but a price is paid for this benefit. In return for the enhanced immunity to nonlinearity-induced spurious tones, the power of the quantization noise introduced by the successive requantizer is significantly higher than that of a comparable ΔΣ modulator. The PLL presented in [7] employs a technique known as phase noise cancellation to overcome this problem at the expense of additional power consumption and circuit area.

No previous publications have addressed the question of whether the tradeoff between immunity to nonlinearity-induced spurious tones and increased quantization

[2] A sequence whose running sum is bounded for all time is said to be DC-free.

noise power observed in the successive requantizer is inevitable. This is an important question because if the tradeoff were just an idiosyncrasy of the successive requantizer, it might be possible to design an improved coarse quantizer with good immunity to spurious tones that is not subject to the tradeoff. This paper answers this question.

The results of the paper prove that spurious tones are inevitably generated for most values of α when the running sum of DC-free quantization noise from a quantizer operating on α is subjected to the type of nonlinear distortion typically imposed by fractional-*N* PLLs. Specifically, if the running sum of the quantization noise, $t[n]$, satisfies $t_{low} < t[n] \leq t_{high}$ for all n, where t_{low} and t_{high} are integers, then subjecting $t[n]$ to kth-order distortion for at least one k in the set $\{1, 2, 3, \ldots, t_{high} - t_{low}\}$ will result in spurious tones for most values of α regardless of how the quantization is performed. The paper also shows that quantizers exist which are optimal in the sense that subjecting the running sum of their quantization noise to kth-order distortion for any value of k in the set $\{1, 2, 3, \ldots, t_{high} - t_{low} - 1\}$ does not result in any spurious tones. Therefore, the results imply a fundamental tradeoff between phase noise power and spurious tone suppression in a PLL.

The remainder of the paper consists of three main sections. Section II describes the details of the spurious tone problem in fractional-*N* PLLs, Section III presents and proves the theoretical results outlined above, and Section IV presents a method of quantization that is optimal in the sense described above.

II. SPURIOUS TONES IN FRACTIONAL-*N* PLLS

A. A Tone Definition Based on the Periodogram

Consider a discrete-time complex-coefficient image-rejection bandpass filter with a positive-frequency passband centered at any non-zero frequency ω_p and an adjustable equivalent noise bandwidth, $\Delta\omega_p$, wherein the passband's peak power gain times $\Delta\omega_p$ is unity. A sequence applied to the filter is said to contain a tone at ω_p if the squared magnitude of the output of the filter grows without bound as $\Delta\omega_p$ is reduced to zero. This description of a tone is consistent with the way that tones are measured in the laboratory using a spectrum analyzer [14].

An example of such a bandpass filter has a length-L impulse response given by

$$h_L[n] = \begin{cases} \dfrac{1}{\sqrt{L}} e^{-j\omega_p(L-1-n)} & \text{if } 0 \le n \le L-1, \\ 0, & \text{otherwise,} \end{cases} \tag{1}$$

where $\Delta\omega_p$ goes to zero as L goes to infinity. If the filter is applied to a sequence, $x[n]$, the squared magnitude of the filter output at time index $n = L - 1$ can be written as

$$I_{x,L}(\omega_p) = \frac{1}{L}\left|\sum_{k=0}^{L-1} x[k]e^{-j\omega_p k}\right|^2. \tag{2}$$

The expression given by (2) for any positive integer L and any $0 \le |\omega_p| \le \pi$ is known as the periodogram [15]. Therefore, the periodogram performs a function analogous to that of a laboratory spectrum analyzer, where increasing L in the periodogram is akin to decreasing the resolution bandwidth of the spectrum analyzer.

Accordingly, a mathematical definition of a tone that reflects the way that tones are measured in the laboratory is as follows.

Definition: Given any $\omega_p \neq 0$, $x[n]$ contains a tone at ω_p if $I_{x,L}(\omega_p)$ is unbounded as $L \to \infty$.

The definition implies that a sequence $x[n]$ is free of tones if and only if $I_{x,L}(\omega)$ is bounded in L for all $0 < |\omega| \leq \pi$.[3]

B. Spurious Tone Generation in Fractional-*N* PLLs

Ideally, a fractional-*N* PLL generates a periodic output signal $v_{out}(t)$ with frequency $f_{PLL} = f_{ref}(N + \alpha)$, where f_{ref} is the frequency of a reference oscillator, N is an integer, and $0 \leq \alpha < 1$. In practice, however, the output signal is more accurately modeled by

$$v_{out}(t) = g(2\pi f_{PLL} t + \theta_{PLL}(t)), \tag{3}$$

where g is a 2π-periodic function and $\theta_{PLL}(t)$ is the phase noise of the PLL [16].

As shown in Fig. 1, a typical fractional-*N* PLL consists of a phase detector, a lowpass loop filter, a voltage controlled oscillator (VCO), a frequency divider, and a noise-shaping coarse quantizer that introduces DC-free quantization noise. The phase detector drives the loop filter with a signal that represents the phase difference between the reference oscillator and frequency divider outputs. The instantaneous frequency of the VCO output signal deviates from its center frequency by an amount proportional to

[3] An alternative definition of a tone could be constructed based on traditional power spectral density (PSD) functions. However, the periodogram-based definition is preferred in this work for two reasons. First, the periodogram can be computed for any signal, whereas the PSD is only defined for a relatively small class of signals. Second, the phase noise performance of PLLs is usually quantified by time averages using laboratory equipment such as spectrum analyzers, not by ensemble averages. In this sense, the periodogram provides a meaningful representation of the power spectrum as used in practice.

the output of the loop filter at each point in time. The frequency divider output is a two-level signal in which the n^{th} and $(n+1)^{th}$ rising edges are separated by $N + y[n]$ cycles of the VCO output, where $y[n]$ for each n is an integer generated by the coarse quantizer. The PLL feedback loop adjusts the output frequency so as to zero the DC component of the phase detector output, causing the output frequency to settle to f_{ref} times the average of $N + y[n]$. If $y[n]$ could be set to α for all n, the PLL would have the desired output frequency. However, practical frequency dividers can only count integer numbers of VCO cycles, so $y[n]$ must be integer-valued. Therefore, the coarse quantizer ensures that $y[n]$ is integer-valued but averages to α in time. This results in the desired PLL output frequency, but the deviations of $y[n]$ from α contribute an extra component to the PLL's phase noise.

In general, $y[n]$ can be viewed as a representation of α quantized to be integer valued, and thus can be written as $y[n] = \alpha + s[n]$, where $s[n]$ is the quantization noise of $y[n]$. As explained in the introduction, it is desirable to engineer both $s[n]$ and its running sum $t[n]$, defined by

$$t[n] = \sum_{k=0}^{n} s[k], \tag{4}$$

to be free of spurious tones and also such that sequences resulting from nonlinearly distorting $s[n]$ and $t[n]$ are free of spurious tones. In practice, it is most critical for $t[n]$ to have these properties, because spurious tones generated by nonlinearly distorting $s[n]$ usually can be sufficiently mitigated by well-known frequency divider linearization techniques such as periodically resynchronizing each frequency divider output rising edge to the next rising edge of the VCO output signal [17].

As described in the introduction, it is usually highly undesirable for the phase noise of a PLL to contain tones, so any tones in a PLL's phase noise are usually referred to as *spurious tones*. Given that this paper describes a spurious tone generation mechanism in PLLs, all tones in the following will be denoted as spurious tones. Nevertheless, from a mathematical point of view there is no distinction between tones and spurious tones.

A sequence $x[n]$ is said to be *immune to spurious tones up to order h* if $x^p[n]$ is free of tones for all positive integers $p \leq h$. Based on simulation and experimental results, the nonlinearities to which $t[n]$ is subjected in a PLL tend to be well-modeled as truncated memoryless power series, i.e. functions of the form

$$f(t[n]) = a_0 + a_1 t[n] + a_2 t^2[n] + ... + a_k t^k[n] \tag{5}$$

for some positive integer k [6], [7], [18]. Thus, mitigating spurious tone generation in a PLL can be achieved by ensuring that $t[n]$ is immune to spurious tones up to a certain order. As explained in the introduction, $s[n]$ is required to be DC-free, which means that $t[n]$ is bounded, so

$$t_{low} < t[n] \leq t_{high} \tag{6}$$

for all n, where t_{low} and t_{high} are integers. Larger values of $t_{high} - t_{low}$ offer more flexibility in the design of the coarse quantizer, which can be exploited to increase the order of the spurious tone immunity of $t[n]$. The results presented in Section III show that the maximum attainable order of spurious tone immunity $t[n]$ can achieve is bounded by ($t_{high} - t_{low} - 1$) regardless of how the quantization is performed.

III. THEORY OF SPURIOUS TONES IN DC-FREE QUANTIZATION NOISE

The following theorem shows that it is not possible to quantize most values of α such that the quantization noise is DC-free and its running sum is immune to spurious tones up to order $t_{high} - t_{low}$. The result is general in that it holds regardless of how the quantization is performed.

Theorem: Let α be a constant that satisfies $0 < \alpha < 1$, let $s[n]$ be a sequence such that

$$y[n] = \alpha + s[n] \tag{7}$$

is integer-valued for all n, and let

$$t[n] = \sum_{k=0}^{n} s[k]\,. \tag{8}$$

If

$$t_{low} < t[n] \le t_{high} \tag{9}$$

for all n, where t_{low} and t_{high} are integers, and

$$\alpha = \frac{P}{Q}, \tag{10}$$

where P and Q are relatively prime integers with $Q > t_{high} - t_{low}$, then

$$I_{t^p,L}(2\pi f) = \frac{1}{L}\left|\sum_{n=0}^{L-1} t^p[n] e^{-j2\pi fn}\right|^2 \tag{11}$$

is unbounded in L for at least one $p \in \{1, 2, \ldots, t_{high} - t_{low}\}$ and at least one $f \in \{\alpha, 2\alpha, \ldots, (Q-1)\alpha\}$.

A practical implication of the theorem is that trying to develop a coarse quantizer applicable to fractional-N PLLs that eliminates the spurious tone generation mechanism

described in Section II-B is futile. The coarse quantizer in any fractional-*N* PLL consists entirely of digital logic and its variables are represented by finite-width data buses, so all variables associated with the coarse quantizer, including α, are rational numbers. In particular, this implies that α satisfies (10). Furthermore, the coarse quantizer in a fractional-*N* PLL is required to have DC-free quantization noise. Thus, any coarse quantizer applicable to a fractional-*N* PLL must satisfy the theorem's hypothesis. The theorem places no other restrictions on the quantizer; the quantization noise can be deterministic or probabilistic and the theorem does not make any assumptions whatsoever about the quantizer's structure.

Another practical implication of the theorem is that the order of immunity to nonlinearity-induced spurious tones of $t[n]$ from the coarse quantizer in a fractional-*N* PLL can only be increased at the expense of increasing the range of values spanned by $t[n]$. The sequence $t[n]$ can be viewed as a lowpass filtered version of the quantization noise, so increasing its range tends to increase the power of the quantization noise at low frequencies where the PLL's loop filter provides little or no attenuation. The portion of $t[n]$ within a fractional-*N* PLL's bandwidth is an additive component of the PLL's phase noise, so all other things being the same, increasing the range of $t[n]$ increases power of the PLL's phase noise [1]. Furthermore, most integrated circuit based fractional-*N* PLLs use a phase-frequency detector and charge pump to implement the phase detector in Fig. 1, so the larger the magnitude of $t[n]$ at any time index n, the longer the current sources in the charge pump are turned on during the nth reference period. Increasing the on-time of the current sources causes more of the current source noise to be converted to phase

noise, so all other things being the same, increasing the range of $t[n]$ also increases the power of the phase noise component contributed by the charge pump.

Proof of the Theorem:

Equations (7) and (8) imply that

$$t[n] = \sum_{k=0}^{n} y[k] - (n+1)\alpha, \tag{12}$$

which can be written as

$$t[n] = \sum_{k=0}^{n} y[k] - \lfloor (n+1)\alpha \rfloor - \langle (n+1)\alpha \rangle, \tag{13}$$

where $\lfloor x \rfloor$ denotes the largest integer less than or equal to x and $\langle x \rangle$ denotes the fractional part of x, i.e. $\langle x \rangle = x - \lfloor x \rfloor$. Let

$$r[n] = \sum_{k=0}^{n} y[k] - \lfloor (n+1)\alpha \rfloor \tag{14}$$

with which (13) can be written as

$$t[n] = r[n] - \langle (n+1)\alpha \rangle, \tag{15}$$

By definition, $r[n]$ is an integer-valued sequence.[4] Furthermore,

$$r[n] \in \{ t_{low} + 1, t_{low} + 2, \ldots, t_{high} \} \tag{16}$$

for all n, because $t[n]$ is bounded according to (9) and the last term in (15) is non-negative and less than 1.

Let

$$I_{t^p,L}(\omega) = \frac{1}{L} \left| \sum_{n=0}^{L-1} t^p[n] e^{-j\omega n} \right|^2. \tag{17}$$

Substituting (15) into (17) results in

[4] It follows from this and (15) that the fractional part of $t[n]$ is periodic, so it consists entirely of spurious tones. The fractional part operator is a memoryless nonlinearity, so this demonstrates that it is not possible for $t[n]$ to be immune to spurious tones for all memoryless nonlinearities.

$$I_{t^p,L}(\omega)=\frac{1}{L}\left|\sum_{n=0}^{L-1}(r[n]-\langle(n+1)\alpha\rangle)^p e^{-j\omega n}\right|^2. \tag{18}$$

Let $L = RQ$, where R is any positive integer, and $\omega = 2\pi i/Q$, where $i \in \{1, 2, \ldots, Q-1\}$. Then (18) can be written as

$$I_{t^p,RQ}\left(\frac{2\pi i}{Q}\right)= \frac{1}{RQ}\left|\sum_{k=0}^{R-1}\sum_{n=0}^{Q-1}\left(r[kQ+n]-\langle(kQ+n+1)\alpha\rangle\right)^p e^{-j\frac{2\pi i}{Q}(kQ+n)}\right|^2. \tag{19}$$

Given that $\alpha = P/Q$, where P and Q are relatively prime integers (so they have no common integer factors other than 1), the smallest value of n greater than zero for which $n\alpha$ is integer-valued is Q. Therefore, $\langle(n+1)\alpha\rangle$ is a periodic sequence with period Q, so

$$\langle(kQ+n+1)\alpha\rangle=\langle(n+1)\alpha\rangle \tag{20}$$

for each integer k. Substituting (20) into (19), interchanging the summations, and rearranging factors gives

$$I_{t^p,RQ}\left(\frac{2\pi i}{Q}\right) =\frac{R}{Q}\left|\sum_{n=0}^{Q-1}\left[\sum_{k=0}^{R-1}\frac{1}{R}\left(r[kQ+n]-\langle(n+1)\alpha\rangle\right)^p\right]e^{-j\frac{2\pi i}{Q}n}\right|^2. \tag{21}$$

Given that $r[kQ + n]$ is integer-valued and bounded according to (16), this can be rewritten as

$$I_{t^p,RQ}\left(\frac{2\pi i}{Q}\right) =\frac{R}{Q}\left|\sum_{n=0}^{Q-1}\left[\sum_{m=t_{low}+1}^{t_{high}}P_R[m,n]\left(m-\langle(n+1)\alpha\rangle\right)^p\right]e^{-j\frac{2\pi i}{Q}n}\right|^2, \tag{22}$$

where

$$P_R\left[m,n\right]=\frac{1}{R}\sum_{k=0}^{R-1}\gamma[k,m,n], \tag{23}$$

and

$$\gamma[k,m,n]=\begin{cases}1, & \text{if } r[kQ+n]=m,\\ 0, & \text{otherwise.}\end{cases} \tag{24}$$

The summation in (23) counts the number of times that $r[kQ + n] = m$ over the R consecutive values of k from 0 to $R - 1$. It follows that $P_R[m, n]$ has the same properties as a probability distribution in m for each n and each R, i.e.,

$$0\le P_R\left[m,n\right]\le 1 \tag{25}$$

and

$$\sum_{m=t_{low}+1}^{t_{high}} P_R\left[m,n\right]=1. \tag{26}$$

Equation (22) can be rewritten as

$$I_{t^p,RQ}\left(\frac{2\pi i}{Q}\right)=\frac{R}{Q}\left|\sum_{n=0}^{Q-1}\beta_R{}^{(p)}\left[n\right]e^{-j\frac{2\pi i}{Q}n}\right|^2, \tag{27}$$

where

$$\beta_R{}^{(p)}\left[n\right]=\sum_{m=t_{low}+1}^{t_{high}} P_R\left[m,n\right]\left(m-\left\langle(n+1)\alpha\right\rangle\right)^p. \tag{28}$$

Thus, the right side of (27) is R/Q times the squared magnitude of the discrete Fourier transform (DFT) of $\beta_R{}^{(p)}[n]$. A necessary condition for the DFT of $\beta_R{}^{(p)}[n]$, i.e.,

$$\sum_{n=0}^{Q-1}\beta_R{}^{(p)}\left[n\right]e^{-j\frac{2\pi i}{Q}n}, \tag{29}$$

to converge to 0 for every $i = 1, 2, \ldots, Q - 1$ as R goes to infinity, and, therefore, for R/Q times the DFT of $\beta_R{}^{(p)}[n]$ to be bounded in R for every $i = 1, 2, \ldots, Q - 1$, is

$$\beta_R{}^{(p)}[n]\to b_p \qquad \text{as} \qquad R\to\infty, \tag{30}$$

where b_p does not depend on n. Given that $L = RQ$, it follows that (30) is also a necessary condition for (11) to remain bounded in L.

Suppose the theorem is false. Then the above implies that there must exist Q probability distributions in m, $P[m, n]$ for $n = 0, 1, 2, \ldots, Q - 1$, each of which must satisfy

$$\sum_{m=t_{low}+1}^{t_{high}} P[m,n]\left(m-\langle (n+1)\alpha \rangle\right)^p = b_p \tag{31}$$

for $p = 1, 2, \ldots, t_{diff}$, where

$$t_{diff} = t_{high} - t_{low}. \tag{32}$$

Additionally, given that $P[m, n]$ for $n = 0, 1, 2, \ldots, Q - 1$ are probability distributions, (31) must hold for $p = 0$ and $b_0 = 1$. Thus, (31) represents $Q(t_{diff} + 1)$ equations that must be satisfied by $t_{diff}Q$ probability values and t_{diff} values of b_p. This can be viewed a linear system of $Q(t_{diff} + 1)$ equations with $t_{diff}Q + t_{diff}$ unknowns. With $Q > t_{diff}$, the system has more equations than unknowns, so if the theorem is false the equations must be linearly dependent.

The equations represented by (31) for each $n \in \{0, 1, 2, \ldots, Q - 1\}$ and all $p \in \{0, 1, \ldots, t_{diff} - 1\}$ can be written as

$$\mathbf{M}(x)\mathbf{p}(x) = \mathbf{b} \tag{33}$$

with values of x given by

$$x = \langle (n+1)\alpha \rangle, \tag{34}$$

where

$$\mathbf{M}(x) = \begin{pmatrix} 1 & 1 & \ldots & 1 \\ (t_{low}+1-x) & (t_{low}+2-x) & \ldots & (t_{high}-x) \\ (t_{low}+1-x)^2 & (t_{low}+2-x)^2 & \ldots & (t_{high}-x)^2 \\ \ldots & \ldots & \ldots & \ldots \\ (t_{low}+1-x)^{t_{diff}-1} & (t_{low}+2-x)^{t_{diff}-1} & \ldots & (t_{high}-x)^{t_{diff}-1} \end{pmatrix}, \tag{35}$$

$$\mathbf{b} = \begin{pmatrix} 1 & b_1 & b_2 & \ldots & b_{t_{diff}-1} \end{pmatrix}^T, \tag{36}$$

and

$$\begin{aligned} &\mathbf{p}\left(\left\langle (n+1)\alpha \right\rangle\right) \\ &\quad = \begin{pmatrix} P[t_{low}+1, n] & P[t_{low}+2, n] & \cdots & P[t_{high}, n] \end{pmatrix}^T. \end{aligned} \tag{37}$$

Furthermore, the equations represented by (31) for each $n \in \{0, 1, 2, \ldots, Q-1\}$ and $p = t_{diff}$ can be written as

$$\mathbf{m}_{t_{diff}}(x)\mathbf{p}(x) = b_{t_{diff}}, \tag{38}$$

with x given by (34) and

$$\begin{aligned} &\mathbf{m}_{t_{diff}}(x) = \\ &\begin{pmatrix} (t_{low}+1-x)^{t_{diff}} & (t_{low}+2-x)^{t_{diff}} & \ldots & (t_{high}-x)^{t_{diff}} \end{pmatrix}. \end{aligned} \tag{39}$$

It follows from the lemma presented in the Appendix that $\mathbf{m}_{t_{diff}}(x)$ can be expressed in terms of $\mathbf{M}(x)$ as

$$\mathbf{m}_{t_{diff}}(x) = \mathbf{r}(x)\mathbf{M}(x), \tag{40}$$

where the kth element of $\mathbf{r}(x)$ is given by

$$(-1)^{t_{diff}-k} \sum_{1 \le i_1 < i_2 < \ldots < i_{t_{diff}-k+1} \le t_{diff}} y_{i_1}(x)\, y_{i_2}(x) \cdots y_{i_{t_{diff}-k+1}}(x), \tag{41}$$

with

$$y_{i_q}(x) = (t_{low} + i_q - x). \tag{42}$$

Therefore, (38) and (40) imply

$$b_{t_{diff}} = \mathbf{r}(x)\mathbf{M}(x)\mathbf{p}(x). \tag{43}$$

Substituting (33) into this result yields

$$b_{t_{diff}} = \mathbf{r}(x)\mathbf{b}. \tag{44}$$

If the theorem is false, (44) must hold for all values of x in the set

$$\{\langle\alpha\rangle,\langle 2\alpha\rangle,\ldots,\langle Q\alpha\rangle\}, \tag{45}$$

with $Q > t_{diff}$. The set contains Q distinct values of x because P and Q are relatively prime integers, so (44) must hold for more than t_{diff} distinct values of x if the theorem is false. It follows from (41) and (42) that the first element of $\mathbf{r}(x)$ is a polynomial in x of degree t_{diff}, and each of the other elements of $\mathbf{r}(x)$ is a polynomial in x of degree less than t_{diff}. Given that the first element of $\mathbf{b}$ is non-zero, this implies that

$$\mathbf{r}(x)\mathbf{b} - b_{t_{diff}} \tag{46}$$

is a polynomial of degree t_{diff}. Therefore, (46) has t_{diff} roots, so there can be at most t_{diff} distinct values of x that satisfy (44). This contradicts the supposition that the theorem is false. ■

The theorem presented above implies that it is not possible to quantize most values of α such that the quantization noise is DC-free and its running sum is immune to spurious tones up to order $t_{high} - t_{low}$. As explained below, this bound on performance is tight in the sense that quantizers exist with the property that the running sum of their quantization noise is immune to spurious tones up to order $t_{high} - t_{low} - 1$. The theorem implies that a quantizer with this property is optimal with respect to spurious tone immunity in the sense that the running sum of its quantization noise has the highest possible order of immunity to spurious tones.

The successive requantizer provides an existence proof that quantizers exist which are optimal with respect to spurious tone immunity. As an example, the successive requantizer proposed in [6] and demonstrated in the fractional-N PLL integrated circuit presented in [7] is shown in Figs. 2 and 3. For this particular successive requantizer, α can be any multiple of 2^{-16} that is non-negative and less than 1. As shown in Fig. 2, the

successive requantizer multiples α by 2^{16} and processes the integer-valued result via a cascade of 16 *quantization blocks*, each of which simultaneously quantizes by one bit and halves each sample of its input sequence. The implementation details of each quantization block are shown in Fig. 3. As proven in [6], $y[n]$ is an integer-valued quantized version of α, its quantization noise is DC-free with $t_{high} - t_{low} = 4$, and the running sum of its quantization noise is immune to spurious tones up to order 3.

The results in [6] are extended in [19] to show that for each positive integer $N_t \geq 2$ there exist multiple successive requantizers that have $t_{high} - t_{low} = 2N_t$ and for which the running sum of their quantization noise is immune to spurious tones up to order $2N_t - 1$. Therefore, each of these successive requantizers is an optimal quantizer with respect to spurious tone immunity in the sense that the running sum of its quantization noise has the highest possible order of immunity to spurious tones.

While the theorem quantifies the relationship between the value of Q and the possible frequencies of the nonlinearity-induced spurious tones, it does not quantify the power of the nonlinearity-induced spurious tones. This is because the theorem is applicable to any quantizer with DC-free quantization noise, whereas the effect of varying Q on quantizer performance for a particular quantizer depends on the quantizer's design. For example, in most delta-sigma modulators with DC-free quantization noise the nonlinearity-induced spurious tone powers are strongly dependent on Q, whereas for the successive requantizer described above computer simulations suggest that they are nearly independent of Q. Thus, the effect of varying Q on quantizer performance must be evaluated in a quantizer specific fashion.

IV. ALTERNATE METHOD OF OPTIMAL QUANTIZATION

The successive requantizer is not the only type of quantizer that is optimal with respect to spurious tone immunity. An alternate method of quantization that is optimal with respect to spurious tone immunity is presented in this section. Unlike the successive requantizer, the idea upon which it is based follows directly from the proof of the theorem presented in Section III, so it gives some insight into the connection between the quantization process and the theorem.

Suppose that a quantized sequence with mean $\alpha = P / Q$, where P and Q are relatively prime integers, is to be generated, and that the running sum of the quantization noise is required to satisfy $-N_t < t[n] \le N_t$ over all n for some positive integer N_t. Thus, $t_{low} = -N_t$ and $t_{high} = N_t$. By the analysis presented in the proof of the theorem up to (31), a necessary condition for $t[n]$ to be immune to spurious tones up to order $t_{high} - t_{low} - 1 = 2N_t - 1$ is that there exist Q probability distributions in m, $P[m, u]$, where $m \in \{-N_t + 1, -N_t + 2, \ldots, N_t\}$ and $u \in \{0, 1, 2, \ldots, Q - 1\}$, which satisfy (31) for $p = 1, 2, \ldots, 2N_t - 1$. It follows from (31) that these probability distributions must satisfy

$$\begin{aligned} &\sum_{m=-N_t+1}^{N_t} P[m,i]\left(m - \langle (i+1)\alpha \rangle\right)^p \\ &\quad = \sum_{m=-N_t+1}^{N_t} P[m,i+1]\left(m - \langle (i+2)\alpha \rangle\right)^p, \end{aligned} \tag{47}$$

for all $i \in \{0, 1, 2, \ldots, Q - 2\}$, and $p \in \{1, 2, 3, \ldots, 2N_t - 1\}$. To be probability distributions, they must also be non-negative and satisfy

$$\sum_{m=-N_t+1}^{N_t} P[m,u] = 1, \tag{48}$$

for all $u \in \{0, 1, 2, \ldots, Q-1\}$. Any set of $P[m, n]$ that satisfy (47) and (48), can be used to generate $r[n]$ such that

$$r[n] \in \{-N_t+1, -N_t+2, ..., N_t\} \tag{49}$$

for all n and

$$\lim_{R\to\infty} \frac{1}{R} \sum_{k=0}^{R-1} \gamma[k,m,u] = P[m,u] \tag{50}$$

where

$$\gamma[k,m,u] = \begin{cases} 1, & \text{if } r[kQ+u] = m, \\ 0, & \text{otherwise.} \end{cases} \tag{51}$$

This can be done either probabilistically or deterministically. For each n, once $r[n]$ is known the running sum of the quantization noise, the quantization noise, and the quantizer output can be calculated using

$$t[n] = r[n] - \langle (n+1)\alpha \rangle, \tag{52}$$

$$s[n] = t[n] - t[n-1], \tag{53}$$

and

$$y[n] = \alpha + s[n], \tag{54}$$

respectively.

For instance, as done in the following examples, $r[n]$ can be generated as a sequence of independent random variables with probability distributions

$$\Pr(r[n] = m) = P[m, n \bmod Q] \tag{55}$$

for all $m \in \{-N_t + 1, -N_t + 2, \ldots, N_t\}$ and all integers n. It follows from (52) that $t^p[n]$ is a sequence of independent random variables, and from (47) that the mean of $t^p[n]$ is

independent of n for $p \in \{1, 2, 3, \ldots, 2N_t - 1\}$. It follows that $t^p[n]$ is white noise and is therefore free of spurious tones for each $p \in \{1, 2, 3, \ldots, 2N_t - 1\}$.

There are many sets of non-negative $P[m, u]$ values that satisfy the system of equations specified by (47) and (48), because the system is under-constrained; it has $(Q - 1)(2N_t - 1) + Q$ equations and $2N_tQ$ unknowns. Therefore, additional constraints can be imposed on the $P[m, u]$ values. For example, imposing additional constraints of the form

$$\sum_{m=-N_t+1}^{N_t} P[m,i]\left(m - \langle (i+1)\alpha \rangle\right)^{2N_t} = \sum_{m=-N_t+1}^{N_t} P[m,u]\left(m - \langle (u+1)\alpha \rangle\right)^{2N_t} \tag{56}$$

for as many $i, u \in \{0, 1, 2, \ldots, Q - 1\}$ as possible has the effect of minimizing spurious tone power in $t^{2N_t}[n]$.

Two quantization noise running sum sequences, $t_1[n]$ and $t_2[n]$, based on the method described above are presented below and demonstrated by simulation to have optimal orders of spurious tone immunity. The magnitude bounds on $t_1[n]$ and $t_2[n]$ are $N_{t1} = 2$ and $N_{t2} = 3$, respectively, and the quantized sequences corresponding to $t_1[n]$ and $t_2[n]$ have means of $\alpha_1 = 1/5$ and $\alpha_2 = 1/7$, respectively. The $P[m, u]$ values found in both cases are presented in matrices $\mathbf{P}_1$ and $\mathbf{P}_2$, defined by

$$\mathbf{P}_k(i, j) = P[-N_{tk} + i, j - 1] \tag{57}$$

for $i \in \{1, 2, \ldots, 2N_{tk}\}$, $j \in \{1, 2, \ldots, Q\}$, and $k = 1$ or 2:

$$\mathbf{P}_1 = \begin{pmatrix} \frac{14}{125} & \frac{7}{125} & \frac{3}{125} & \frac{1}{125} & \frac{1}{5} \\ \frac{73}{125} & \frac{64}{125} & \frac{51}{125} & \frac{37}{125} & \frac{3}{5} \\ \frac{37}{125} & \frac{51}{125} & \frac{64}{125} & \frac{73}{125} & \frac{1}{5} \\ \frac{1}{125} & \frac{3}{125} & \frac{7}{125} & \frac{14}{125} & 0 \end{pmatrix}, \tag{58}$$

$$\mathbf{P}_2 = \begin{pmatrix} \frac{132}{16807} & \frac{66}{16807} & \frac{30}{16807} & \frac{12}{16807} & \frac{4}{16807} & \frac{1}{16807} & \frac{5}{343} \\ \frac{137}{780} & \frac{2190}{16807} & \frac{273}{2945} & \frac{97}{1538} & \frac{687}{16807} & \frac{185}{7368} & \frac{78}{343} \\ \frac{236}{465} & \frac{880}{1821} & \frac{272}{611} & \frac{738}{1861} & \frac{860}{2519} & \frac{724}{2551} & \frac{177}{343} \\ \frac{724}{2551} & \frac{860}{2519} & \frac{738}{1861} & \frac{272}{611} & \frac{880}{1821} & \frac{236}{465} & \frac{78}{343} \\ \frac{185}{7368} & \frac{687}{16807} & \frac{97}{1538} & \frac{273}{2945} & \frac{2190}{16807} & \frac{137}{780} & \frac{5}{343} \\ \frac{1}{16807} & \frac{4}{16807} & \frac{12}{16807} & \frac{30}{16807} & \frac{66}{16807} & \frac{132}{16807} & 0 \end{pmatrix}. \tag{59}$$

Figs. 4 and 5 show the estimated power spectra of $t_1^{\,p}[n]$ for $p \in \{1, 2, 3, 4\}$ and $t_2^{\,q}[n]$ for $q \in \{1, 2, \ldots, 6\}$. The figures demonstrate that spurious tones in $t_1^{\,p}[n]$ are present only when $p = 2N_{t1} = 4$ and that spurious tones in $t_2^{\,q}[n]$ are present only when $q = 2N_{t2} = 6$. This supports the assertion that both examples represent optimal quantization in terms of spurious tone immunity.

APPENDIX

The following lemma is used in the proof of the theorem in Section III.

Lemma: Given arbitrary $a_1, a_2, \ldots, a_n$, let $\mathbf{V}$ be the following nxn matrix:

$$\mathbf{V} = \begin{pmatrix} 1 & 1 & 1 & \ldots & 1 \\ a_1 & a_2 & a_3 & \ldots & a_n \\ a_1^{\,2} & a_2^{\,2} & a_3^{\,2} & \ldots & a_n^{\,2} \\ \ldots & \ldots & \ldots & \ldots & \ldots \\ a_1^{\,n-1} & a_2^{\,n-1} & a_3^{\,n-1} & \ldots & a_n^{\,n-1} \end{pmatrix}. \tag{60}$$

Then, the row vector

$$\mathbf{v}_n = \begin{pmatrix} a_1^{\,n} & a_2^{\,n} & a_3^{\,n} & \ldots & a_n^{\,n} \end{pmatrix} \tag{61}$$

can be expressed as

$$\mathbf{v}_n = \mathbf{r} \cdot \mathbf{V}, \tag{62}$$

where $\mathbf{r}$ is a row vector whose elements are given by

$$\begin{aligned} \mathbf{r}(1) &= (-1)^{n-1} \sum_{1 \le i_1 < i_2 < \ldots < i_n \le n} a_{i_1} a_{i_2} \cdots a_{i_n}, \\ \mathbf{r}(2) &= (-1)^{n-2} \sum_{1 \le i_1 < i_2 < \ldots < i_{n-1} \le n} a_{i_1} a_{i_2} \cdots a_{i_{n-1}}, \\ &\vdots \\ \mathbf{r}(n) &= \sum_{1 \le i_1 \le n} a_{i_1}. \end{aligned} \tag{63}$$

Proof:

Consider the polynomial

$$P(x) = (x - a_1)(x - a_2) \cdots (x - a_n), \tag{64}$$

which can be expanded as

$$\begin{aligned} P(x) = x^n - x^{n-1} \sum_{1 \le i_1 \le n} a_{i_1} + x^{n-2} \sum_{1 \le i_1 < i_2 \le n} a_{i_1} a_{i_2} - \ldots \\ + (-1)^n \sum_{1 \le i_1 < i_2 < \ldots < i_n \le n} a_{i_1} a_{i_2} \ldots a_{i_n}. \end{aligned} \tag{65}$$

It follows from (64) that a_k is a root of $P(x)$ for any $k \in \{1, 2, \ldots, n\}$, i.e.

$$P(a_k) = 0. \tag{66}$$

Additionally, it is seen from (65) that $P(a_k)$ can be expressed as

$$P(a_k) = a_k{}^n - (\mathbf{r}\cdot\mathbf{V})(k), \tag{67}$$

where $(\mathbf{r}\cdot\mathbf{V})(k)$ is the kth element of the vector $\mathbf{r}\cdot\mathbf{V}$. Therefore, (66) and (67) yield

$$(\mathbf{r}\cdot\mathbf{V})(k) = a_k{}^n, \tag{68}$$

which proves the result. ■

ACKNOWLEDGEMENTS

Chapter 1, in full, has been published in the IEEE Transactions on Signal Processing, volume 61, number 16, pages 4172-4180, August 2013. E. Familier, I. Galton, 2013. The dissertation author is the primary investigator and author of this paper. Professor Ian Galton supervised the research which forms the basis for this paper.

FIGURES

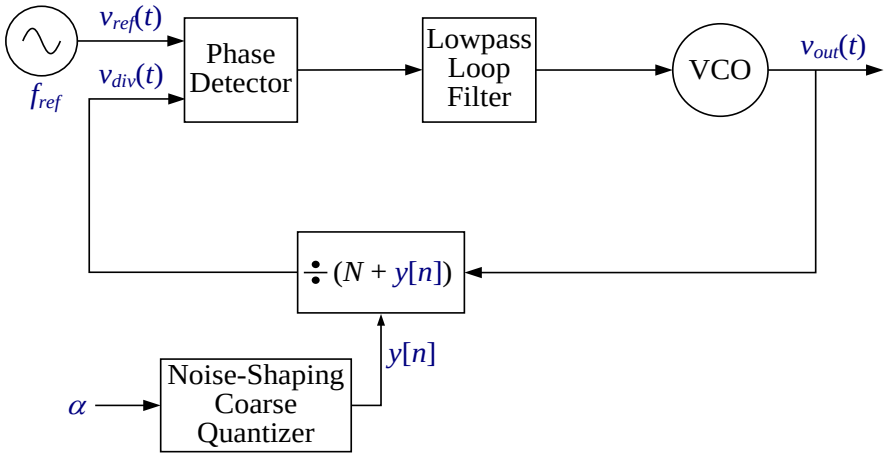

Figure 1: Block diagram of a fractional-*N* PLL.

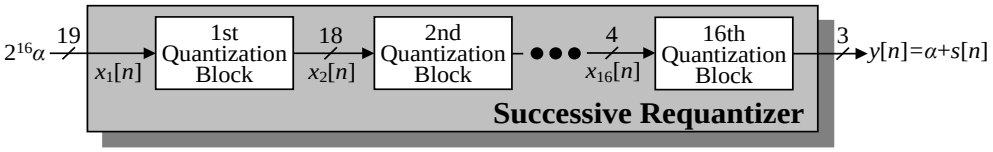

Figure 2: High-level diagram of an example successive requantizer.

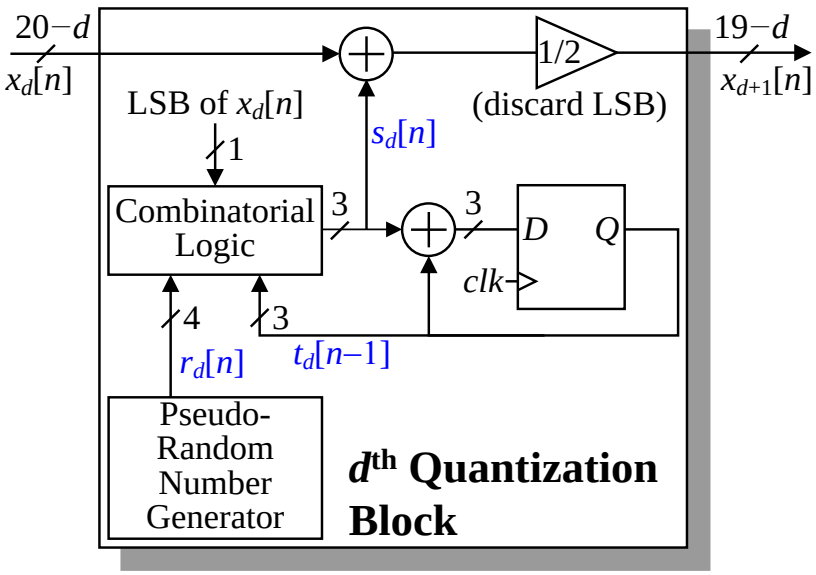

Combinatorial Logic Truth Table:

LSB of $x_d[n] = 0$		
$t_d[n-1]$	$r_d[n]$	$s_d[n]$
2	≥ 0 and ≤ 3	0
2	≤ −1 or ≥ 4	−2
1	≤ −1 or ≥ 6	0
1	≥ 0 and ≤ 5	−2
0	0 or 1	2
0	≤ −1 or ≥ 4	0
0	2 or 3	−2
−1	≤ −1 or ≥ 6	0
−1	≥ 0 and ≤ 5	2
−2	≥ 0 and ≤ 3	0
−2	≤ −1 or ≥ 4	2

LSB of $x_d[n] = 1$		
$t_d[n-1]$	$r_d[n]$	$s_d[n]$
2	≤ −1 or ≥ 4	−1
2	≥ 0 and ≤ 3	−3
1	≥ 1 and ≤ 3	1
1	≤ −1 or ≥ 4	−1
1	0	−3
0	≥ 0	1
0	≤ −1	−1
−1	≥ 1 and ≤ 3	−1
−1	≤ −1 or ≥ 4	1
−1	0	3
−2	≤ −1 or ≥ 4	1
−2	≥ 0 and ≤ 3	3

Figure 3: Details of each quantization block within the example successive requantizer.

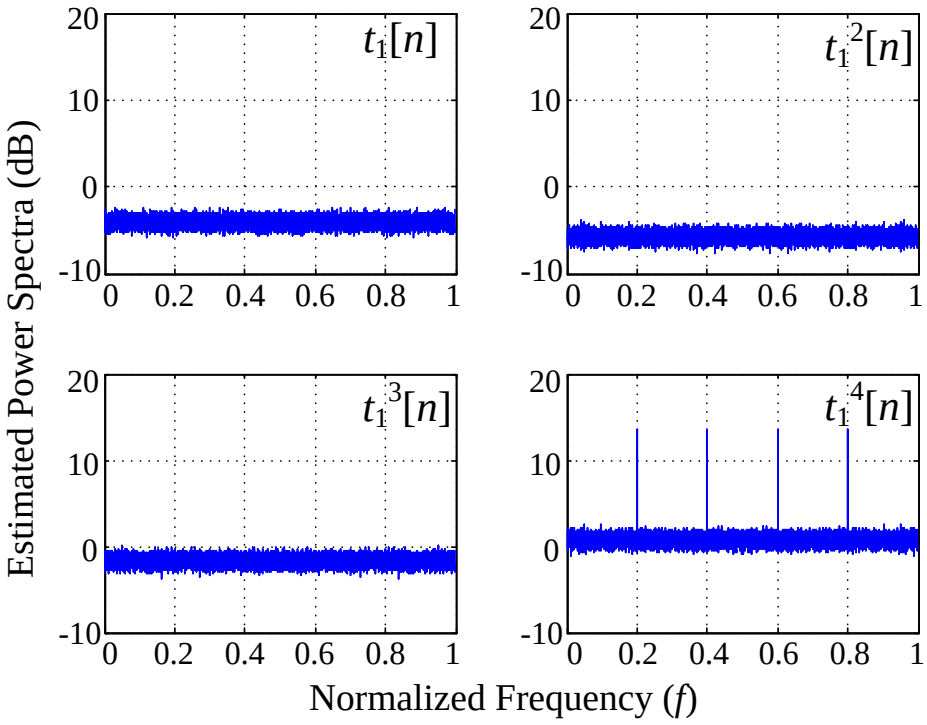

Figure 4: Estimated power spectra of an optimal quantization noise running sum sequence bounded by 2 when raised to different powers.

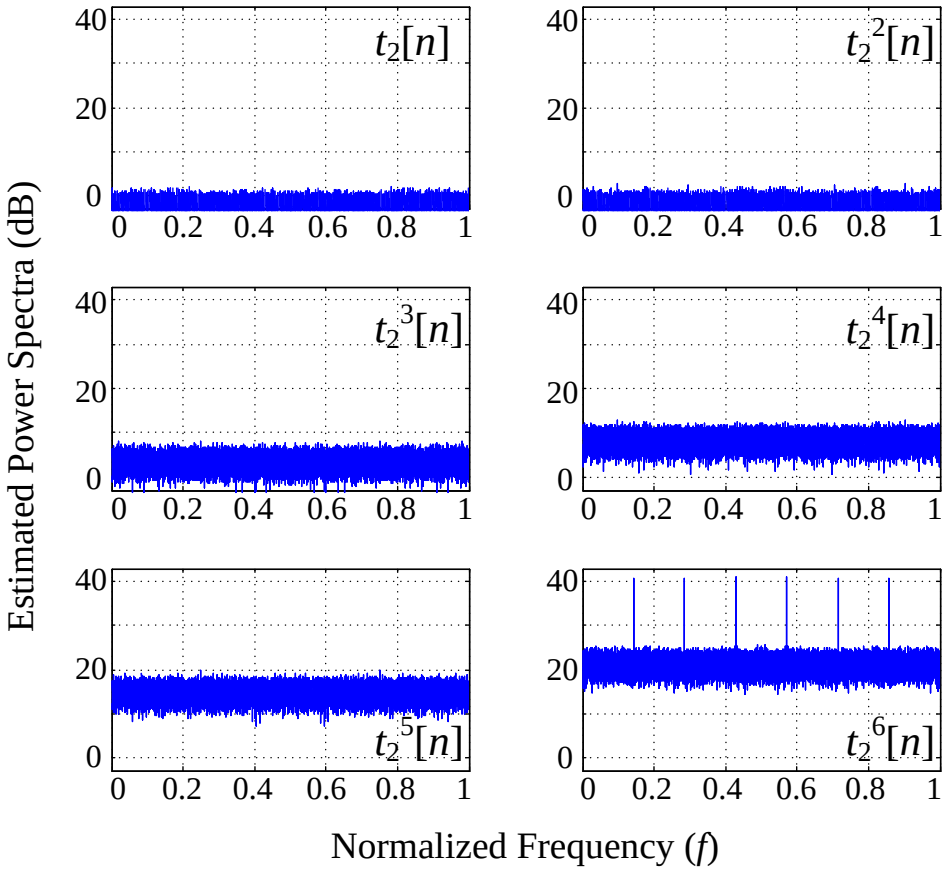

Figure 5: Estimated power spectra of an optimal quantization noise running sum sequence bounded by 3 when raised to different powers**.**

REFERENCES

1. B. Razavi, Phase-Locking in High-Performance Systems: From Devices to Architectures, Wiley-Interscience, 2003.

2. T. H. Lee, *The Design of CMOS Radio-Frequency Integrated Circuits*, Second Edition, Cambridge University Press, 2003.

3. S. Ting, A. H. Sayed, "Digital Suppression of Spurious PLL Tones in A/D Converters," *IEEE Transactions on Signal Processing*, vol. 59, no. 11, pp. 5275-5288, November 2011.

4. B. De Muer, M. Steyaert, "A CMOS Monolithic ΔΣ-Controlled Fractional-N Frequency Synthesizer for DCS-1800," *IEEE Journal of Solid-State Circuits*, vol. 37, no. 7, July 2002.

5. S. Pamarti, L. Jansson, I. Galton, "A Wideband 2.4GHz ΔΣ Fractional-N PLL with 1 Mb/s In-Loop Modulation," *IEEE Journal of Solid-State Circuits*, vol. 39, no. 1, pp. 49-62, January 2004.

6. A. Swaminathan, A. Panigada, E. Masry, I. Galton, "A Digital Requantizer with Shaped Requantization Noise that Remains Well Behaved after Nonlinear Distortion," *IEEE Transactions on Signal Processing*, vol. 55, no. 11, pp. 5382-5394, November 2007.

7. K. J. Wang, A. Swaminathan, I. Galton, "Spurious Tone Suppression Techniques Applied to a Wide-Bandwidth 2.4 GHz Fractional-*N* PLL," *IEEE Journal of Solid-State Circuits*, vol. 43, issue 12, pp. 2787-2797, December 2008.

8. H. Jian, Z. Xu, Y. Wu, F. Chang, "A Compact 0.8-6GHz Fractional-N PLL with Binary-Weighted D/A Differentiator and Offset-Frequency Δ–Σ Modulator for Noise and Spurs Cancellation," *2009 Symposium on VLSI Circuits*, pp. 186-187, 16-18 June 2009.

9. P. Su, S. Pamarti, "Mismatch Shaping Techniques to Linearize Charge Pump Errors in Fractional-N PLLs," *IEEE Transactions on Circuits and Systems–I: Regular Papers*, vol. 57, no. 6, June 2010.

10. K. Hosseini, B. Fitzgibbon, M.P. Kennedy, "Observations Concerning the Generation of Spurious Tones in Digital Delta-Sigma Modulators Followed by a Memoryless Nonlinearity," *IEEE Transactions on Circuits and Systems–II: Express Briefs*, vol. 58, no. 11, November 2011.

11. B. Miller, B. Conley, "A Multiple Modulator Fractional Divider," *Annual IEEE*

Symposium on Frequency Control, vol. 44, pp. 559-568, March 1990.

12. B. Miller, B. Conley, "A Multiple Modulator Fractional Divider," *IEEE Transactions on Instrumentation and Measurement*, vol. 40, no. 3, pp. 578-583, June 1991.

13. T. A. Riley, M. A. Copeland, T. A. Kwasniewski, "Delta-Sigma Modulation in Fractional-N Frequency Synthesis," *IEEE Journal of Solid-State Circuits*, vol. 28, no. 5, pp. 553-559, May 1993.

14. Agilent Technologies, Inc, *Agilent Spectrum Analysis Basics*, Application Note 150, August 2006.

15. A. V. Oppenheim, R. W. Schafer, J. R. Buck, *Discrete-Time Signal Processing*, Second Edition, Englewood Cliffs, NJ: Prentice-Hall, 1999.

16. A. Hajimiri, T. H. Lee, "A General Theory of Phase Noise in Electrical Oscillators," *IEEE Journal of Solid-State Circuits*, vol. 33, no. 2, pp.179-194, February 1998.

17. L. Lin, L. Tee, P. R. Gray, "A 1.4 GHz Differential Low-Noise CMOS Frequency Synthesizer using a Wideband PLL Architecture," *IEEE ISSCC Digest of Technical Papers*, pp. 204-205, February 2000.

18. H. Hedayati, B. Bakkaloglu, W. Khalil, "Closed-loop Nonlinear Modeling of Wideband ΔΣ Fractional-N Frequency Synthesizers," *IEEE Transactions on Microwave Theory and Techniques*, vol. 54, no. 10, pp. 3654-3663, October 2006.

19. E. Familier, C. Venerus, I. Galton, "A Class of Quantizers with DC-Free Quantization Noise and Optimal Immunity to Nonlinearity-Induced Spurious Tones," *IEEE Transactions on Signal Processing*, vol. 61, no. 17, 2013.

CHAPTER 2

A CLASS OF QUANTIZERS WITH DC-FREE QUANTIZATION NOISE AND OPTIMAL IMMUNITY TO NONLINEARITY-INDUCED SPURIOUS TONES

Abstract—Fractional-*N* phase-locked loops (PLLs) typically use noise-shaping coarse quantizers to control their instantaneous output frequency. The resulting quantization noise and its running sum inevitably get distorted by non-ideal analog components within the PLL, which induces undesirable spurious tones in the PLL's output signal. A recently proposed quantizer, called a successive requantizer, has been shown to mitigate this problem. Its quantization noise and the running sum of its quantization noise can be subjected to up to 5th-order and 3rd-order nonlinear distortion, respectively, without inducing spurious tones. This paper extends the previously published successive requantizer results to design successive requantizers whose quantization noise running sum sequences can attain such immunity to nonlinearity-induced spurious tones up to arbitrarily high orders of distortion. It also presents successive requantizers whose

Manuscript received November 8, 2012; revised February 22, 2013; accepted April 01, 2013. Date of publication May 16, 2013; date of current version August 07, 2013. The associate editor coordinating the review of this manuscript and approving it for publication was Prof. Ljubisa Stankovic. This work was supported by the National Science Foundation under Award 0914748.
The authors are with the Department of Electrical and Computer Engineering, University of California at San Diego, La Jolla, CA 92093-0407 USA (e-mail: galton@ucsd.edu).
Color versions of one or more of the figures in this paper are available online at http://ieeexplore.ieee.org.
Digital Object Identifier 10.1109/TSP.2013.2263503

quantization noise and quantization noise running sum sequences have optimally reduced susceptibility to nonlinearity-induced spurious tones.

I. INTRODUCTION

Fractional-*N* phase locked loops (PLLs) are widely used to synthesize local oscillator signals in communication systems [1], [2]. They typically use noise-shaping coarse quantizers, most commonly implemented as digital delta-sigma (ΔΣ) modulators, to quantize digital sequences that control their output frequency. Each quantized sequence can be viewed as the sum of the quantizer's input sequence plus *DC-free quantization noise* [3]–[5].[6] In practical PLLs, the quantization noise and its running sum inevitably are subjected to nonlinear distortion from analog circuit imperfections within the PLL. This has the undesirable effect of inducing spurious tones in the sequences, even when the undistorted sequences are free of spurious tones [6]–[12]. Spurious tones induced in this fashion are referred to as *nonlinearity-induced spurious tones*.

Most communication applications require the power of spurious tones to be very low, as they ultimately appear in the PLL's output signal and can be critically harmful to communication system performance. One way to minimize spurious tone power is to make the analog circuitry of the PLL very linear. Unfortunately, improving analog circuit linearity tends to increase power dissipation and integrated circuit area significantly. Alternatively, the coarse quantizer can be designed to ensure that the quantization noise

[6] A sequence whose running sum is bounded for all time is said to be DC-free.

and its running sum remain free of spurious tones even when subjected to the type of nonlinear distortion commonly imposed within the PLL.

A sequence $x[n]$ is said to be immune to spurious tones up to order h if $x^p[n]$, for $p = 1, 2,\ldots, h$, are free of spurious tones. A recently proposed quantizer, called a successive requantizer, was introduced in [6] and implemented as part of a phase-noise cancelling PLL in [7] to mitigate the power of nonlinearity-induced spurious tones. Its quantization noise and the running sum of its quantization noise are immune to spurious tones up to orders 5 and 3, respectively.

This paper extends the previously published successive requantizer results to design successive requantizers with higher immunity to nonlinearly-induced spurious tones. It proves that the order up to which the quantization noise running sum of a successive requantizer is immune to spurious tones can be arbitrarily increased at the expense of increasing the range of values spanned by the quantization noise running sum. In a PLL, increasing this range tends to increase the quantization noise power, and, therefore, the phase noise. Hence, a tradeoff exists between enhanced immunity to nonlinearity-induced spurious tones and increased phase noise power. The paper also presents successive requantizers that are optimal in the sense that their quantization noise and quantization noise running sum are immune to spurious tones up to the maximum possible orders for the range of values spanned by the quantization noise running sum.

II. SUCCESSIVE REQUANTIZER BACKGROUND

A. Spectral Properties of Interest

The periodogram of any sequence $x[n]$ is defined as

$$I_{x,L}(\omega) = \frac{1}{L}\left|\sum_{n=0}^{L-1} x[n]e^{-j\omega n}\right|^2 \tag{69}$$

for any positive integer L [13]. By definition, $x[n]$ contains a tone at $\omega_n \neq 0$ if $I_{x,L}(\omega)$ is unbounded at $\omega = \omega_n$ as $L \to \infty$ [6], [14]. In a PLL, the nonlinearities to which the quantization noise sequence $s[n]$ and the quantization noise running sum sequence

$$t[n] = \sum_{k=0}^{n} s[k] \tag{70}$$

are subjected tend to be well-modeled as truncated memoryless power series [7]. Therefore, this work focuses on the properties of $I_{s^q,L}(\omega)$ and $I_{t^p,L}(\omega)$ for integer values of q and p up to some maximum values.

B. Successive Requantizer Architecture

As shown in Fig. 6, a typical fractional-N PLL consists of a phase detector, a lowpass loop filter, a voltage controlled oscillator (VCO), a frequency divider, and a noise-shaping coarse quantizer that introduces DC-free quantization noise. Its purpose is to generate a periodic or frequency modulated output signal with an instantaneous frequency of $(N + x[n])f_{ref}$, where N is a positive integer, $x[n]$ is a sequence of fractional values, and f_{ref} is the frequency of a reference oscillator. In most applications $x[n]$ is constant, and in other applications it varies slowly. The PLL's feedback loop adjusts the

output frequency to be f_{ref} times the average of the divider modulus $N + x_K[n]$. If $x_K[n]$ could be set to $x[n]$ for all n, the PLL would have the desired output frequency. However, practical frequency dividers can only count integer numbers of VCO cycles, so $x_K[n]$ must be integer-valued. Therefore, the coarse quantizer ensures that $x_K[n]$ is integer-valued but averages to $x[n]$ in time. This results in the desired PLL output frequency, although the deviations of $x_K[n]$ from $x[n]$ contribute an extra component to the PLL's phase noise. As explained in the introduction, the coarse quantizer can be implemented as the successive requantizer presented in [6].

The high-level architecture of the successive requantizer is shown in Figs. 7 and 8, wherein all node variables are integer-valued sequences in two's complement format. The successive requantizer consists of K serially-connected quantization blocks, each of which quantizes its input by 1 bit, so the successive requantizer quantizes its input by K bits. Its input,

$$x_0[n] = 2^K x[n], \tag{71}$$

is a B-bit sequence which satisfies $|x_0[n]| \le 2^{B-2}$ for all n. The dth quantization block's input, $x_d[n]$, and output, $x_{d+1}[n]$, are related through

$$x_{d+1}[n] = \frac{1}{2}\left(x_d[n] + s_d[n]\right), \tag{72}$$

where $s_d[n]$ is a sequence generated by the quantization block's *sequence generator*. The sequence generator (Fig. 8) generates $s_d[n]$ as a function of the *parity sequence*, $o_d[n]$, which at each time, n, is 1 if $s_d[n]$ is odd and 0 if $s_d[n]$ is even. It chooses $s_d[n]$ to have the same parity as $x_d[n]$ for each n so that $x_{d+1}[n]$ is an integer-valued sequence, and to have a sufficiently small magnitude that the two's complement representation of $x_{d+1}[n]$

requires one less bit than that of $x_d[n]$. Hence, the output of the successive requantizer is a two's complement integer-valued sequence given by

$$x_K[n] = 2^{-K} x_0[n] + s[n] = x[n] + s[n], \tag{73}$$

where

$$s[n] = \sum_{d=0}^{K-1} 2^{d-K} s_d[n] \tag{74}$$

is the quantization noise. The running sum of $s_d[n]$ is

$$t_d[n] = \sum_{k=0}^{n} s_d[k], \tag{75}$$

so (74) implies that the running sum of the quantization noise can be written as

$$t[n] = \sum_{d=0}^{K-1} 2^{d-K} t_d[n]. \tag{76}$$

The lowest integer bound on the magnitude of each $t_d[n]$ sequence is denoted as N_t, so $|t_d[n]| \le N_t$ for all d and n. Therefore, it follows from (76) that $|t[n]| < N_t$ for all n.

As shown in [6], if the sequence generator is designed such that the probability mass function (pmf) of $s_d[n]$ for each n depends only on $o_d[n]$ and $t_d[n-1]$, then $t_d[n]$ is a discrete-valued Markov random sequence conditioned on $o_d[n]$. Hence, for any parity sequence, $o_d[n]$, the evolution of $t_d[n]$ from times u to $u + m$ can be represented by an m-step $(2N_t + 1)\times(2N_t + 1)$ state transition matrix, $\mathbf{A}_{\{o_d[n]\}}[u, m]$, where the element on the ith row and jth column is

$$\begin{aligned}\left(\mathbf{A}_{\{o_d[n]\}}[u,m]\right)(i,j) = \Pr(&t_d[u+m] = \mathbf{t}(j) \mid t_d[u] = \mathbf{t}(i), \\ &o_d[n]; n = u+1, u+2, \ldots, u+m)\end{aligned} \tag{77}$$

and

$$\mathbf{t} = (N_t \quad N_t - 1 \quad \ldots \quad -N_t)^T. \tag{78}$$

It follows from the properties of state transition matrices that for $m > 1$ $\mathbf{A}_{\{o_d[n]\}}[u, m]$ can be expanded as a product of one-step state transition matrices as

$$\begin{aligned}&\mathbf{A}_{\{o_d[n]\}}[u,m]\\&\quad=\mathbf{A}_{\{o_d[n]\}}[u,1]\mathbf{A}_{\{o_d[n]\}}[u+1,1]\cdots\mathbf{A}_{\{o_d[n]\}}[u+m-1,1].\end{aligned}\tag{79}$$

As is also shown in [6], $\mathbf{A}_{\{o_d[n]\}}[v - 1, 1]$ at each time index v is equal to one of two one-step state transition matrices, denoted as $\mathbf{A_e}$ and $\mathbf{A_o}$: when $o_d[v] = 0$, $\mathbf{A}_{\{o_d[n]\}}[v - 1, 1] = \mathbf{A_e}$, and when $o_d[v] = 1$, $\mathbf{A}_{\{o_d[n]\}}[v - 1, 1] = \mathbf{A_o}$. It follows from (75) that

$$s_d[n]=t_d[n]-t_d[n-1],\tag{80}$$

so the $\mathbf{A_e}$ and $\mathbf{A_o}$ matrices describe the probabilistic behavior of each $s_d[n]$ sequence and determine the orders up to which $s[n]$ and $t[n]$ are immune to spurious tones. In any given successive requantizer they completely specify the required behavior of the combinatorial logic block and, conversely, can be deduced from the combinatorial logic block.

Each $t_d[n]$ sequence satisfies $|t_d[n]| \le N_t$ for all n, so it follows from (80) that each $s_d[n]$ sequence satisfies $|s_d[n]| \le 2N_t$ for all n. Therefore, (74) implies that $|s[n]| < 2N_t$ for all n, and that the output of the successive requantizer, given by (73), satisfies $|x_K[n]| \le 2N_t$ for all n. Since $x_K[n]$ is represented by a $(B - K)$-bit sequence,

$$B-K\ge\log_2\ 4N_t+1\tag{81}$$

must hold.

Figs. 7 and 9 imply that the dth quantization block of the successive requantizer contains combinatorial logic that depends on the $\mathbf{A_e}$ and $\mathbf{A_o}$ matrices, a pseudo-random number generator, a $(B - d)$-bit adder, a $\lceil \log_2\ 4N_t + 1 \rceil$-bit adder, and $\lceil \log_2\ 4N_t + 1 \rceil$ flip

flops, where $\lceil x \rceil$ denotes the smallest integer greater than x. With K blocks, where K is usually close to B in magnitude, the computational complexity of the successive requantizer is a logarithmic function of N_t and a quadratic function of B. As an example, the implementation of the successive requantizer in 0.18 μm 1P6M CMOS technology in [7], for which $N_t = 3$ and $K = 19$, and the related pseudo-random number generator, requires 1049 gates, 114 flip flops, and 232 1-bit adders, and occupies an area of 0.142 mm^2.

C. Example Successive Requantizers

If the combinatorial logic implements the truth table shown in Fig. 9(a), then $N_t = 1$,

$$\mathbf{A_e} = \begin{pmatrix} 1 & 0 & 0 \\ 0 & 1 & 0 \\ 0 & 0 & 1 \end{pmatrix}, \text{ and } \mathbf{A_o} = \begin{pmatrix} 0 & 1 & 0 \\ 1/2 & 0 & 1/2 \\ 0 & 1 & 0 \end{pmatrix}. \quad (82)$$

It can be verified from the results presented in [15] that in this case $t[n]$ and $s[n]$ are free of spurious tones. However, the results presented in [14] and simulations support the conclusion that spurious tones are generated for some successive requantizer input sequences when $t[n]$ or $s[n]$ are subjected to second-order nonlinear distortion. Therefore, $t[n]$ and $s[n]$ are immune to spurious tones only up to order 1.

As proven in [7], if the combinatorial logic implements the truth table shown in Fig. 9(b), then $N_t = 2$,

$$\mathbf{A_e} = \begin{pmatrix} 1/4 & 0 & 3/4 & 0 & 0 \\ 0 & 5/8 & 0 & 3/8 & 0 \\ 1/8 & 0 & 3/4 & 0 & 1/8 \\ 0 & 3/8 & 0 & 5/8 & 0 \\ 0 & 0 & 3/4 & 0 & 1/4 \end{pmatrix}, \text{ and}$$
$$\mathbf{A_o} = \begin{pmatrix} 0 & 3/4 & 0 & 1/4 & 0 \\ 3/16 & 0 & 3/4 & 0 & 1/16 \\ 0 & 1/2 & 0 & 1/2 & 0 \\ 1/16 & 0 & 3/4 & 0 & 3/16 \\ 0 & 1/4 & 0 & 3/4 & 0 \end{pmatrix}. \quad (83)$$

In this case it follows from the results in [6] and [14] that $t[n]$ and $s[n]$ are immune to spurious tones up to orders 3 and 5, respectively.

D. Additional Successive Requantizer Properties

The $\mathbf{A_e}$ matrices in the examples presented above have the property that $\mathbf{A_e}(i, j) = 0$ whenever $i + j$ is odd, and $\mathbf{A_o}(i, j) = 0$ whenever $i + j$ is even; such matrices are referred to as even-entries matrices and odd-entries matrices, respectively. As is evident in the example $\mathbf{A_e}$ and $\mathbf{A_o}$ matrices presented above, the row vectors of both even-entries and odd-entries matrices alternate between two types of vectors: vectors whose odd-indexed elements are zero, referred to as even-entries vectors, and vectors whose even-indexed elements are zero, referred to as odd-entries vectors. For example, an even-entries vector $\mathbf{v_e}$ is such that $\mathbf{v_e}(i) = 0$ whenever i is odd.

These properties of $\mathbf{A_e}$ and $\mathbf{A_o}$ hold in general as a result of (80). For any n at which $o_d[n] = 0$, $s_d[n]$ is even, so (80) implies that the probability that $t_d[n]$ and $t_d[n-1]$ have different parities is zero. Similarly, for any n at which $o_d[n] = 1$, $s_d[n]$ is odd, so the probability that $t_d[n]$ and $t_d[n-1]$ have the same parity is zero. This implies that the

successive requantizer is such that $\mathbf{A_e}$ matrices are always even-entries matrices, and $\mathbf{A_o}$ matrices are always odd-entries matrices.

Not only are the $\mathbf{A_e}$ and $\mathbf{A_o}$ matrices for any given successive requantizer even-entries and odd-entries $(2N_t + 1)\times(2N_t + 1)$ stochastic matrices, respectively, as described above, but the converse is also true: any even-entries and odd-entries $(2N_t + 1)\times(2N_t + 1)$ stochastic matrices can be used as the $\mathbf{A_e}$ and $\mathbf{A_o}$ matrices, respectively, with which to design a successive requantizer. This is because any such matrices provide a complete description of the pmf of $s_d[n]$ conditioned on $o_d[n]$ and $t_d[n-1]$ at each n, and any chosen pmf can be realized with arbitrarily high accuracy using combinatorial logic elements and a pseudo-random number generator.

It is convenient to define a $(2N_t + 1)\times(4N_t + 1)$ stochastic matrix that describes the evolution of $s_d[n]$ from times u to $u + m$, with elements given by

$$\begin{aligned}\left(\mathbf{S}_{\{o_d[n]\}}[u,m]\right)(i,j) = \Pr(&s_d[u+m] = \mathbf{s}(j) \mid t_d[u] = \mathbf{t}(i),\\ &o_d[n]; n = u+1, u+2, \ldots, u+m)\end{aligned} \tag{84}$$

where

$$\mathbf{s} = (2N_t \quad 2N_t - 1 \quad \ldots \quad -2N_t)^T. \tag{85}$$

As shown in [6], the dependence of the pmf of $s_d[n]$ on $o_d[n]$ implies that, at each time v, $\mathbf{S}_{\{o_d[n]\}}[v-1, 1]$ is equal to one of two matrices, denoted as $\mathbf{S_e}$ and $\mathbf{S_o}$. When $o_d[v] = 0$, $\mathbf{S}_{\{o_d[n]\}}[v-1, 1] = \mathbf{S_e}$, and when $o_d[v] = 1$, $\mathbf{S}_{\{o_d[n]\}}[v-1, 1] = \mathbf{S_o}$. With (77) and (84) this implies that for $m > 1$

$$\begin{aligned}&\mathbf{S}_{\{o_d[n]\}}[u,m]\\ &\quad = \mathbf{A}_{\{o_d[n]\}}[u,m-1]\left(\mathbf{S_e}\left(1-o_d[u+m]\right) + \mathbf{S_o}o_d[u+m]\right).\end{aligned} \tag{86}$$

Equation (84) implies that each nonzero element in $\mathbf{S_e}$ and $\mathbf{S_o}$ is equal to an element in $\mathbf{A_e}$ and $\mathbf{A_o}$, respectively. Specifically, for i, j, and k such that $\mathbf{s}(k) = \mathbf{t}(j) - \mathbf{t}(i)$, the element in the ith row and kth column of $\mathbf{S_e}$ is equal to that in the ith row and jth column of $\mathbf{A_e}$, and the element in the ith row and kth column of $\mathbf{S_o}$ is equal to that in the ith row and jth column of $\mathbf{A_o}$. Hence, $\mathbf{S_e}$ and $\mathbf{S_o}$ can be deduced from $\mathbf{A_e}$ and $\mathbf{A_o}$ as

$$\mathbf{S}_{\mathbf{x}}(i, j) = \begin{cases} \mathbf{A}_{\mathbf{x}}(i, j+i-2N_t-1), & \text{if } 2N_t+2-i \le j \le 4N_t+2-i, \\ 0, & \text{if } j \le 2N_t+1-i, j \ge 4N_t+3-i \end{cases} \tag{87}$$

for $\mathbf{x} = \mathbf{e}$ or $\mathbf{o}$.

III. OPTIMAL QUANTIZATION IN TERMS OF IMMUNITY TO SPURIOUS TONES

A. Theory on Optimal Quantization

The one-step state transition matrices, $\mathbf{A_e}$ and $\mathbf{A_o}$, are said to ensure order-p $t[n]$-convergence if there is a constant b_p such that

$$\lim_{m\to\infty} \mathbf{A}_{\{o_d[n]\}}[u, m]\mathbf{t}^{(p)} = b_p \mathbf{1}_{2N_t+1} \tag{88}$$

for all parity sequences $\{o_d[n], d = 0, 1, \ldots, K-1\}$ and any integer u, where

$$\mathbf{t}^{(p)} = \begin{pmatrix} N_t^{\,p} & (N_t-1)^p & \ldots & (-N_t)^p \end{pmatrix}^T, \tag{89}$$

$\mathbf{1}_{2N_t+1}$ is a length-($2N_t$ + 1) vector whose elements are all 1, and the convergence of the vector sequence in (88) is exponential.[7] Similarly, they are said to ensure order-q $s[n]$-convergence if there is a constant c_q such that

$$\lim_{m\to\infty} \mathbf{S}_{\{o_d[n]\}}[u,m]\mathbf{s}^{(q)} = c_q \mathbf{1}_{2N_t+1} \tag{90}$$

for all parity sequences $\{o_d[n], d = 0, 1,\ldots, K-1\}$ and any integer u, where

$$\mathbf{s}^{(q)} = \left(\left(2N_t\right)^q \quad \left(2N_t - 1\right)^q \quad \ldots \quad \left(-2N_t\right)^q \right)^T, \tag{91}$$

and the convergence of the vector sequence in (90) is exponential.

Theorems 1 and 2 state sufficient conditions for $t[n]$ and $s[n]$, respectively, to be immune to spurious tones up to any given order.

Theorem 1: Suppose that $\mathbf{A_e}$ and $\mathbf{A_o}$ ensure order-p $t[n]$-convergence for all positive integers $p \le h_t$, where h_t is a positive integer. Then, $t[n]$ is immune to spurious tones up to order h_t.

Proof: The proof is identical to that of Theorem 1 in [6] except with equation (29) in [6] replaced by

$$\left| E\left\{ t^p[n_1] t^p[n_2] - C_{t^p} \right\} \right| \le D_1 \alpha^{|n_2 - n_1|} + D_2 \alpha^{\min\{n_1, n_2\}} \tag{92}$$

for some positive constants D_1 and D_2 and a constant $0 < \alpha < 1$, (31) in [6] replaced by

[7] A length-m vector sequence $\mathbf{b}[0]$, $\mathbf{b}[1]$, … converges exponentially to a vector $\mathbf{b}$ if there exist constants $C \ge 0$ and $0 < \alpha < 1$ such that $|\mathbf{b}[n] - \mathbf{b}| \le C\alpha^n \mathbf{1}_m$ for all integers $n \ge 0$.

$$
\begin{aligned}
|J_{2,1}| &\le \frac{1}{L}\sum_{\substack{n_1=0\\ n_1\neq n_2}}^{L-1}\sum_{n_2=0}^{L-1}\left(D_1\alpha^{|n_1-n_2|}+D_2\alpha^{\min\{n_1,n_2\}}\right)\\
&\le \frac{D_1}{L}\sum_{n_1=0}^{L-1}\sum_{n_2=0}^{L-1}\alpha^{|n_1-n_2|}+\frac{D_2}{L}\left(\sum_{0\le n_1<n_2\le L-1}\alpha^{n_1}+\sum_{0\le n_2<n_1\le L-1}\alpha^{n_2}\right)\\
&\le \frac{D_1}{L}\sum_{n_1=0}^{L-1}\left(2\sum_{n=0}^{L-1}\alpha^{n}\right)+D_2\left(2\sum_{n=0}^{L-1}\alpha^{n}\right)\\
&\le 2\left(D_1+D_2\right)\frac{1-\alpha^{L}}{1-\alpha}\le 2\left(D_1+D_2\right)\frac{1}{1-\alpha},
\end{aligned}
\tag{93}
$$

and Lemma 1 in [6] replaced by Lemma 1 in the appendix of this paper. ■

Theorem 2: Suppose that $\mathbf{A_e}$ and $\mathbf{A_o}$ ensure order-q $s[n]$-convergence for all positive integers $q \le h_s$, where h_s is a positive integer. Then, $s[n]$ is immune to spurious tones up to order h_s.

Proof: The proof is identical to that of Theorem 2 in [6] except with p replaced by q, equation (36) in [6] replaced by

$$
\left|E\left\{s^q[n_1]s^q[n_2]-C_{s^q}\right\}\right| \le E_1\beta^{|n_2-n_1|}+E_2\beta^{\min\{n_1,n_2\}} \tag{94}
$$

for some positive constants E_1 and E_2 and a constant $0 < \beta < 1$, and Lemma 2 in [6] replaced by Lemma 2 in the appendix of this paper. ■

Theorem 3 provides sufficient conditions on $\mathbf{A_e}$ and $\mathbf{A_o}$ for $t[n]$ to be immune to spurious tones up to order $2N_t - 1$.

Theorem 3: Let $\mathbf{A_e}$ and $\mathbf{A_o}$ be $(2N_t + 1)\times(2N_t + 1)$ matrices with elements that satisfy

$$
\mathbf{A_e}(i,j)=\begin{cases}\dfrac{1}{2^{2N_t-1}}\dbinom{2N_t}{j-1}+\left(\mathbf{Q}^T\mathbf{P}\mathbf{Q}\right)(i,j), & \text{if } i+j \text{ is even},\\ 0, & \text{if } i+j \text{ is odd},\end{cases} \tag{95}
$$

$$\mathbf{A_o}(i,j)=\begin{cases}0, & \text{if } i+j \text{ is even,}\\ \dfrac{1}{2^{2N_t-1}}\dbinom{2N_t}{j-1}+\left(\mathbf{Q}^T\mathbf{P}\mathbf{Q}\right)(i,j), & \text{if } i+j \text{ is odd,}\end{cases} \tag{96}$$

where N_t is any integer greater than 1, $\mathbf{Q}$ is the $N_t\times(2N_t+1)$ matrix

$$\mathbf{Q}=\begin{pmatrix}1 & 0 & \ldots & 0 & 0 & 0 & \ldots & 0 & -1\\ 0 & 1 & \ldots & 0 & 0 & 0 & \ldots & -1 & 0\\ \ldots & \ldots & \ldots & \ldots & \ldots & \ldots & \ldots & \ldots & \ldots\\ 0 & 0 & \ldots & 1 & 0 & -1 & \ldots & 0 & 0\end{pmatrix} \tag{97}$$

and $\mathbf{P}$ is any $N_t\times N_t$ matrix whose elements satisfy

$$|\mathbf{P}(i,j)|\le\frac{1}{2^{2N_t-1}}\binom{2N_t}{j-1} \tag{98}$$

and for each row i

$$|\mathbf{P}(i,j)|\ne\frac{1}{2^{2N_t-1}}\binom{2N_t}{j-1} \tag{99}$$

for at least one $j\in\{2,4,\ldots,N_t\}$ if N_t is even and one $j\in\{1,3,\ldots,N_t\}$ if N_t is odd. Then, $t[n]$ is immune to spurious tones up to order $2N_t-1$.

Note that the $\mathbf{A_e}$ and $\mathbf{A_o}$ matrices given by (83) satisfy the conditions of Theorem 3. Specifically, (95) and (96) with

$$\mathbf{P}=\begin{pmatrix}1/8 & 1/4\\ 1/16 & 1/8\end{pmatrix} \tag{100}$$

yield the $\mathbf{A_e}$ and $\mathbf{A_o}$ matrices given by (83).

Proof of Theorem 3: It is first shown that $\mathbf{A_e}$ and $\mathbf{A_o}$ are valid one-step state transition matrices for the successive requantizer, i.e. that they are stochastic even-entries and odd-entries matrices, respectively. These results are then used to show that Theorem 1 holds for $h_t=2N_t-1$, which completes the proof.

By definition, $\mathbf{A_e}$ and $\mathbf{A_o}$ are even-entries and odd-entries matrices, respectively. To show that they are stochastic matrices, it is sufficient to show that all their elements are nonnegative and that the sum of the elements on each row of each matrix is 1.

It follows from (95) and (96) that a sufficient condition for the elements of $\mathbf{A_e}$ and $\mathbf{A_o}$ to be nonnegative is

$$\left|\left(\mathbf{Q}^T\mathbf{P}\mathbf{Q}\right)(i,j)\right| \le \frac{1}{2^{2N_t-1}}\binom{2N_t}{j-1} \tag{101}$$

for all $i, j \in \{1, 2,\ldots, 2N_t + 1\}$. The matrix $\mathbf{Q}$ can be written as

$$\mathbf{Q} = \left(\mathbf{I}_{N_t}, \mathbf{0}_{N_t}, -\mathbf{J}_{N_t}\right), \tag{102}$$

where $\mathbf{I}_{N_t}$ is the $N_t \times N_t$ identity matrix, $\mathbf{0}_{N_t}$ is a length-N_t vector whose elements are all 0, and $\mathbf{J}_{N_t}$ is the $N_t \times N_t$ *exchange matrix*, i.e. the $N_t \times N_t$ matrix for which all the elements in the anti-diagonal are 1 and all other elements are 0. Thus,

$$\mathbf{Q}^T\mathbf{P}\mathbf{Q} = \begin{pmatrix} \mathbf{P} & \mathbf{0}_{N_t} & -\mathbf{P}\mathbf{J}_{N_t} \\ \mathbf{0}_{N_t}{}^T & 0 & \mathbf{0}_{N_t}{}^T \\ -\mathbf{J}_{N_t}\mathbf{P} & \mathbf{0}_{N_t} & \mathbf{J}_{N_t}\mathbf{P}\mathbf{J}_{N_t} \end{pmatrix}. \tag{103}$$

The definition of exchange matrices implies that

$$\left(\mathbf{P}\mathbf{J}_{N_t}\right)(i,j) = \mathbf{P}(i, N_t + 1 - j), \tag{104}$$

$$\left(\mathbf{J}_{N_t}\mathbf{P}\right)(i,j) = \mathbf{P}(N_t + 1 - i, j), \text{ and} \tag{105}$$

$$\left(\mathbf{J}_{N_t}\mathbf{P}\mathbf{J}_{N_t}\right)(i,j) = \mathbf{P}(N_t + 1 - i, N_t + 1 - j) \tag{106}$$

for all $i, j \in \{1, 2,\ldots, N_t\}$. Combining (105) and (106) yields

$$\left(\mathbf{J}_{N_t}\mathbf{P}\mathbf{J}_{N_t}\right)(i,j) = \left(\mathbf{J}_{N_t}\mathbf{P}\right)(i, N_t + 1 - j), \tag{107}$$

which with (103) and (104) implies

$$\left(\mathbf{Q}^T\mathbf{P}\mathbf{Q}\right)(i,j) = -\left(\mathbf{Q}^T\mathbf{P}\mathbf{Q}\right)(i, 2N_t + 2 - j) \tag{108}$$

for all $i, j \in \{1, 2,\ldots, 2N_t + 1\}$. It follows from (98), (103), and (105) that (101) is satisfied for all $j \in \{1, 2,\ldots, N_t\}$ and $i \in \{1, 2,\ldots, 2N_t + 1\}$. This, with (108), implies that

$$\left|\left(\mathbf{Q}^T\mathbf{P}\mathbf{Q}\right)(i,j)\right| \le \begin{cases} \dfrac{1}{2^{2N_t-1}}\dbinom{2N_t}{j-1}, & \text{if } 1 \le j \le N_t+1, \\ \dfrac{1}{2^{2N_t-1}}\dbinom{2N_t}{2N_t+1-j}, & \text{if } N_t+2 \le j \le 2N_t+1 \end{cases} \tag{109}$$

for all $i \in \{1, 2,\ldots, 2N_t + 1\}$. Binomial coefficients have the property that

$$\binom{2N_t}{j-1} = \binom{2N_t}{2N_t+1-j} \tag{110}$$

for all $j \in \{1, 2,\ldots, 2N_t + 1\}$, so (109) is equivalent to (101) for all $i, j \in \{1, 2,\ldots, 2N_t + 1\}$. This completes the proof that the elements of $\mathbf{A_e}$ and $\mathbf{A_o}$ are nonnegative.

To show that $\mathbf{A_e}$ and $\mathbf{A_o}$ are stochastic matrices, it remains to show that the sum of the elements in each of their rows is 1. It follows from (95) and (96) that the sum of the elements on the ith row of $\mathbf{A_e}$ or $\mathbf{A_o}$ can either be written as

$$\frac{1}{2^{2N_t-1}}\sum_{j=1,\,j\text{ odd}}^{2N_t+1}\binom{2N_t}{j-1} + \sum_{j=1,\,j\text{ odd}}^{2N_t+1}\left(\mathbf{Q}^T\mathbf{P}\mathbf{Q}\right)(i,j) \quad \text{or} \tag{111}$$

$$\frac{1}{2^{2N_t-1}}\sum_{j=2,\,j\text{ even}}^{2N_t}\binom{2N_t}{j-1} + \sum_{j=2,\,j\text{ even}}^{2N_t}\left(\mathbf{Q}^T\mathbf{P}\mathbf{Q}\right)(i,j). \tag{112}$$

It follows from (108) that the second sum in each of (111) and (112) is 0. The first sums in (111) and (112) can be rewritten as

$$\frac{1}{2^{2N_t}}\left[\sum_{j=1}^{2N_t+1}\binom{2N_t}{j-1} - \sum_{j=1}^{2N_t+1}\binom{2N_t}{j-1}(-1)^j\right] \quad \text{and} \tag{113}$$

$$\frac{1}{2^{2N_t}}\left[\sum_{j=1}^{2N_t+1}\binom{2N_t}{j-1} + \sum_{j=1}^{2N_t+1}\binom{2N_t}{j-1}(-1)^j\right], \tag{114}$$

respectively. The Binomial Theorem implies that the first and second sums in each of (113) and (114) equal $(1+1)^{2N_t}$ and $(1-1)^{2N_t}$, respectively. Thus, (113) and (114) each evaluate to 1, so the sum of the elements on each row of $\mathbf{A_e}$ and $\mathbf{A_o}$ is 1.

To complete the proof of the theorem it is sufficient to prove that $\mathbf{A_e}$ and $\mathbf{A_o}$ ensure order-p $t[n]$-convergence for all positive integers $p \le 2N_t - 1$ so that Theorem 1 can be applied. This is done in two parts. First, it is shown that $\mathbf{A_e}$ and $\mathbf{A_o}$ are centrosymmetric[8], that all their even-entries row vectors have at least $1 + \lfloor N_t / 2 \rfloor$ nonzero entries, and that all their odd-entries row vectors have at least $1 + \lfloor (N_t + 1)/2 \rfloor$ nonzero entries.[9] With Lemma 3 in the appendix, this shows that $\mathbf{A_e}$ and $\mathbf{A_o}$ ensure order-p $t[n]$-convergence for all odd positive integers $p \le 2N_t - 1$. Second, it is shown that for each even positive integer $p \le 2N_t - 1$

$$\mathbf{A_e}\mathbf{t}^{(p)} = \mathbf{A_o}\mathbf{t}^{(p)} = b_p \mathbf{1}_{2N_t+1} \tag{115}$$

for some constant b_p. With Lemma 4 in the appendix, this shows that $\mathbf{A_e}$ and $\mathbf{A_o}$ ensure order-p $t[n]$-convergence for all even positive integers $p \le 2N_t - 1$.

Combining (104) and (105) yields

$$\left(\mathbf{P}\mathbf{J}_{N_t}\right)(i, j) = \left(\mathbf{J}_{N_t}\mathbf{P}\right)(N_t + 1 - i, N_t + 1 - j) \tag{116}$$

for all $i, j \in \{1, 2, \ldots, N_t\}$. This, with (103) and (106), implies that

$$\left(\mathbf{Q}^T\mathbf{P}\mathbf{Q}\right)(i, j) = \left(\mathbf{Q}^T\mathbf{P}\mathbf{Q}\right)(2N_t + 2 - i, 2N_t + 2 - j) \tag{117}$$

for all $i, j \in \{1, 2, \ldots, 2N_t + 1\}$. It follows from (110) and (117) that

---

[8] An $N \times M$ matrix $\mathbf{A}$ is said to be centrosymmetric if $\mathbf{A}(i, j) = \mathbf{A}(N + 1 - i, M + 1 - j)$ for all $i \in \{1, 2, \ldots, N\}$ and $j \in \{1, 2, \ldots, M\}$.

[9] For any number x, $\lfloor x \rfloor$ denotes the largest integer not greater than x.

$$\frac{1}{2^{2N_t-1}}\binom{2N_t}{j-1}+\left(\mathbf{Q}^T\mathbf{PQ}\right)(i,j)=\frac{1}{2^{2N_t-1}}\binom{2N_t}{(2N_t+2-j)-1} +\left(\mathbf{Q}^T\mathbf{PQ}\right)(2N_t+2-i,2N_t+2-j) \tag{118}$$

for all $i, j \in \{1, 2, \ldots, 2N_t + 1\}$. This, with (95) and (96), implies that $\mathbf{A_e}$ and $\mathbf{A_o}$ are centrosymmetric.

Let $\mathbf{v_o}$ be any odd-entries row vector of either $\mathbf{A_e}$ or $\mathbf{A_o}$. It follows from (95) and (96) that there is a value of $i \in \{1, 2,\ldots, 2N_t + 1\}$ such that the elements of $\mathbf{v_o}$ can be written as

$$\mathbf{v_o}(j)= \begin{cases} \frac{1}{2^{2N_t-1}}\binom{2N_t}{j-1}+\left(\mathbf{Q}^T\mathbf{PQ}\right)(i,j), & \text{if } j=1,3,\ldots,\text{or } 2N_t+1, \\ 0, & \text{if } j=2,4,\ldots,\text{or } 2N_t. \end{cases} \tag{119}$$

It follows from (110) that

$$\frac{1}{2^{2N_t-1}}\binom{2N_t}{N_t+1-k}=\frac{1}{2^{2N_t-1}}\binom{2N_t}{N_t+1+k} \tag{120}$$

and from (108) that

$$\left(\mathbf{Q}^T\mathbf{PQ}\right)(i,N_t+1-k)=-\left(\mathbf{Q}^T\mathbf{PQ}\right)(i,N_t+1+k) \tag{121}$$

for each $k \in \{1, 2,\ldots, N_t\}$. Therefore, it is not possible for (119) to be zero for both $j = N_t + 1 - k$ and $j = N_t + 1 + k$ for any $k \in \{1, 3,\ldots, N_t\}$ if N_t is odd or any $k \in \{2, 4,\ldots, N_t\}$ if N_t is even. As indicated by (103), $(\mathbf{Q}^T\mathbf{PQ})(i, N_t + 1) = 0$, so if N_t is even then $\mathbf{v_o}(N_t + 1)$ is nonzero. Equations (103), (105), and (121) with the theorem's stated conditions under which (99) holds imply that if N_t is odd there is a value of $k \in \{1, 3, \ldots, N_t\}$ for which (119) is nonzero for both $j = N_t + 1 - k$ and $j = N_t + 1 + k$. These results imply that $\mathbf{v_o}$ has at least $1 + N_t / 2$ nonzero elements if N_t is even and at least $1 + (N_t + 1) / 2$ nonzero elements if N_t is odd, or, equivalently, that $\mathbf{v_o}$ has at least $1 + \lfloor (N_t + 1)/2 \rfloor$ regardless of

whether N_t is even or odd. Almost identical reasoning leads to the conclusion that each even-entries row vector of either $\mathbf{A_e}$ or $\mathbf{A_o}$ has at least $1 + \lfloor N_t / 2 \rfloor$ nonzero entries.

Suppose p is even. It follows from (78), (95), and (96) that the ith element of $\mathbf{A_e t}^{(p)}$ or $\mathbf{A_o t}^{(p)}$ can be written as

$$\sum_{j=2,\, j \text{ even}}^{2N_t} (N_t + 1 - j)^p \cdot \left(\frac{1}{2^{2N_t - 1}} \binom{2N_t}{j-1} + \left(\mathbf{Q}^T \mathbf{P} \mathbf{Q}\right)(i, j) \right) \tag{122}$$

or

$$\sum_{j=1,\, j \text{ odd}}^{2N_t+1} (N_t + 1 - j)^p \cdot \left(\frac{1}{2^{2N_t - 1}} \binom{2N_t}{j-1} + \left(\mathbf{Q}^T \mathbf{P} \mathbf{Q}\right)(i, j) \right). \tag{123}$$

Given that

$$\left(N_t + 1 - j\right)^p = \left(N_t + 1 - (2N_t + 2 - j)\right)^p \tag{124}$$

for all $j \in \{1, 2, \ldots, 2N_t + 1\}$, (122) and (123) can be rewritten as

$$\begin{aligned} &\frac{1}{2^{2N_t - 1}} \sum_{j=2,\, j \text{ even}}^{2N_t} \left(N_t + 1 - j\right)^p \binom{2N_t}{j-1} \\ &\quad + \sum_{j=2,\, j \text{ even}}^{N_t} \left(N_t + 1 - j\right)^p \Big[\left(\mathbf{Q}^T \mathbf{P} \mathbf{Q}\right)(i, j) \\ &\qquad + \left(\mathbf{Q}^T \mathbf{P} \mathbf{Q}\right)(i, 2N_t + 2 - j) \Big] \end{aligned} \tag{125}$$

and

$$\begin{aligned} &\frac{1}{2^{2N_t - 1}} \sum_{j=1,\, j \text{ odd}}^{2N_t+1} \left(N_t + 1 - j\right)^p \binom{2N_t}{j-1} \\ &\quad + \sum_{j=1,\, j \text{ odd}}^{N_t} \left(N_t + 1 - j\right)^p \Big[\left(\mathbf{Q}^T \mathbf{P} \mathbf{Q}\right)(i, j) \\ &\qquad + \left(\mathbf{Q}^T \mathbf{P} \mathbf{Q}\right)(i, 2N_t + 2 - j) \Big], \end{aligned} \tag{126}$$

respectively. It follows from (108) that the second sums in (125) and (126) equal 0. Therefore, subtracting (125) from (126) yields

$$\frac{1}{2^{2N_t-1}}\sum_{j=1}^{2N_t+1}\left(N_t+1-j\right)^p(-1)^j\binom{2N_t}{j-1}. \tag{127}$$

The expression in (127) is 0 for each $p \in \{2, 4,\ldots, 2N_t - 2\}$ [16]. Thus, for each such p, (122) and (123) are equal, so there exists a value b_p such that (115) holds. ■

Theorem 4 proves that Theorem 2 cannot hold for $h_s = 4N_t - 2$, although as shown by example in the next section it can hold for $h_s = 4N_t - 3$.

Theorem 4: There do not exist $\mathbf{A_e}$ and $\mathbf{A_o}$ matrices such that Theorem 2 holds for $h_s = 4N_t - 2$.

Proof: The proof is by contradiction. Suppose Theorem 2 holds for $h_s = 4N_t - 2$. Let u be any integer and $o_d[n]$ be a parity sequence that satisfies

$$o_d[u+m]=\begin{cases}0, & \text{if } m \text{ is even,}\\ 1, & \text{if } m \text{ is odd}\end{cases} \tag{128}$$

for all positive integers m. By Lemma 5, $\mathbf{A}_{\{o_d[n]\}}[u, m]$ is either an even-entries or an odd-entries matrix for each positive integer m, so its row vectors alternate between even-entries and odd-entries vectors. For each m, let $\mathbf{v_e}[m]$ be an even-entries row vector in $\mathbf{A}_{\{o_d[n]\}}[u, m]$. It is first shown that

$$\lim_{m\to\infty}\sum_{j=2}^{4N_t}\left(\mathbf{v_e}[2m]\mathbf{S_o}-\mathbf{v_e}[2m-1]\mathbf{S_e}\right)(j)\cdot(2N_t+1-j)^q=0 \tag{129}$$

for all $q \in \{0, 1,\ldots, 4N_t - 2\}$. This is then used to prove that

$$\lim_{m\to\infty}\left(\mathbf{v_e}[2m]\mathbf{S_o}-\mathbf{v_e}[2m-1]\mathbf{S_e}\right)=\mathbf{0}_{4N_t+1}{}^T. \tag{130}$$

Finally, it is shown that

$$\lim_{m\to\infty}\left(\mathbf{v_e}[2m]\mathbf{S_o}-\mathbf{v_e}[2m-1]\mathbf{S_e}\right)\cdot\begin{pmatrix}0 & 1 & 0 & 1 & \ldots & 0\end{pmatrix}^T=1. \tag{131}$$

However, (130) implies that

$$\lim_{m\to\infty}\left(\mathbf{v_e}[2m]\mathbf{S_o}-\mathbf{v_e}[2m-1]\mathbf{S_e}\right)\cdot\begin{pmatrix}0 & 1 & 0 & 1 & \ldots & 0\end{pmatrix}^T=0, \tag{132}$$

which contradicts (131), so Theorem 2 must not hold for $h_s = 4N_t - 2$.

By assumption, $\mathbf{A_e}$ and $\mathbf{A_o}$ ensure order-q $s[n]$-convergence for each positive integer $q \leq 4N_t - 2$. With (86), this implies that, for each such q,

$$\begin{aligned}\lim_{m\to\infty} \mathbf{A}_{\{o_d[n]\}}[u, m-1]\left(\mathbf{S_e}\left(1-o_d[u+m]\right)+\mathbf{S_o}o_d[u+m]\right)\mathbf{s}^{(q)} \\ = c_q \mathbf{1}_{2N_t+1}\end{aligned} \tag{133}$$

for some constant c_q. Given (128), (133) implies that

$$\lim_{m\to\infty} \mathbf{A}_{\{o_d[n]\}}[u, 2m-1]\mathbf{S_e}\mathbf{s}^{(q)} = c_q \mathbf{1}_{2N_t+1} \text{ and} \tag{134}$$

$$\lim_{m\to\infty} \mathbf{A}_{\{o_d[n]\}}[u, 2m]\mathbf{S_o}\mathbf{s}^{(q)} = c_q \mathbf{1}_{2N_t+1}, \tag{135}$$

so

$$\lim_{m\to\infty} \mathbf{v_e}[2m-1]\mathbf{S_e}\mathbf{s}^{(q)} = c_q \text{ and} \tag{136}$$

$$\lim_{m\to\infty} \mathbf{v_e}[2m]\mathbf{S_o}\mathbf{s}^{(q)} = c_q . \tag{137}$$

Therefore, for $q \in \{1, 2, \ldots, 4N_t - 2\}$,

$$\lim_{m\to\infty} \left(\mathbf{v_e}[2m]\mathbf{S_o} - \mathbf{v_e}[2m-1]\mathbf{S_e}\right)\mathbf{s}^{(q)} = 0 , \tag{138}$$

or, equivalently,

$$\lim_{m\to\infty} \sum_{j=1}^{4N_t+1} \left(\mathbf{v_e}[2m]\mathbf{S_o} - \mathbf{v_e}[2m-1]\mathbf{S_e}\right)(j)\cdot\mathbf{s}^{(q)}(j) = 0 . \tag{139}$$

Since $\mathbf{S_e}$ and $\mathbf{S_o}$ are stochastic matrices,

$$\mathbf{S_e}\mathbf{1}_{4N_t+1} = \mathbf{S_o}\mathbf{1}_{4N_t+1} = \mathbf{1}_{2N_t+1}. \tag{140}$$

Given that $\mathbf{A}_{\{o_d[n]\}}[u, m]$ is a stochastic matrix for each m, this implies that

$$\begin{aligned}\lim_{m\to\infty} \mathbf{A}_{\{o_d[n]\}}[u, m]\mathbf{S_e}\mathbf{1}_{4N_t+1} &= \lim_{m\to\infty} \mathbf{A}_{\{o_d[n]\}}[u, m]\mathbf{S_o}\mathbf{1}_{4N_t+1} \\ &= \lim_{m\to\infty} \mathbf{A}_{\{o_d[n]\}}[u, m]\mathbf{1}_{2N_t+1} = \mathbf{1}_{2N_t+1},\end{aligned} \tag{141}$$

so (134) and (135) and, consequently, (139) also hold for $q = 0$.

Note that if $j = 1$, (87) implies that $\mathbf{S_e}(i, j) = \mathbf{S_o}(i, j) = 0$ for all i except $i = 2N_t + 1$, and if $j = 4N_t + 1$, (87) implies that $\mathbf{S_e}(i, j) = \mathbf{S_o}(i, j) = 0$ for all i except $i = 1$. Additionally,

since, for each m, $\mathbf{v_e}[m]$ is an even-entries vector, $(\mathbf{v_e}[m])(1) = (\mathbf{v_e}[m])(2N_t + 1) = 0$. Thus, for $j \in \{1, 4N_t + 1\}$ and each m,

$$\left(\mathbf{v_e}[2m]\mathbf{S_o} - \mathbf{v_e}[2m-1]\mathbf{S_e}\right)(j) = 0. \tag{142}$$

This implies that (139) can be rewritten as

$$\lim_{m\to\infty} \sum_{j=2}^{4N_t} \left(\mathbf{v_e}[2m]\mathbf{S_o} - \mathbf{v_e}[2m-1]\mathbf{S_e}\right)(j) \cdot \mathbf{s}^{(q)}(j) = 0. \tag{143}$$

This, with (85), implies that (129) holds for $q \in \{0, 1,\ldots, 4N_t - 2\}$.

Equation (129) for all $q \in \{0, 1,\ldots, 4N_t - 2\}$ can be written in matrix form as

$$\lim_{m\to\infty} \mathbf{x}[m] \cdot \mathbf{M} = \mathbf{0}_{4N_t-1}{}^T, \tag{144}$$

where $\mathbf{x}[m]$ is the length-$(4N_t - 1)$ subvector of $(\mathbf{v_e}[2m]\mathbf{S_o} - \mathbf{v_e}[2m - 1]\mathbf{S_e})$ formed by rows 2 through $4N_t$, i.e.

$$\left(\mathbf{x}[m]\right)(j) = \left(\mathbf{v_e}[2m]\mathbf{S_o} - \mathbf{v_e}[2m-1]\mathbf{S_e}\right)(j+1) \tag{145}$$

for $1 \le j \le 4N_t - 1$, and $\mathbf{M}$ is the $(4N_t - 1)\times(4N_t - 1)$ matrix

$$\begin{pmatrix} 1 & (2N_t-1)^1 & (2N_t-1)^2 & \ldots & (2N_t-1)^{4N_t-2} \\ 1 & (2N_t-2)^1 & (2N_t-2)^2 & \ldots & (2N_t-2)^{4N_t-2} \\ 1 & (2N_t-3)^1 & (2N_t-3)^2 & \ldots & (2N_t-3)^{4N_t-2} \\ \ldots & \ldots & \ldots & \ldots & \ldots \\ 1 & (-2N_t+1)^1 & (-2N_t+1)^2 & \ldots & (-2N_t+1)^{4N_t-2} \end{pmatrix}. \tag{146}$$

Matrix $\mathbf{M}$ is a square Vandermonde matrix [17]. No two elements in the second column of $\mathbf{M}$ are equal to each other, so it follows from the properties of Vandermonde matrices that the determinant of $\mathbf{M}$ is nonzero, which implies that $\mathbf{M}$ is invertible. Right multiplying both sides of (144) by the inverse of $\mathbf{M}$ yields

$$\lim_{m\to\infty} \mathbf{x}[m] = \mathbf{0}_{4N_t-1}{}^T. \tag{147}$$

Since (142) holds for $j \in \{1, 4N_t + 1\}$, (147) implies that (130) holds.

Given that $\mathbf{A_e}$ is an even-entries matrix, $\mathbf{A_e}(i, j + i - 2N_t - 1) = 0$ whenever j is even, because $i + (j + i - 2N_t - 1)$ is odd. Therefore, (87) implies that $\mathbf{S_e}(i, j) = 0$ whenever j is even. In particular, it follows that the sum of the even-indexed entries in each row of $\mathbf{S_e}$ is 0. Given that $\mathbf{A_o}$ is an odd-entries matrix, $\mathbf{A_o}(i, j + i - 2N_t - 1) = 0$ whenever j is odd, because $i + (j + i - 2N_t - 1)$ is even. Therefore, (87) implies that $\mathbf{S_o}(i, j) = 0$ whenever j is odd, so the even-indexed entries in each row of $\mathbf{S_o}$ include all of the row's non-zero entries. It follows that the sum of these entries must be unity because $\mathbf{S_o}$ is a stochastic matrix. These results imply that

$$\begin{aligned}\lim_{m\to\infty}\left(\mathbf{v_e}[2m]\mathbf{S_o} - \mathbf{v_e}[2m-1]\mathbf{S_e}\right)\cdot\begin{pmatrix}0 & 1 & 0 & 1 & \ldots & 0\end{pmatrix}^T \\ = \lim_{m\to\infty}\mathbf{v_e}[2m]\mathbf{1}_{2N_t+1}.\end{aligned} \tag{148}$$

This is equivalent to (131), because $\mathbf{v_e}[m]$ is a row vector of a stochastic matrix. ■

B. Optimal Successive Requantizers

Given any quantizer, let o_t and o_s denote the orders up to which $t[n]$ and $s[n]$, respectively, are immune to spurious tones, and let N_t denote the smallest integer for which $|t[n]| \le N_t$ over all n. The design strategy for the successive requantizer presented in this paper is to find $\mathbf{A_e}$ and $\mathbf{A_o}$ matrices that maximize the values of o_t and o_s.

The results of [14] prove that $o_t \le 2N_t - 1$ regardless of the quantizer used. Theorem 3 shows that for a successive requantizer, there exist $\mathbf{A_e}$ and $\mathbf{A_o}$ matrices that ensure $o_t = 2N_t - 1$. Thus, successive requantizers are optimal quantizers in terms of the order up to which $t[n]$ can be immune to spurious tones.

In this paper, $\mathbf{A_e}$ and $\mathbf{A_o}$ matrices for $N_t = 2$, 3, 4, and 5 are presented for which $o_t = 2N_t - 1$ and which satisfy Theorem 2 for $h_s = 4N_t - 3$, which implies that $o_s = 4N_t - 3$.

As proven by Theorem 4, $4N_t - 3$ is the maximum value of h_s for which Theorem 2 can hold. Thus, the matrices presented are optimal in the sense that o_t and h_s are as large as possible for the corresponding values of N_t.

The procedure to find the $\mathbf{A_e}$ and $\mathbf{A_o}$ matrices is to use (95)–(97) and find the elements of matrix $\mathbf{P}$ by solving the system of equations

$$\begin{aligned}\mathbf{A_e}\mathbf{S_e}\mathbf{s}^{(q)} &= \mathbf{A_e}\mathbf{S_o}\mathbf{s}^{(q)} = \mathbf{A_o}\mathbf{S_e}\mathbf{s}^{(q)} \\ &= \mathbf{A_o}\mathbf{S_o}\mathbf{s}^{(q)} = c_q\mathbf{1}_{2N_t+1},\end{aligned} \tag{149}$$

with $\mathbf{S_e}$ and $\mathbf{S_o}$ given by (87), for all even positive integers $q \leq 4N_t - 4$ and any constants $c_2, c_4, \ldots, c_{4N_t-4}$, following the constraints specified in Theorem 3. By Theorem 3, these $\mathbf{A_e}$ and $\mathbf{A_o}$ matrices guarantee that $o_t = 2N_t - 1$. As shown in the proof of Theorem 3, $\mathbf{A_e}$ and $\mathbf{A_o}$ satisfy the conditions of Lemma 3 in the appendix, so $\mathbf{A_e}$ and $\mathbf{A_o}$ ensure order-q $s[n]$-convergence for all odd q. Additionally, since the system of equations specified by (149) holds, it follows from Lemma 6 in the appendix that $\mathbf{A_e}$ and $\mathbf{A_o}$ ensure order-q $s[n]$-convergence for all even positive integers $q \leq 4N_t - 4$. Thus, $h_s = 4N_t - 3$.

For each N_t, the system of equations specified by (149) was solved using Matlab's solve() function [18]. For $N_t = 2$, the $\mathbf{A_e}$ and $\mathbf{A_o}$ matrices found are those presented in [6] and given by (83). For each $N_t = 3$, 4, and 5, $\mathbf{P}_{N_t}$, i.e., the $\mathbf{P}$ matrix from which $\mathbf{A_e}$ and $\mathbf{A_o}$ can be constructed using (95)–(97), is

$$\mathbf{P}_3 = \begin{pmatrix} \frac{1}{32} & \frac{1}{8} & \frac{1}{32} \\ \frac{1}{48} & \frac{1}{12} & \frac{5}{48} \\ \frac{3}{160} & \frac{1}{24} & \frac{5}{96} \end{pmatrix}, \tag{150}$$

$$\mathbf{P}_4 = \begin{pmatrix} \frac{1}{128} & \frac{3}{64} & \frac{63}{400} & \frac{21}{64} \\ \frac{3}{512} & \frac{9}{256} & \frac{7}{128} & -\frac{63}{640} \\ \frac{7}{3200} & \frac{1}{64} & \frac{7}{128} & \frac{1}{16} \\ \frac{3}{512} & \frac{3}{80} & \frac{1}{32} & \frac{7}{256} \end{pmatrix}, \text{ and} \tag{151}$$

$$\mathbf{P}_5 = \begin{pmatrix} \frac{1}{512} & \frac{1}{64} & \frac{355}{6083} & -\frac{3}{640} & -\frac{458}{1193} \\ \frac{1}{640} & \frac{1}{80} & \frac{51}{1000} & \frac{39}{1600} & \frac{337}{2122} \\ \frac{67}{64000} & \frac{37}{3200} & \frac{380}{7179} & \frac{177}{8053} & \frac{139}{6736} \\ \frac{3}{64000} & \frac{67}{6400} & \frac{101}{7578} & \frac{3}{80} & \frac{51}{1280} \\ -\frac{1}{512} & \frac{67}{6400} & \frac{31}{2560} & \frac{41}{1600} & \frac{104}{8781} \end{pmatrix}, \tag{152}$$

respectively.

The immunity to spurious tones achieved for each N_t suggests that o_s can be increased by increasing N_t, but this result has yet to be proven theoretically for arbitrary values of N_t.

A quantization noise sequence, $s[n]$, was generated by simulating a successive requantizer with $N_t = 3$, wherein $\mathbf{A_e}$ and $\mathbf{A_o}$ are constructed from the $\mathbf{P}_3$ matrix in (150). Fig. 10 shows estimated power spectra of $s[n]$ before and after the application of 8th and 9th order distortion, and Fig. 11 shows estimated power spectra of the running sum of the

quantization noise $t[n]$ before and after the application of 5^{th} and 6^{th} order distortion. As expected, the power spectra of $s^p[n]$ for $p = 1$, 8, and 9 and $t^p[n]$ for $p = 1$ and 5 show no visible spurious tones, as $o_s = 4N_t - 3 = 9$ and $o_t = 2N_t - 1 = 5$, while that of $t^6[n]$ shows spurious tones. Similarly, a quantization noise sequence, $s[n]$, was generated by simulating a successive requantizer with $N_t = 4$, wherein $\mathbf{A_e}$ and $\mathbf{A_o}$ are constructed from the $\mathbf{P}_4$ matrix in (151). Fig. 12 shows estimated power spectra of $s[n]$ before and after the application of 12^{th} and 13^{th} order distortion, and Fig. 13 shows estimated power spectra of the running sum of the quantization noise $t[n]$ before and after the application of 7^{th} and 8^{th} order distortion. As expected, the power spectra of $s^p[n]$ for $p = 1$, 12, and 13 and $t^p[n]$ for $p = 1$ and 7 show no visible spurious tones, as $o_s = 4N_t - 3 = 13$ and $o_t = 2N_t - 1 = 7$, while that of $t^8[n]$ shows spurious tones. Simulations of successive requantizers for which $N_t = 5$, with $\mathbf{A_e}$ and $\mathbf{A_o}$ as constructed from the $\mathbf{P}_5$ matrix in (152) can also be performed to corroborate that, for this case, $o_s = 4N_t - 3$ and $o_t = 2N_t - 1$ as well.

APPENDIX

Lemma 1: Suppose the conditions of Theorem 1 are satisfied. Then, for each $p \leq h_t$ and each set of parity sequences $\{o_d[n], d = 0, 1, \ldots, K - 1\}$, there exists a constant C_{t^p}, positive constants D_1, D_2, and a constant $0 < \alpha < 1$ such that for integers $n_1 \neq n_2$ (92) holds.

Proof: Without loss of generality, let $n_2 > n_1$. It follows from (76) that $t^p[n_1]t^p[n_2]$ can be expressed as

$$2^{-2pK}\left(\sum_{c_1=0}^{K-1}2^{c_1}t_{c_1}[n_1]\right)\left(\sum_{c_2=0}^{K-1}2^{c_2}t_{c_2}[n_1]\right)\ldots\left(\sum_{c_p=0}^{K-1}2^{c_p}t_{c_p}[n_1]\right)$$
$$\times\left(\sum_{d_1=0}^{K-1}2^{d_1}t_{d_1}[n_2]\right)\left(\sum_{d_2=0}^{K-1}2^{d_2}t_{d_2}[n_2]\right)\ldots\left(\sum_{d_p=0}^{K-1}2^{d_p}t_{d_p}[n_2]\right), \tag{153}$$

so $E\{t^p[n_1]t^p[n_2]\}$ can be written as

$$2^{-2pK}\sum_{c_1=0}^{K-1}\cdots\sum_{c_p=0}^{K-1}\sum_{d_1=0}^{K-1}\cdots\sum_{d_p=0}^{K-1}2^{c_1+\ldots+c_p+d_1+\ldots+d_p}$$
$$\times E\left\{\prod_{i=1}^{p}t_{d_i}[n_2]t_{c_i}[n_1]\right\}. \tag{154}$$

The above expression is a linear combination of terms of the form

$$Q(n_1,n_2)=E\left\{\prod_{j=0}^{K-1}t_j{}^{p_j}[n_1]t_j{}^{q_j}[n_2]\right\}, \tag{155}$$

where p_j and q_j are non-negative integers less than or equal to p for all $j \in \{0, 1,\ldots, K-1\}$. It thus suffices to establish a bound for $Q(n_1, n_2)$ of the form

$$\left|Q(n_1,n_2)-C_3\right|\le C_1\alpha^{n_2-n_1}+C_2\alpha^{n_1} \tag{156}$$

for some constant C_3 and some positive constants C_1 and C_2.

Equation (155) can be written in terms of conditional expectations as follows:

$$Q(n_1,n_2)=E\left\{\prod_{i=0}^{K-1}t_i{}^{p_i}[n_1]E\left\{\prod_{j=0}^{K-1}t_j{}^{q_j}[n_2]\,|\,t_d[n_1];\right.\right.$$
$$\left.\left.d=0,1,\ldots,K-1\right\}\right\}. \tag{157}$$

By the law of total expectation, the inner expectation in (157) can be conditioned on additional variables as long as the outer expectation in (157) is computed over all possible values of those additional variables. Thus, (157) can be rewritten as

$$Q(n_1, n_2) = E\left\{\prod_{i=0}^{K-1} t_i^{\,p_i}[n_1] E\left\{\prod_{j=0}^{K-1} t_j^{\,q_j}[n_2] \,|\, t_d[n_1], o_d[n]; \right.\right. \\ \left.\left. d = 0,1,...,K-1, n = n_1+1,...,n_2\right\}\right\}. \tag{158}$$

As proven in [6], the inner expectation in the right side of (158) equals

$$\prod_{j=0}^{K-1} E\left\{t_j^{\,q_j}[n_2] \,|\, t_j[n_1], o_j[n]; n = n_1+1,...,n_2\right\}. \tag{159}$$

Therefore, $Q(n_1, n_2)$ can be rewritten as

$$Q(n_1, n_2) = E\left\{\prod_{i=0}^{K-1} t_i^{\,p_i}[n_1] \prod_{j=0}^{K-1} E\left\{t_j^{\,q_j}[n_2] \,|\, t_j[n_1], o_j[n]; \right.\right. \\ \left.\left. n = n_1+1,...,n_2\right\}\right\}. \tag{160}$$

By the conditions of the lemma, for each $j \in \{0, 1, \ldots, K-1\}$, the vector sequence $\{\mathbf{A}_{\{o_j[n]\}}[n_1, n_2 - n_1]\,\mathbf{t}^{(q_j)}, n_2 = n_1 + 1, n_1 + 2, \ldots\}$ converges exponentially to $b_{q_j}\mathbf{1}_{2N_t+1}$ as $n_2 - n_1 \to \infty$. Thus, there exist constants $C_{q_j} \geq 0$ and $0 < \alpha < 1$ such that

$$\left|\mathbf{A}_{\{o_j[n]\}}[n_1, n_2 - n_1]\mathbf{t}^{(q_j)} - b_{q_j}\mathbf{1}_{2N_t+1}\right| \leq C_{q_j}\alpha^{n_2-n_1}\mathbf{1}_{2N_t+1}. \tag{161}$$

It follows from (77) that the ith entry of the vector $\mathbf{A}_{\{o_j[n]\}}[n_1, n_2 - n_1]\,\mathbf{t}^{(q_j)}$ can be written as

$$\sum_{k=1}^{2N_t+1} \Pr\left(t_j[n_2] = \mathbf{t}(k) \,|\, t_j[n_1] = \mathbf{t}(i), o_j[n]; \right. \\ \left. n = n_1+1,...,n_2\right) \cdot \mathbf{t}^{(q_j)}(k) \\ = E\left\{t_j^{\,q_j}[n_2] \,|\, t_j[n_1] = \mathbf{t}(i), o_j[n]; n = n_1+1,...,n_2\right\}. \tag{162}$$

This, with (161), implies that

$$\left|E\left\{t_j^{\,q_j}[n_2] \,|\, t_j[n_1], o_j[n]; n = n_1+1,...,n_2\right\} - b_{q_j}\right| \\ \leq C_{q_j}\alpha^{n_2-n_1}. \tag{163}$$

It follows that

$$\left|\prod_{j=0}^{K-1} E\left\{t_j{}^{q_j}[n_2]\,|\,t_j[n_1], o_j[n]; n = n_1+1,\ldots,n_2\right\} - \prod_{j=0}^{K-1} b_{q_j}\right| \leq C_q \alpha^{n_2-n_1} \tag{164}$$

for some positive constant C_q.

Consider the expression

$$\left|Q(n_1,n_2) - E\left\{\prod_{j=0}^{K-1} b_{q_j} \prod_{i=0}^{K-1} t_i{}^{p_i}[n_1]\right\}\right|. \tag{165}$$

Using (160), this expression can be rewritten as

$$\left|E\left\{\prod_{i=0}^{K-1} t_i{}^{p_i}[n_1]\left(\prod_{j=0}^{K-1} E\left\{t_j{}^{q_j}[n_2]\,|\,t_j[n_1], o_j[n]; n = n_1+1,\ldots,n_2\right\} - \prod_{j=0}^{K-1} b_{q_j}\right)\right\}\right|. \tag{166}$$

Given that, for any random variable x, $|E\{x\}| \leq E\{|x|\}$, the expression in (166) is less than or equal to

$$E\left\{\prod_{i=0}^{K-1}\left|t_i{}^{p_i}[n_1]\right| \cdot \left|\prod_{j=0}^{K-1} E\left\{t_j{}^{q_j}[n_2]\,|\,t_j[n_1], o_j[n]; n = n_1+1,\ldots,n_2\right\} - \prod_{j=0}^{K-1} b_{q_j}\right|\right\}. \tag{167}$$

Since the magnitude of each $t_i[n]$ sequence is bounded by N_t and each p_i is less than or equal to p, the expression in (167) is itself less than or equal to

$$
\begin{aligned}
& N_t^{pK} E\left\{\left|\prod_{j=0}^{K-1} E\left\{t_j^{q_j}[n_2] \mid t_j[n_1], o_j[n];\right.\right.\right. \\
& \qquad \left.\left.\left. n = n_1+1, \ldots, n_2\right\} - \prod_{j=0}^{K-1} b_{q_j}\right|\right\} \\
& \le N_t^{pK} \max_{t_j[n_1]} \left\{\left|\prod_{j=0}^{K-1} E\left\{t_j^{q_j}[n_2] \mid t_j[n_1], o_j[n];\right.\right.\right. \\
& \qquad \left.\left.\left. n = n_1+1, \ldots, n_2\right\} - \prod_{j=0}^{K-1} b_{q_j}\right|\right\}.
\end{aligned} \tag{168}
$$

With (164), (165)–(168) imply that

$$
\left| Q(n_1, n_2) - E\left\{\prod_{j=0}^{K-1} b_{q_j} \prod_{i=0}^{K-1} t_i^{p_i}[n_1]\right\}\right| \le C_1 \alpha^{n_2 - n_1} \tag{169}
$$

for some constant $C_1 \ge 0$. By similar reasoning, it can be established that

$$
\left| E\left\{\prod_{j=0}^{K-1} b_{q_j} \prod_{i=0}^{K-1} t_i^{p_i}[n_1]\right\} - \prod_{j=0}^{K-1} b_{q_j} \prod_{i=0}^{K-1} b_{p_i}\right| \le C_2 \alpha^{n_1} \tag{170}
$$

for some constant $C_2 \ge 0$. Using the triangle inequality,

$$
\begin{aligned}
& \left| Q(n_1, n_2) - \prod_{j=0}^{K-1} b_{q_j} \prod_{i=0}^{K-1} b_{p_i}\right| \\
& \quad \le \left| Q(n_1, n_2) - E\left\{\prod_{j=0}^{K-1} b_{q_j} \prod_{i=0}^{K-1} t_i^{p_i}[n_1]\right\}\right| \\
& \quad + \left| E\left\{\prod_{j=0}^{K-1} b_{q_j} \prod_{i=0}^{K-1} t_i^{p_i}[n_1]\right\} - \prod_{j=0}^{K-1} b_{q_j} \prod_{i=0}^{K-1} b_{p_i}\right|.
\end{aligned} \tag{171}
$$

Therefore, it follows from (169)–(171) that (156) holds. ■

Lemma 2: Suppose the conditions of Theorem 2 are satisfied. Then, for each $q \le h_s$ and each set of parity sequences $\{o_d[n], d = 0, 1, \ldots, K-1\}$, there exists a constant C_{s^q}

, positive constants E_1, E_2, and a constant $0 < \beta < 1$ such that for integers $n_1 \neq n_2$ (94) holds.

The proof is identical to that of Lemma 1 except with $s[n]$, c_{q_j}, and $\mathbf{S}_{\{o_d[n]\}}[n_1, n_2 - n_1]$ playing the roles of $t[n]$, b_{q_j}, and $\mathbf{A}_{\{o_d[n]\}}[n_1, n_2 - n_1]$, respectively. ■

Lemma 3: Suppose that $\mathbf{A_e}$ and $\mathbf{A_o}$ are centrosymmetric, that all their odd-entries row vectors contain at least $1 + \lfloor (N_t + 1)/2 \rfloor$ nonzero entries, and that all their even-entries row vectors contain at least $1 + \lfloor N_t/2 \rfloor$ nonzero entries. Then, $\mathbf{A_e}$ and $\mathbf{A_o}$ ensure order-p $t[n]$-convergence and order-q $s[n]$-convergence for all odd positive integers p and q.

Proof: Let $o_d[n]$ be any parity sequence, u be any integer, and p and q be any odd integers. It is first shown that $\mathbf{A_e}$ and $\mathbf{A_o}$ ensure order-p $t[n]$-convergence.

It follows from (78) that the elements of $\mathbf{t}^{(p)}$ satisfy

$$\mathbf{t}^{(p)}(j) = -\mathbf{t}^{(p)}(2N_t + 2 - j). \tag{172}$$

For any integers m_1 and $m_2 > 0$, (79) implies that $\mathbf{A}_{\{o_d[n]\}}[m_1, m_2]$ is either a one-step state transition matrix or can be expanded as a product of such matrices. Since each such matrix equals $\mathbf{A_e}$ or $\mathbf{A_o}$, the conditions of the lemma imply that $\mathbf{A}_{\{o_d[n]\}}[m_1, m_2]$ is centrosymmetric or can be expanded as a product of centrosymmetric matrices. Therefore, by the properties of centrosymmetric matrices, $\mathbf{A}_{\{o_d[n]\}}[m_1, m_2]$ is centrosymmetric [19]. This, together with (172), implies that the elements of $\mathbf{A}_{\{o_d[n]\}}[m_1, m_2]\mathbf{t}^{(p)}$ satisfy

$$\begin{aligned}\left(\mathbf{A}_{\{o_d[n]\}}[m_1,m_2]\mathbf{t}^{(p)}\right)(i) &= \sum_{j=1}^{2N_t+1}\left(\mathbf{A}_{\{o_d[n]\}}[m_1,m_2]\right)(i,j)\mathbf{t}^{(p)}(j) = \\ -\sum_{j=1}^{2N_t+1}&\left(\mathbf{A}_{\{o_d[n]\}}[m_1,m_2]\right)(2N_t+2-i,2N_t+2-j)\mathbf{t}^{(p)}(2N_t+2-j),\end{aligned} \tag{173}$$

where the last expression can be rewritten as

$$-\sum_{j=1}^{2N_t+1}\left(\mathbf{A}_{\{o_d[n]\}}[m_1,m_2]\right)(2N_t+2-i,j)\cdot\mathbf{t}^{(p)}(j)\,. \tag{174}$$

Thus, the elements of $\mathbf{A}_{\{o_d[n]\}}[m_1, m_2]\mathbf{t}^{(p)}$ satisfy

$$\begin{aligned}&\left(\mathbf{A}_{\{o_d[n]\}}[m_1,m_2]\mathbf{t}^{(p)}\right)(i) \\ &\quad=-\left(\mathbf{A}_{\{o_d[n]\}}[m_1,m_2]\mathbf{t}^{(p)}\right)(2N_t+2-i).\end{aligned} \tag{175}$$

Let m be any integer greater than 1. Given (79), $\mathbf{A}_{\{o_d[n]\}}[u, m]\mathbf{t}^{(p)}$ can be written as

$$\mathbf{A}_{\{o_d[n]\}}[u,1]\mathbf{A}_{\{o_d[n]\}}[u+1,m-1]\mathbf{t}^{(p)}. \tag{176}$$

Therefore, the ith element of $\mathbf{A}_{\{o_d[n]\}}[u, m]\mathbf{t}^{(p)}$ equals

$$\begin{aligned}&\left(\mathbf{A}_{\{o_d[n]\}}[u,m]\mathbf{t}^{(p)}\right)(i) = \\ &\sum_{j=1}^{2N_t+1}\left(\mathbf{A}_{\{o_d[n]\}}[u,1]\right)(i,j)\cdot\left(\mathbf{A}_{\{o_d[n]\}}[u+1,m-1]\mathbf{t}^{(p)}\right)(j).\end{aligned} \tag{177}$$

Let $(A_{i,1}, A_{i,2},\ldots, A_{i,2N_t+1})$ be a permutation of

$$\left(\left(\mathbf{A}_{o_d[n]}[u,1]\right)(i,j),\ j=1,2,...,2N_t+1\right) \tag{178}$$

which satisfies

$$A_{i,1}\geq A_{i,2}\geq\ldots\geq A_{i,2N_t+1} \tag{179}$$

and $(t_1, t_2,\ldots, t_{2N_t+1})$ a permutation of

$$\left(\left(\mathbf{A}_{o_d[n]}[u+1,m-1]\mathbf{t}^{(p)}\right)(j),\ j=1,2,...,2N_t+1\right) \tag{180}$$

which satisfies

$$t_1 \geq t_2 \geq \ldots \geq t_{2N_t+1}. \tag{181}$$

Then, it follows from (177) and from the rearrangement inequality that

$$\left(\mathbf{A}_{\{o_d[n]\}}[u,m]\mathbf{t}^{(p)}\right)(i) \leq \sum_{j=1}^{2N_t+1} A_{i,j}t_j \,. \tag{182}$$

Given (175) and that the elements of $\mathbf{A}_{\{o_d[n]\}}[u, 1]$ are all nonnegative, $A_{i,j}t_j \leq 0$ for $j \in \{N_t + 1, N_t + 2, \ldots, 2N_t + 1\}$. Thus, (182) implies that

$$\left(\mathbf{A}_{\{o_d[n]\}}[u,m]\mathbf{t}^{(p)}\right)(i) \leq \sum_{j=1}^{N_t} A_{i,j}t_j \leq t_1 \sum_{j=1}^{N_t} A_{i,j} \,. \tag{183}$$

It is now shown that

$$\sum_{j=1}^{N_t} A_{i,j} < \sum_{j=1}^{2N_t+1} A_{i,j} = 1. \tag{184}$$

Since $\mathbf{A}_{\{o_d[n]\}}[u, 1]$ is stochastic, all of its elements are nonnegative, and the sum of the elements in each of its rows is 1. Additionally, since it equals either $\mathbf{A_e}$ or $\mathbf{A_o}$, $\mathbf{A}_{\{o_d[n]\}}[u, 1]$ is either an even-entries or an odd-entries matrix, so its row vectors alternate between even-entries and odd-entries vectors. Suppose N_t is even. If the ith row of $\mathbf{A}_{\{o_d[n]\}}[u, 1]$ is an even-entries row then $A_{i,j} = 0$ for $j \in \{1, 3, \ldots, 2N_t + 1\}$. By the conditions of the lemma, $A_{i,j}$ is nonzero for at least $1 + N_t / 2$ values of $j \in \{2, 4, \ldots, N_t, N_t + 2, \ldots, 2N_t\}$, so it is nonzero for at least 1 value of $j \in \{N_t + 2, N_t + 4, \ldots, 2N_t\}$, which implies that (184) holds. Similarly, if the ith row of $\mathbf{A}_{\{o_d[n]\}}[u, 1]$ is an odd-entries row then $A_{i,j} = 0$ for $j \in \{2, 4, \ldots, 2N_t\}$. By the conditions of the lemma, $A_{i,j}$ is nonzero for at least $1 + N_t / 2$ values of $j \in \{1, 3, \ldots, N_t - 1, N_t + 1, \ldots, 2N_t + 1\}$, so it is nonzero for at least one value of $j \in \{N_t + 1, N_t +$

3,…, $2N_t + 1\}$, which implies that (184) holds. Now suppose N_t is odd. If the ith row of $\mathbf{A}_{\{o_d[n]\}}[u, 1]$ is an even-entries row then $A_{i,j} = 0$ for $j \in \{1, 3,\ldots, 2N_t + 1\}$. By the conditions of the lemma, $A_{i,j}$ is nonzero for at least $1 + (N_t - 1) / 2$ values of $j \in \{2, 4,\ldots, N_t - 1, N_t + 1,\ldots, 2N_t\}$, so it is nonzero for at least 1 value of $j \in \{N_t + 1, N_t + 3,\ldots, 2N_t\}$, which implies that (184) holds. Similarly, if the ith row of $\mathbf{A}_{\{o_d[n]\}}[u, 1]$ is an odd-entries row then $A_{i,j} = 0$ for $j \in \{2, 4,\ldots, 2N_t\}$. By the conditions of the lemma, $A_{i,j}$ is nonzero for at least $1 + (N_t + 1) / 2$ values of $j \in \{1, 3,\ldots, N_t, N_t + 2,\ldots, 2N_t + 1\}$, so it is nonzero for at least 1 value of $j \in \{N_t + 2, N_t + 4,\ldots, 2N_t + 1\}$, which implies that (184) holds.

It follows from (183) and (184) that

$$\begin{aligned}&\max_i \left\{\left(\mathbf{A}_{\{o_d[n]\}}[u, m]\mathbf{t}^{(p)}\right)(i)\right\}\\ &\quad \le (1-\beta)\max_i \left\{\left(\mathbf{A}_{\{o_d[n]\}}[u+1, m-1]\mathbf{t}^{(p)}\right)(i)\right\},\end{aligned} \tag{185}$$

where β is the smallest nonzero element of $\mathbf{A_e}$ and $\mathbf{A_o}$, i.e.

$$\beta = \min\left\{\min_{i,j}\{\mathbf{A_e}(i, j) \ne 0\}, \min_{i,j}\{\mathbf{A_o}(i, j) \ne 0\}\right\}. \tag{186}$$

Since (185) holds for any integers u and $m > 1$, it follows that, for $m > 2$,

$$\begin{aligned}&\max_i \left\{\left(\mathbf{A}_{\{o_d[n]\}}[u, m]\mathbf{t}^{(p)}\right)(i)\right\}\\ &\quad \le (1-\beta)^2 \max_i \left\{\left(\mathbf{A}_{\{o_d[n]\}}[u+2, m-2]\mathbf{t}^{(p)}\right)(i)\right\} \le \ldots\\ &\quad \le (1-\beta)^{m-1} \max_i \left\{\left(\mathbf{A}_{\{o_d[n]\}}[u+m-1, 1]\mathbf{t}^{(p)}\right)(i)\right\}\\ &\quad \le (1-\beta)^{m-1} \max_i \left\{\mathbf{t}^{(p)}(i)\right\},\end{aligned} \tag{187}$$

where the last inequality holds because $\mathbf{A}_{\{o_d[n]\}}[u + m - 1, 1]$ is stochastic, so all of its elements are nonnegative and the sum of the elements in each of its rows is 1. Thus,

$$\lim_{m\to\infty}\left[\max_i \left\{\left(\mathbf{A}_{\{o_d[n]\}}[u, m]\mathbf{t}^{(p)}\right)(i)\right\}\right] = 0 \tag{188}$$

with exponential convergence.

Note now that (175) implies that

$$\begin{aligned}&\min_i\left\{\left(\mathbf{A}_{\{o_d[n]\}}[u,m]\mathbf{t}^{(p)}\right)(i)\right\}\\&\quad=-\max_i\left\{\left(\mathbf{A}_{\{o_d[n]\}}[u,m]\mathbf{t}^{(p)}\right)(i)\right\}\end{aligned}\tag{189}$$

for each m, so

$$\lim_{m\to\infty}\left[\min_i\left\{\left(\mathbf{A}_{\{o_d[n]\}}[u,m]\mathbf{t}^{(p)}\right)(i)\right\}\right]=0\tag{190}$$

with exponential convergence as well. Hence, (188), (190), and the squeeze theorem from calculus imply that $\mathbf{A_e}$ and $\mathbf{A_o}$ ensure order-p $t[n]$-convergence.

The proof that $\mathbf{A_e}$ and $\mathbf{A_o}$ ensure order-q $s[n]$-convergence is similar. It follows from (85) that the elements of $\mathbf{s}^{(q)}$ satisfy

$$\mathbf{s}^{(q)}(j)=-\mathbf{s}^{(q)}(4N_t+2-j)\,.\tag{191}$$

Given that $\mathbf{A_e}$ and $\mathbf{A_o}$ are centrosymmetric, (87) implies that $\mathbf{S_e}$ and $\mathbf{S_o}$ are also centrosymmetric. For any integers m_1 and $m_2 > 0$, (79), (86), and the conditions of the lemma imply that $\mathbf{S}_{\{o_d[n]\}}[m_1, m_2]$ is centrosymmetric or can be expanded as a product of centrosymmetric matrices. Therefore, $\mathbf{S}_{\{o_d[n]\}}[m_1, m_2]$ is centrosymmetric. This, together with (191), implies that the elements of $\mathbf{S}_{\{o_d[n]\}}[m_1, m_2]\mathbf{s}^{(q)}$ satisfy

$$\begin{aligned}&\left(\mathbf{S}_{\{o_d[n]\}}[m_1,m_2]\mathbf{s}^{(q)}\right)(i)\\&\quad=-\left(\mathbf{S}_{\{o_d[n]\}}[m_1,m_2]\mathbf{s}^{(q)}\right)(2N_t+2-i).\end{aligned}\tag{192}$$

The rest of the proof follows from reasoning similar to that presented above from (175) to (190). ■

Lemma 4: Let

$$\mathbf{A_e t}^{(p)} = \mathbf{A_o t}^{(p)} = b_p \mathbf{1}_{2N_t+1} \tag{193}$$

for some integer p and some constant b_p. Then, $\mathbf{A_e}$ and $\mathbf{A_o}$ ensure order-p $t[n]$-convergence.

Proof: Let $o_d[n]$ be any parity sequence and u be any integer. It follows from (79) that for each integer $m > 1$ $\mathbf{A}_{\{o_d[n]\}}[u, m]$ can be written as

$$\mathbf{A}_{\{o_d[n]\}}[u,m] = \mathbf{A}_{\{o_d[n]\}}[u,m-1]\mathbf{A}_{\{o_d[n]\}}[u+m-1,1]. \tag{194}$$

Since $\mathbf{A}_{\{o_d[n]\}}[u + m - 1, 1]$ equals either $\mathbf{A_e}$ or $\mathbf{A_o}$, (193) and (194) imply that

$$\mathbf{A}_{\{o_d[n]\}}[u,m]\mathbf{t}^{(p)} = b_p \mathbf{A}_{\{o_d[n]\}}[u,m-1]\mathbf{1}_{2N_t+1}. \tag{195}$$

Additionally, $\mathbf{A}_{\{o_d[n]\}}[u, m - 1]$ is stochastic, so

$$\mathbf{A}_{\{o_d[n]\}}[u,m-1]\mathbf{1}_{2N_t+1} = \mathbf{1}_{2N_t+1}. \tag{196}$$

Therefore,

$$\mathbf{A}_{\{o_d[n]\}}[u,m]\mathbf{t}^{(p)} = b_p \mathbf{1}_{2N_t+1}, \tag{197}$$

so for each integer $m \geq 1$

$$\left|\mathbf{A}_{\{o_d[n]\}}[u,m]\mathbf{t}^{(p)} - b_p \mathbf{1}_{2N_t+1}\right| \leq \mathbf{0}_{2N_t+1}, \tag{198}$$

which proves the lemma. ■

Lemma 5: Given any parity sequence $o_d[n]$ and any integers u and $m > 0$, $\mathbf{A}_{\{o_d[n]\}}[u, m]$ is either an even-entries or an odd-entries matrix.

Proof: It follows from (80) that

$$\begin{aligned}\sum_{k=u+1}^{u+m} s_d[k] &= \sum_{k=u+1}^{u+m} \left(t_d[k] - t_d[k-1]\right) \\ &= t_d[u+m] - t_d[u].\end{aligned} \tag{199}$$

Since $s_d[n]$ and $o_d[n]$ have the same parity at each n, the parity of each $s_d[k]$, for $k = u + 1, u + 2, \ldots, u + m$, is fixed, i.e., each $s_d[k]$ is either even or odd. Therefore, the parity of the sum in the left side of (199) is also fixed. If the sum is even, (199) implies that the

probability that $t_d[u + m]$ and $t_d[u]$ have different parities is zero. Similarly, if it is odd, the probability that $t_d[u + m]$ and $t_d[u]$ have the same parity is zero. Therefore, (77) implies that $\mathbf{A}_{\{o_d[n]\}}[u, m]$ is either an even-entries or an odd-entries matrix. ■

Lemma 6: Let (149) hold for some integer q and some constant c_q. Then, $\mathbf{A_e}$ and $\mathbf{A_o}$ ensure order-q $s[n]$-convergence.

Proof: Let $o_d[n]$ be any parity sequence and u be any integer. It follows from (79) and (86) that for each integer $m > 2$ $\mathbf{S}_{\{o_d[n]\}}[u, m]$ can be written as

$$\mathbf{A}_{\{o_d[n]\}}[u, m-2]\mathbf{A}_{\{o_d[n]\}}[u+m-2, 1]\mathbf{S}_{\{o_d[n]\}}[u+m-1, 1]. \quad (200)$$

The rest of the proof is almost identical to the proof of Lemma 4, with $\mathbf{A}_{\{o_d[n]\}}[u + m – 2, 1]\mathbf{S}_{\{o_d[n]\}}[u + m – 1, 1]$, $\mathbf{s}^{(q)}$, and c_q playing the roles of $\mathbf{A}_{\{o_d[n]\}}[u + m – 1, 1]$, $\mathbf{t}^{(p)}$, and b_p, respectively. ■

ACKNOWLEDGEMENTS

The authors would like to acknowledge Guglielmo Lockhart for helpful discussions relating to this work.

Chapter 2, in full, has been published in the IEEE Transactions on Signal Processing, volume 61, number 17, pages 4270-4283, September 2013. E. Familier, C. Venerus, I. Galton, 2013. The dissertation author is the primary investigator and author of this paper. Professor Ian Galton supervised the research which forms the basis for this paper.

FIGURES

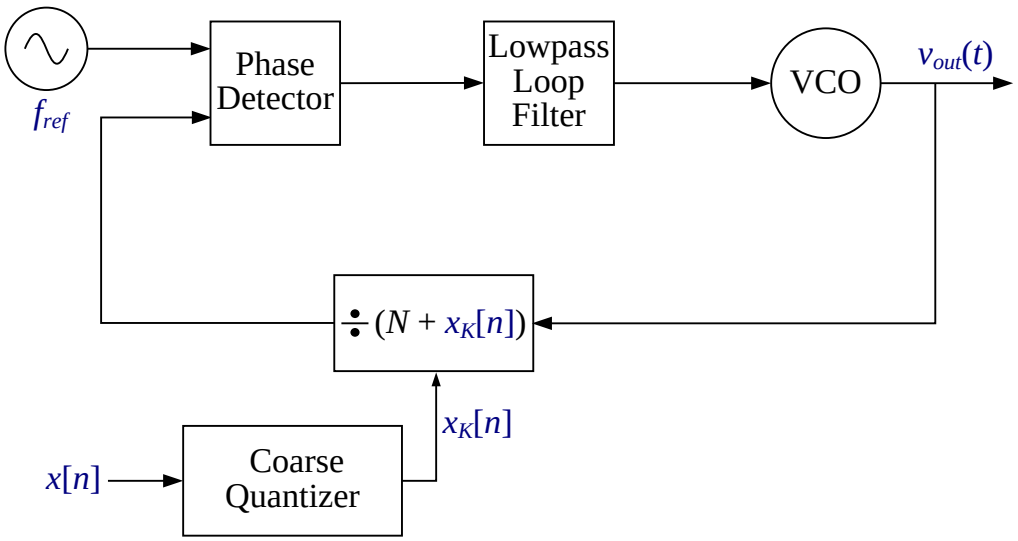

Figure 6: Block diagram of a fractional-*N* PLL.

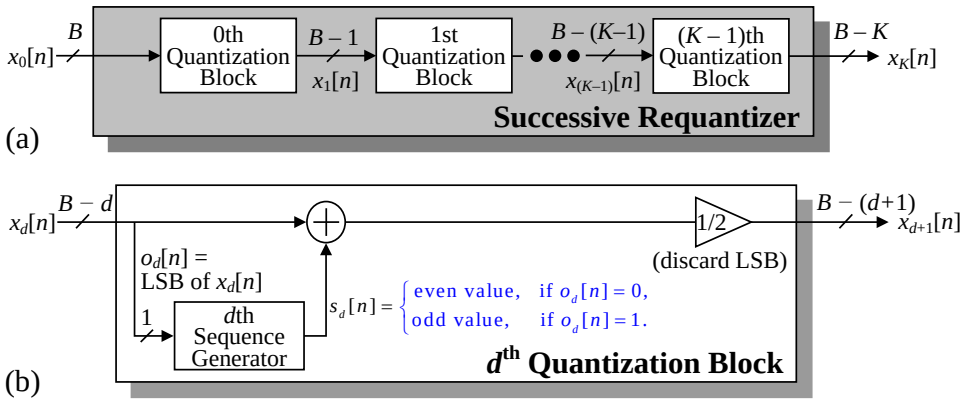

Figure 7: High-level block diagram of a successive requantizer.

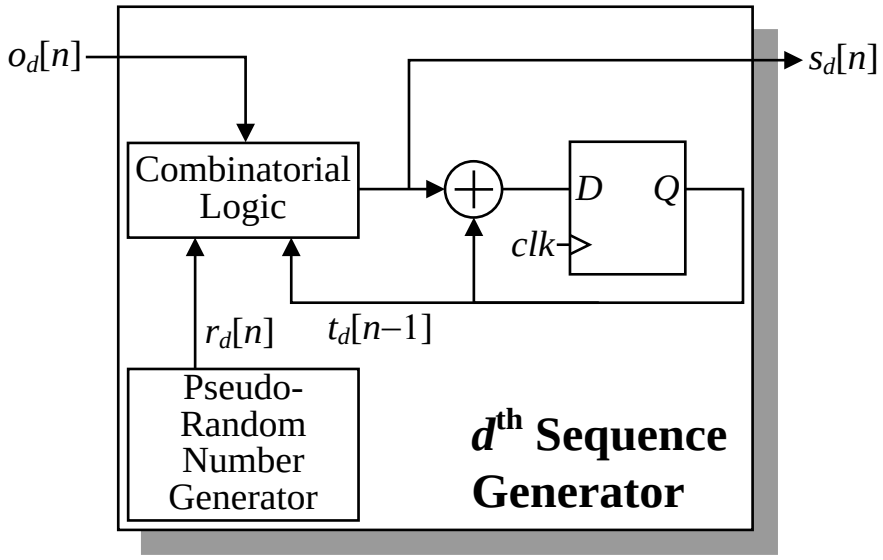

Figure 8: Block diagram of a sequence generator.

Combinatorial Logic Truth Tables:

Case $N_t = 1$, $r_d[n]$ in {–1, 0}

$o_d[n] = 0$		
$t_d[n-1]$	$r_d[n]$	$s_d[n]$
1	−1 or 0	0
0	−1 or 0	0
−1	−1 or 0	0

$o_d[n] = 1$		
$t_d[n-1]$	$r_d[n]$	$s_d[n]$
1	−1 or 0	−1
0	−1	−1
0	0	1
−1	−1 or 0	1

(a)

Case $N_t = 2$, $r_d[n]$ in {–8, –7,…, 7}

$o_d[n] = 0$		
$t_d[n-1]$	$r_d[n]$	$s_d[n]$
2	≥ 0 and ≤ 3	0
2	≤ −1 or ≥ 4	−2
1	≤ −1 or ≥ 6	0
1	≥ 0 and ≤ 5	−2
0	0 or 1	2
0	≤ −1 or ≥ 4	0
0	2 or 3	−2
−1	≤ −1 or ≥ 6	0
−1	≥ 0 and ≤ 5	2
−2	≥ 0 and ≤ 3	0
−2	≤ −1 or ≥ 4	2

$o_d[n] = 1$		
$t_d[n-1]$	$r_d[n]$	$s_d[n]$
2	≤ −1 or ≥ 4	−1
2	≥ 0 and ≤ 3	−3
1	≥ 1 and ≤ 3	1
1	≤ −1 or ≥ 4	−1
1	0	−3
0	≥ 0	1
0	≤ −1	−1
−1	≥ 1 and ≤ 3	−1
−1	≤ −1 or ≥ 4	1
−1	0	3
−2	≤ −1 or ≥ 4	1
−2	≥ 0 and ≤ 3	3

(b)

Figure 9: Example combinatorial logic truth tables of sequence generators corresponding to the one-step state transition matrices in (a) equation (82) and (b) equation (83). In both cases, $r_d[n]$ is a sequence of independent and identically distributed random variables which follow a uniform distribution.

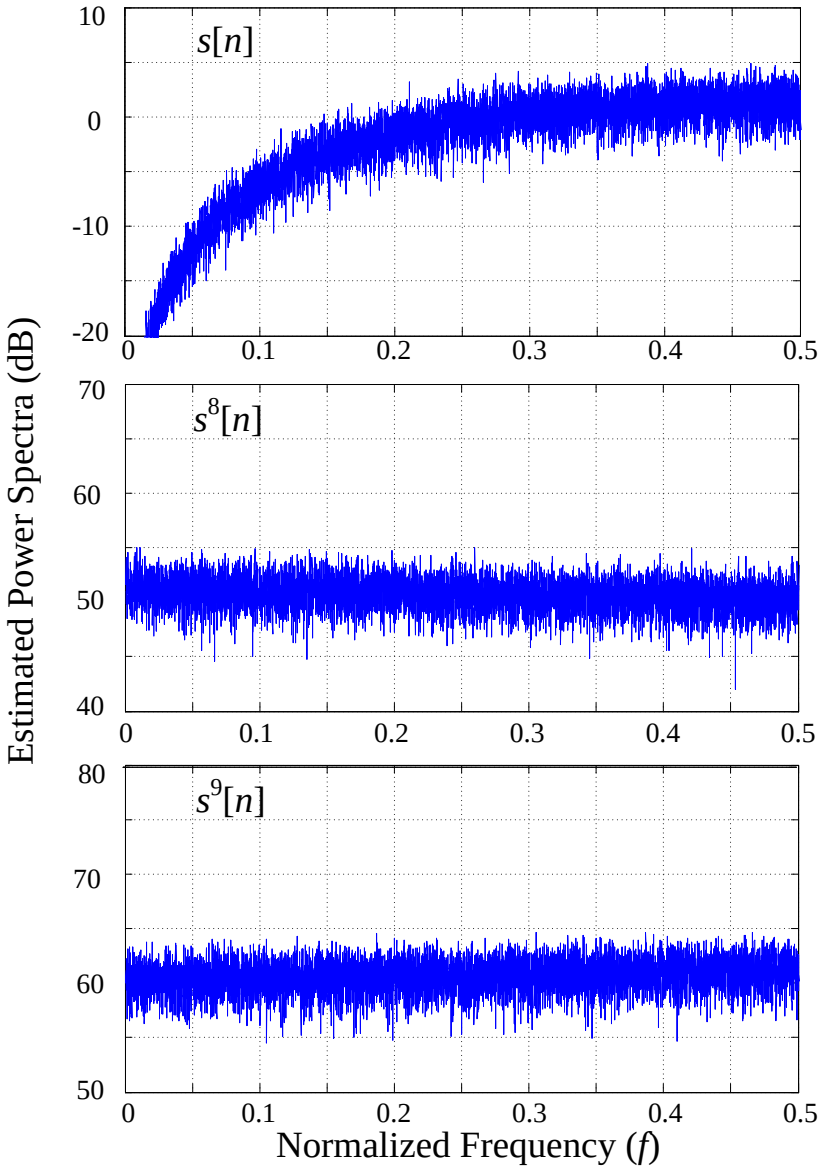

Figure 10: Estimated power spectra of the quantization noise of a simulated successive requantizer for which $N_t = 3$ before and after the application of 8th and 9th order nonlinear distortion.

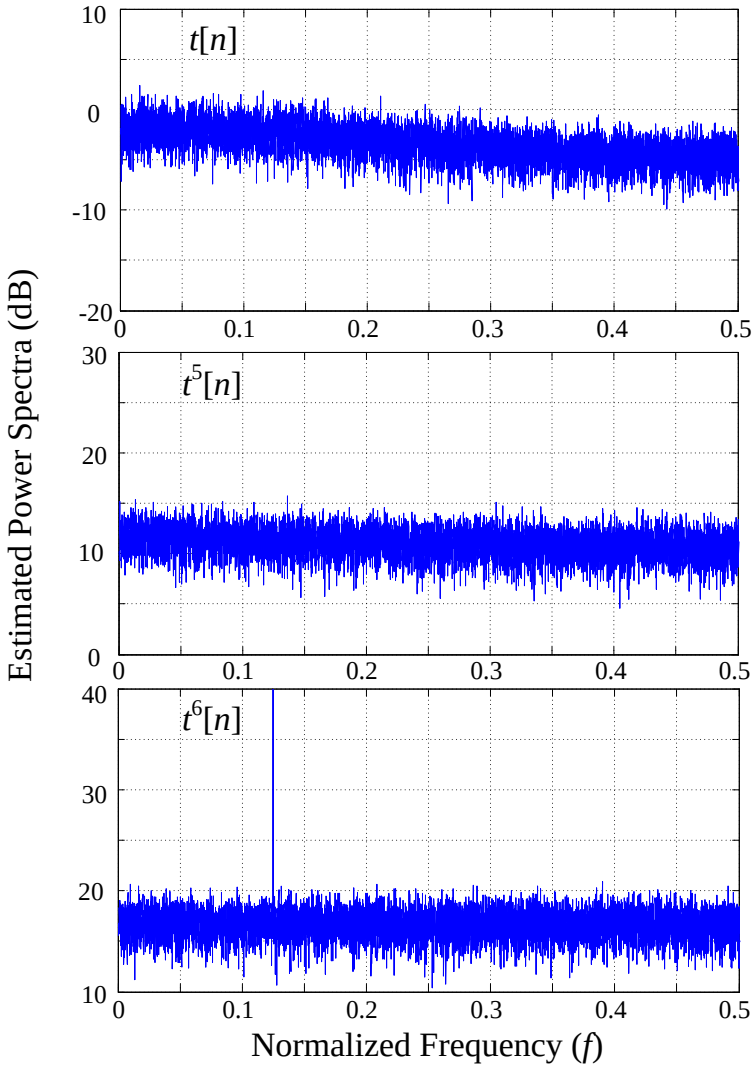

Figure 11: Estimated power spectra of the running sum of the quantization noise of a simulated successive requantizer for which $N_t = 3$ before and after the application of 5th and 6th order nonlinear distortion.

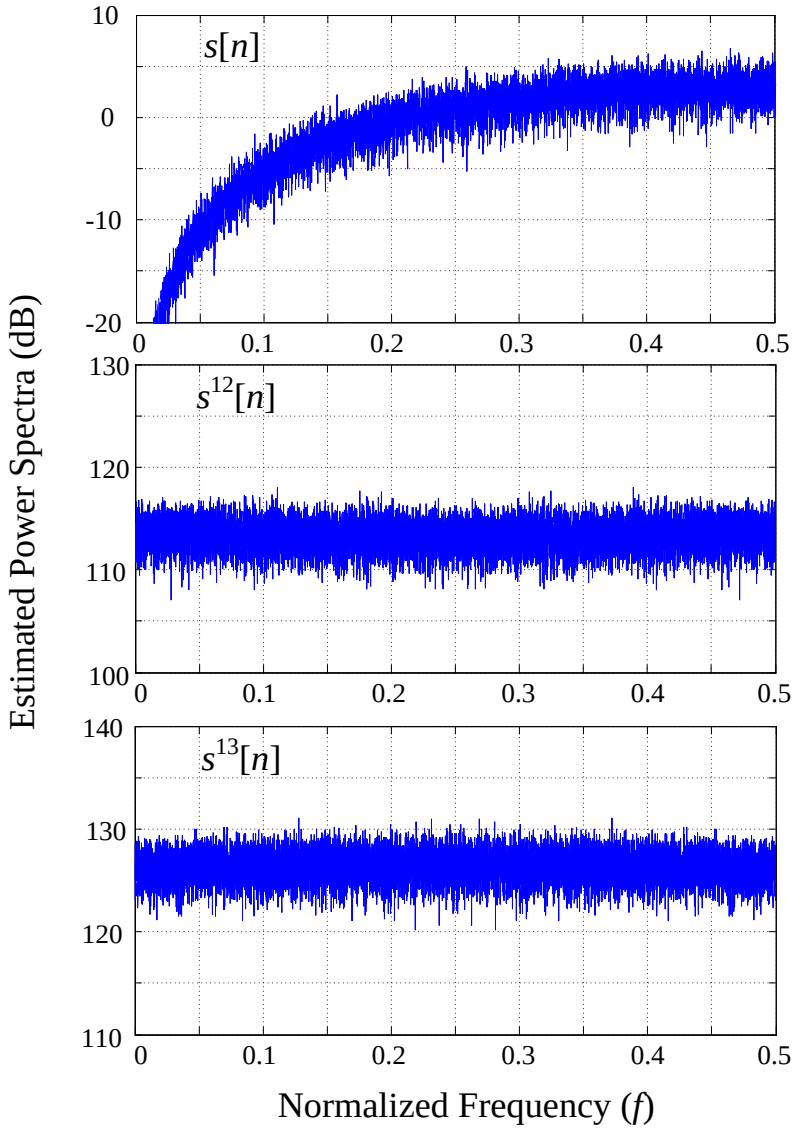

Figure 12: Estimated power spectra of the quantization noise of a simulated successive requantizer for which N_t = 4 before and after the application of 12th and 13th order nonlinear distortion.

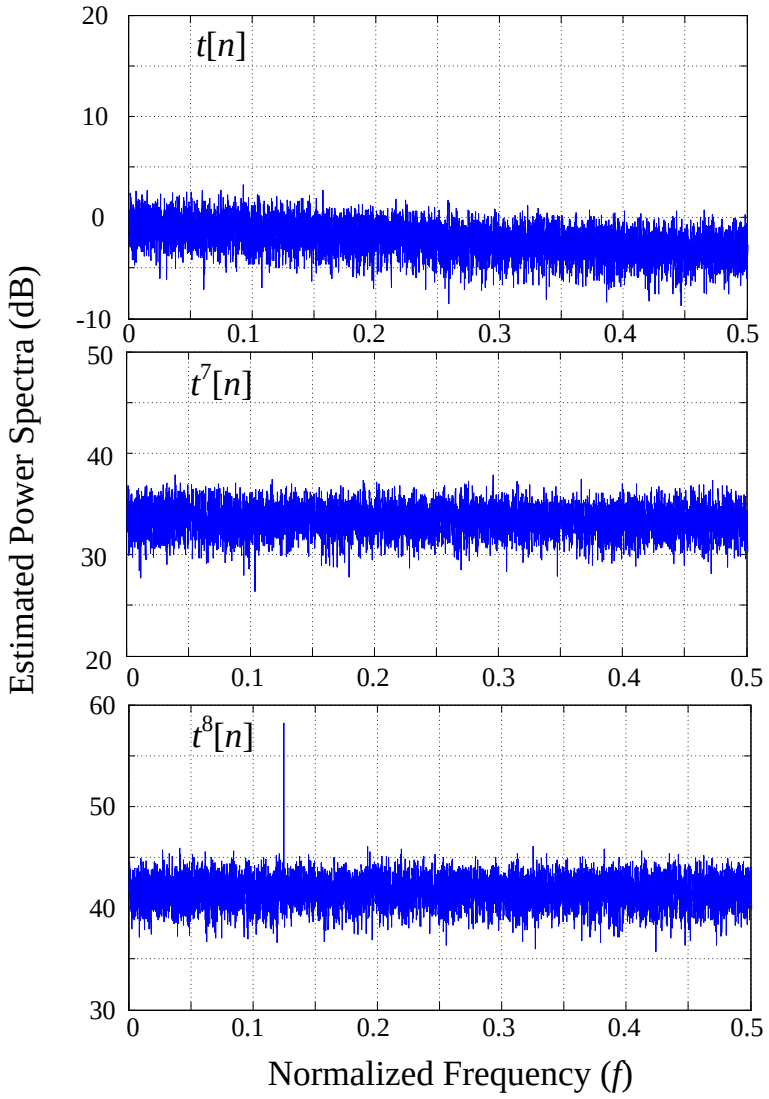

Figure 13: Estimated power spectra of the running sum of the quantization noise of a simulated successive requantizer for which $N_t = 4$ before and after the application of 7th and 8th order nonlinear distortion.

REFERENCES

1. B. Razavi, Phase-Locking in High-Performance Systems: From Devices to Architectures, Wiley-Interscience, 2003.

2. T. H. Lee, *The Design of CMOS Radio-Frequency Integrated Circuits*, Second Edition, Cambridge University Press, 2003.

3. B. Miller, B. Conley, "A Multiple Modulator Fractional Divider," *Annual IEEE Symposium on Frequency Control*, vol. 44, pp. 559-568, March 1990.

4. B. Miller, B. Conley, "A Multiple Modulator Fractional Divider," *IEEE Transactions on Instrumentation and Measurement*, vol. 40, no. 3, pp. 578-583, June 1991.

5. T. A. Riley, M. A. Copeland, T. A. Kwasniewski, "Delta-Sigma Modulation in Fractional-N Frequency Synthesis," *IEEE Journal of Solid-State Circuits*, vol. 28, no. 5, pp. 553-559, May 1993.

6. B. De Muer, M. Steyaert, "A CMOS Monolithic ΔΣ-Controlled Fractional-N Frequency Synthesizer for DCS-1800," *IEEE Journal of Solid-State Circuits*, vol. 37, no. 7, July 2002.

7. S. Pamarti, L. Jansson, I. Galton, "A Wideband 2.4GHz ΔΣ Fractional-N PLL with 1 Mb/s In-Loop Modulation," *IEEE Journal of Solid-State Circuits*, vol. 39, no. 1, pp. 49-62, January 2004.

8. A. Swaminathan, A. Panigada, E. Masry, I. Galton, "A Digital Requantizer with Shaped Requantization Noise that Remains Well Behaved after Nonlinear Distortion," *IEEE Transactions on Signal Processing*, vol. 55, no. 11, pp. 5382-5394, November 2007.

9. K. J. Wang, A. Swaminathan, I. Galton, "Spurious Tone Suppression Techniques Applied to a Wide-Bandwidth 2.4 GHz Fractional-*N* PLL," *IEEE Journal of Solid-State Circuits*, vol. 43, issue 12, pp. 2787-2797, December 2008.

10. H. Jian, Z. Xu, Y. Wu, F. Chang, "A Compact 0.8-6GHz Fractional-N PLL with Binary-Weighted D/A Differentiator and Offset-Frequency Δ–Σ Modulator for Noise and Spurs Cancellation," *2009 Symposium on VLSI Circuits*, pp. 186-187, 16-18 June 2009.

11. P. Su, S. Pamarti, "Mismatch Shaping Techniques to Linearize Charge Pump Errors in Fractional-N PLLs," *IEEE Transactions on Circuits and Systems–I: Regular Papers*, vol. 57, no. 6, June 2010.

12. K. Hosseini, B. Fitzgibbon, M.P. Kennedy, "Observations Concerning the Generation of Spurious Tones in Digital Delta-Sigma Modulators Followed by a Memoryless Nonlinearity," *IEEE Transactions on Circuits and Systems–II: Express Briefs*, vol. 58, no. 11, November 2011.

13. A. V. Oppenheim, R. W. Schafer, J. R. Buck, *Discrete-Time Signal Processing*, Second Edition, Englewood Cliffs, NJ: Prentice-Hall, 1999.

14. E. Familier, I. Galton, "A Fundamental Limitation on DC-Free Quantization Noise with respect to Nonlinearity-Induced Spurious Tones," *IEEE Transactions on Signal Processing*, vol. 61, no. 16, 2013.

15. J. Welz, I. Galton, "A tight signal-band power bound on mismatch noise in a mismatch shaping digital-to-analog converter," *IEEE Transactions on Information Theory*, vol. 50, no. 4, pp. 593-607, April 2004.

16. S. M. Ruiz, "An Algebraic Identity Leading to Wilson's Theorem," *The Mathematical Gazette*, vol. 80, no. 489, pp. 579-582, November 1996.

17. A. Klinger, "The Vandermonde Matrix," *The American Mathematical Monthly* , vol. 74, no. 5, pp. 571-574 , May 1967.

18. Mathworks Documentation Center (R2012b), retrieved October 2012 from http://www.mathworks.com/help/symbolic/solve.html.

19. J. R. Weaver, "Centrosymmetric (Cross-Symmetric) Matrices, their Basic Properties, Eigenvalues, Eigenvectors," *American Mathematical Monthly*, vol. 92, pp. 711-717, December 1985.

CHAPTER 3

SECOND AND THIRD-ORDER NOISE SHAPING DIGITAL QUANTIZERS FOR LOW PHASE NOISE AND NONLINEARITY-INDUCED SPURIOUS TONES IN FRACTIONAL-N PLLS

Abstract—Noise shaping digital quantizers, most commonly digital delta-sigma (ΔΣ) modulators, are used in fractional-*N* phase-locked loops (PLLs) to enable fractional frequency tuning. Unfortunately, their quantization noise is subjected to nonlinear distortion because of the PLL's inevitable non-ideal analog circuit behavior, which induces spurious tones in the PLL's phase error. Successive requantizers have been proposed as ΔΣ modulator replacements with the advantage that they reduce the power of these spurious tones. However, the quantization noise from previously published successive requantizers is only first-order highpass shaped, so it usually causes more PLL phase noise than that from the second-order and third-order ΔΣ modulators commonly used in PLLs. This paper presents second-order and third-order successive requantizers to address this limitation. Additionally, successive requantizer design options are presented that result in either lower-power spurious tones or lower phase noise compared to ΔΣ modulators when used in PLLs.

This work was supported by the National Science Foundation.
The authors are with the Department of Electrical and Computer Engineering, University of California at San Diego, La Jolla, CA 92093-0407 USA (e-mail: eythanfc@gmail.com).
Color versions of one or more of the figures in this paper are available online at http://ieeexplore.ieee.org.

I. INTRODUCTION

Fractional-*N* phase-locked loops (PLLs) typically incorporate all-digital delta-sigma (ΔΣ) modulators to enable fractional frequency tuning [1]–[3]. A ΔΣ modulator's output sequence can be written as the sum of its input sequence plus *quantization noise*. The quantization noise causes the PLL's phase error to contain a component proportional to a lowpass filtered version of the running sum of the quantization noise [4][11]. In practice, non-ideal analog circuit behavior in the PLL causes the PLL's phase error to also contain components proportional to nonlinearly distorted versions of both the quantization noise and its running sum. Unfortunately, these nonlinearly distorted sequences contain spurious tones, even when the quantization noise and its running sum are free of spurious tones [5]–[15]. This is problematic in high-performance applications such as wireless communication systems which tend to be extremely sensitive to spurious tones.

The successive requantizer was proposed in [7] as a digital ΔΣ modulator replacement to address this issue. The nonlinearities to which the quantization noise and its running sum are subjected in PLLs tend to be well approximated by truncated memoryless power series [7], [8]. Therefore, the successive requantizer in [8] was designed to produce quantization noise, $s[n]$, with the property that $s^p[n]$ for p = 1, 2, 3, 4, and 5 are free of spurious tones, and such that its running sum, $t[n]$, has the property that $t^p[n]$ for p = 1, 2, and 3 are free of spurious tones. The successive requantizer was

[11] In this paper, a PLL's *phase error* refers to the difference between the PLL's actual and ideal phases and a PLL's *phase noise* refers to all stochastic components of its phase error (e.g. such as those caused by thermal noise).

demonstrated in a PLL with record-setting spurious tone performance in [8]. Unfortunately, its quantization noise is only first-order highpass shaped, whereas most ΔΣ modulators used in PLLs have second-order or third-order highpass shaped quantization noise to reduce the quantization noise contribution to the PLL's phase noise [4].[12] This issue was addressed in [8] via a quantization noise cancelation technique at the expense of increased PLL circuit area and power consumption.

This paper presents extensions of previously published results that enable successive requantizers with second-order and third-order highpass shaped quantization noise to address this limitation. It also presents design techniques that optimize the successive requantizers to either minimize PLL phase noise or spurious tone power depending on the PLL's target specifications.

In both cases, the successive requantizers achieve higher than first-order quantization noise shaping in return for not ensuring that $s^p[n]$ for $p \geq 2$ is free of spurious tones. In practice, this is not a significant limitation because in most PLLs the frequency divider output edges are resynchronized to voltage controlled oscillator edges which tends to make the nonlinear distortion applied to $s[n]$ negligible [4]. Therefore, the design option presented in the paper to minimize spurious tones focuses on nonlinearity applied to the quantization noise running sum at the expense of only a slight increase in PLL phase noise. Specifically, it ensures that $t^p[n]$ for $p = 1, 2, \ldots, h$ are free of spurious tones, where h is a positive integer. The other design option results in successive requantizers

[12] A sequence is said to be first-order highpass shaped if its running sum is bounded but the running sum of its running sum (i.e. its double running sum) is not bounded. Similarly, a sequence is said to be second-order highpass shaped if both its running sum and its double running sum are bounded but its triple running sum is not bounded.

that, like ΔΣ modulators, do not ensure that $t^p[n]$ is free of spurious tones for $p \geq 2$. Instead, they offer the advantage of introducing lower PLL phase noise than their ΔΣ modulator counterparts when used in typical PLLs.

Therefore, the contribution of this paper is a family of replacements for the commonly-used second-order and third-order ΔΣ modulators in fractional-*N* PLLs, each member of which either improves PLL spurious-tone performance at the expense of slightly higher PLL phase noise or lowers PLL phase noise. Unlike previous work, this is achieved without the high area and power consumption of phase noise cancellation techniques.

The paper consists of four main sections. Section II presents the second-order successive requantizer architecture. Section III presents two second-order successive requantizer designs which highlight a tradeoff between nonlinearity-induced spurious tone power and low-frequency quantization noise power. Section IV presents a second-order successive requantizer with lower low-frequency quantization noise power than a second-order ΔΣ modulator. Section V presents a third-order successive requantizer with lower low-frequency quantization noise power than a third-order ΔΣ modulator.

II. SECOND-ORDER SUCCESSIVE REQUANTIZER ARCHITECTURE

A high-level diagram of a successive requantizer is shown in Fig. 14. Its sequences are all integer-valued and represented in two's complement format. It processes a *B*-bit input sequence $x_0[n]$ through *K* serially-connected *quantization blocks*

to produce a $(B - K)$-bit output sequence $x_K[n]$. The dth quantization block, for each $d = 0, 1, \ldots, K-1$, divides its input, $x_d[n]$, by two and quantizes the result by one bit such that its output sequence has the form

$$x_{d+1}[n] = \frac{x_d[n] + s_d[n]}{2}, \tag{201}$$

where $s_d[n]/2$ can be viewed as quantization noise. The $s_d[n]$ *sequence generator* generates $s_d[n]$ to have the same parity as $x_d[n]$ for all n (otherwise $x_{d+1}[n]$ would not be integer-valued) and with a small enough magnitude that $x_{d+1}[n]$ can be represented with one less bit than $x_d[n]$. As explained in [7], it follows that the output of the successive requantizer can be written as

$$x_K[n] = 2^{-K} x_0[n] + s[n], \tag{202}$$

where

$$s[n] = \sum_{d=0}^{K-1} 2^{d-K} s_d[n] \tag{203}$$

is the quantization noise of the successive requantizer.

The running sums of $s_d[n]$ and $s[n]$ are defined as

$$t_d[n] = \sum_{k=0}^{n} s_d[k], \quad t[n] = \sum_{k=0}^{n} s[k], \tag{204}$$

respectively. Therefore, (203) implies that

$$t[n] = \sum_{d=0}^{K-1} 2^{d-K} t_d[n]. \tag{205}$$

It follows from (203)–(205) that the statistical properties of $s[n]$ and $t[n]$ are determined by the behavior of the $s_d[n]$ sequence generators.

A first-order $s_d[n]$ sequence generator, i.e. one in which $s_d[n]$ is first-order highpass shaped, is shown in Fig. 15 [7]. It contains a pseudo-random number generator that outputs a sequence of independent, identically and uniformly distributed pseudo-random variables $r_d[n]$, a delayed accumulator block that takes $s_d[n]$ and outputs $t_d[n-1]$, and a combinatorial logic block that generates $s_d[n]$ as a function of the lowest significant bit (LSB) of $x_d[n]$, $t_d[n-1]$, and $r_d[n]$ such that $t_d[n]$ is bounded for all n. It follows that $t_d[n]$ is a deterministic function of $t_d[n-1]$, the parity of $x_d[n]$, and $r_d[n]$.

Fig. 16 shows the proposed second-order $s_d[n]$ sequence generator. It contains a pseudo-random number generator that outputs $r_d[n]$ as in the first-order case, a combinatorial logic block, and two difference blocks. As shown in the figure, the combinatorial logic block generates a bounded sequence $u_d[n]$ conditioned on its delayed version $u_d[n-1]$, a *parity sequence* $o_d[n]$, and $r_d[n]$. As can be seen from Fig. 16,

$$t_d[n] = u_d[n] - u_d[n-1] \tag{206}$$

and

$$s_d[n] = t_d[n] - t_d[n-1], \tag{207}$$

so $u_d[n]$ is the running sum of $t_d[n]$ and the double running sum of $s_d[n]$. Unlike in the first-order $s_d[n]$ sequence generator, in the second-order $s_d[n]$ sequence generator both the running sum and the double running sum of $s_d[n]$ are bounded, so $s_d[n]$ is second-order highpass shaped.

As described above, $s_d[n]$ must have the same parity as $x_d[n]$ for all n, i.e.

$$x_d[n] \bmod 2 = s_d[n] \bmod 2. \tag{208}$$

This imposes some restrictions on the combinatorial logic. It can be seen from Fig. 16 that

$$o_d[n] = \left(x_d[n] + t_d[n-1]\right) \bmod 2 \tag{209}$$

which, with (206), can be written as

$$o_d[n] = \left(x_d[n] + u_d[n-1] - u_d[n-2]\right) \bmod 2 . \tag{210}$$

Equations (206) and (207) imply that

$$s_d[n] = u_d[n] - 2u_d[n-1] + u_d[n-2] . \tag{211}$$

For any integers a and b, [(a mod 2) + (b mod 2)] mod 2 = (a + b) mod 2, and (2a) mod 2 = 0, so it follows from (208), (210), and (211) that the combinatorial logic must generate $u_d[n]$ such that

$$\left(u_d[n] + u_d[n-1]\right) \bmod 2 = o_d[n] . \tag{212}$$

The number of bits in the successive requantizer output is determined by the range of values covered by $x_0[n]$ and by the $s_d[n]$ sequences. It follows from (201) that for each $0 \le m \le K-1$

$$x_m[n] + s_m[n] = 2^{-m} x_0[n] + \sum_{d=0}^{m} 2^{d-m} s_d[n] \tag{213}$$

and

$$x_{m+1}[n] = 2^{-m-1} x_0[n] + \sum_{d=0}^{m} 2^{d-m-1} s_d[n] . \tag{214}$$

Let N_s be the smallest positive integer greater than or equal to 2 such that

$$\left|s_d[n]\right| \le N_s \text{ for all } n \text{ and each } d \in \{0,1,...,K-1\} . \tag{215}$$

If the range of the input to the successive requantizer is restricted as

$$-2^K \le x_0[n] \le 0\,, \tag{216}$$

it follows from (213)–(215) that

$$-2N_s - 2^{K-m} < x_m[n] + s_m[n] < 2N_s \text{ for } 0 \le m \le K-1 \tag{217}$$

and

$$-N_s - 2^{K-m} < x_m[n] < N_s \quad \text{for } 1 \le m \le K\,. \tag{218}$$

This implies that $x_m[n] + s_m[n]$ for $0 \le m \le K-1$ and $x_m[n]$ for $1 \le m \le K$ can be represented with $\left\lceil \log_2\left(2^{K-m+1}N_s\right)\right\rceil$ bits, where, for any value x, $\lceil x \rceil$ is the smallest integer greater than or equal to x. The dth quantization block represents $x_d[n]$ and $x_d[n] + s_d[n]$ with $B - d$ bits and $x_{d+1}[n]$ with $B - (d + 1)$ bits, so it follows that the successive requantizer requires at least $B = K + 1 + \left\lceil \log_2\left(N_s\right)\right\rceil$ bits for its input, or, equivalently, $1 + \left\lceil \log_2\left(N_s\right)\right\rceil$ bits for its output.

For example, if $N_s = 8$, as in some of the example successive requantizers in the following section, and (216) holds, the successive requantizer input must have at least $B = K + 4$ bits, and its output must have at least 4 bits to cover the range $\{-8, -7, \ldots, 7\}$. A similar analysis yields that if the range of $x_0[n]$ is restricted as

$$-2^K \le x_0[n] \le 2^K \tag{219}$$

then the successive requantizer requires at least $B = K + 2 + \left\lceil \log_2\left(N_s\right)\right\rceil$ bits for its input, or, equivalently, $2 + \left\lceil \log_2\left(N_s\right)\right\rceil$ bits for its output.

As illustrated via examples in the next sections, the choice of N_s represents a tradeoff between PLL spurious tone performance and quantization noise power: increasing N_s provides flexibility which can be used to improve spurious tone performance, but it also tends to increase quantization noise power [12].

It follows from Figs. 14 and 16 that the computational complexity of the successive requantizer is a logarithmic function of N_s and a quadratic function of the number of quantization blocks K. The dth pseudo-random number generator can be implemented with a modified linear-feedback shift register (LFSR) that simultaneously generates multiple bits that are well-modeled as zero-mean, white, and independent of each other [16].

III. SECOND-ORDER SUCCESSIVE REQUANTIZERS WITH HIGH IMMUNITY TO SPURIOUS TONES

The combinatorial logic block of a second-order $s_d[n]$ sequence generator can be described by two *state transition matrices*, $\mathbf{A_e}$ and $\mathbf{A_o}$, which define the probability mass function (pmf) of $u_d[n]$ conditioned on $u_d[n-1]$ and $o_d[n]$ for each n. Specifically, if $u_d[n]$ takes values in $\{N_u, N_u - 1, \ldots, -N_u\}$, where N_u is a positive integer, then $\mathbf{A_e}$ and $\mathbf{A_o}$ are $(2N_u + 1)\times(2N_u + 1)$ matrices with elements

$$\begin{aligned}\mathbf{A_e}(i, j) &= \Pr(u_d[n] = \mathbf{u}(j) \mid u_d[n-1] = \mathbf{u}(i), o_d[n] = 0), \\ \mathbf{A_o}(i, j) &= \Pr(u_d[n] = \mathbf{u}(j) \mid u_d[n-1] = \mathbf{u}(i), o_d[n] = 1)\end{aligned} \quad (220)$$

for all i, $j \in \{1, 2, \ldots, 2N_u + 1\}$, where

$$\mathbf{u} = \begin{pmatrix} N_u & (N_u - 1) & \ldots & -N_u \end{pmatrix}^T .^{13} \tag{221}$$

The combinatorial logic block is deterministic, so the probabilities in (220) arise from the random sequence, $r_d[n]$, which is assumed, by design, to be uniformly distributed for all n. This implies that the probabilities in (220) must be of the form $k / 2^b$, where $k \in \{0, 1, \ldots, 2^b\}$ and b is the number of bits used to represent $r_d[n]$[14]. The only other requirements the state transition matrices must satisfy are that their rows add to 1–so that the pmf is valid–and that

$$\begin{aligned} \mathbf{A_e}(i, j) &= 0 \quad \forall \quad i + j : \text{odd and} \\ \mathbf{A_o}(i, j) &= 0 \quad \forall \quad i + j : \text{even.} \end{aligned} \tag{222}$$

The last requirement is needed to satisfy (212). Equation (221) implies that if $i + j$ is even then $\mathbf{u}(i) + \mathbf{u}(j)$ is even, whereas if $i + j$ is odd then $\mathbf{u}(i) + \mathbf{u}(j)$ is odd. This and (220) imply that if $\mathbf{A_e}(i, j) \neq 0$ for some odd $i + j$, there is a non-zero probability that $u_d[n - 1] + u_d[n]$ is odd when $o_d[n] = 0$, which contradicts (212). Similarly, if $\mathbf{A_o}(i, j) \neq 0$ for some even $i + j$, there is a non-zero probability that $u_d[n - 1] + u_d[n]$ is even when $o_d[n] = 1$, which contradicts (212) as well.

As an example, if $N_u = 2$ and $r_d[n] \in \{-8, -7, \ldots, 7\}$, then

---

[13] In this paper, the ith entry of a vector $\mathbf{v}$ is denoted by $\mathbf{v}(i)$, whereas the ith row, jth column entry of a matrix $\mathbf{M}$ is denoted by $\mathbf{M}(i, j)$.

[14] Since $u_d[n]$ conditioned on $u_d[n - 1]$ and $o_d[n]$ is a deterministic function of $r_d[n]$, the 2^b values $r_d[n]$ can take map to $M \leq 2^b$ values of $u_d[n]$ for each $u_d[n - 1]$ and $o_d[n]$. Since $r_d[n]$ is uniformly distributed, the probability that $u_d[n] = u$ equals $k / 2^b$, where k is the number of different $r_d[n]$ values that map to u.

$$\mathbf{A_e} = \begin{pmatrix} 1/4 & 0 & 3/4 & 0 & 0 \\ 0 & 5/8 & 0 & 3/8 & 0 \\ 1/8 & 0 & 3/4 & 0 & 1/8 \\ 0 & 3/8 & 0 & 5/8 & 0 \\ 0 & 0 & 3/4 & 0 & 1/4 \end{pmatrix} \text{ and}$$
$$\mathbf{A_o} = \begin{pmatrix} 0 & 3/4 & 0 & 1/4 & 0 \\ 3/16 & 0 & 3/4 & 0 & 1/16 \\ 0 & 1/2 & 0 & 1/2 & 0 \\ 1/16 & 0 & 3/4 & 0 & 3/16 \\ 0 & 1/4 & 0 & 3/4 & 0 \end{pmatrix} \quad (223)$$

describe valid behavior for the combinatorial logic block. A truth table for combinatorial logic that implements the behavior specified by (223) can be constructed from (220) and (221) with $N_u = 2$. For example, the elements in the third row of $\mathbf{A_e}$, i.e. 1 / 8, 0, 3 / 4, 0, and 1 / 8, are the probabilities that $u_d[n] = \boldsymbol{u}(1) = 2$, $u_d[n] = \boldsymbol{u}(2) = 1$, $u_d[n] = \boldsymbol{u}(3) = 0$, $u_d[n] = \boldsymbol{u}(4) = -1$, and $u_d[n] = \boldsymbol{u}(5) = -2$, respectively, conditioned on $u_d[n - 1] = \boldsymbol{u}(3) = 0$ and $o_d[n] = 0$. Therefore, if $u_d[n - 1] = 0$ and $o_d[n] = 0$, the combinatorial logic must set $u_d[n] = 2$ with probability 1 / 8, $u_d[n] = 0$ with probability 3 / 4, and $u_d[n] = -2$ with probability 1 / 8. Given that $r_d[n]$ is uniformly distributed among the sixteen integers from –8 to 7, one way to do this is to map two of these integers to $u_d[n] = 2$, another two to $u_d[n] = -2$, and the rest to $u_d[n] = 0$; e.g., set $u_d[n] = -2$ if $r_d[n] = 0$ or 1, $u_d[n] = 2$ if $r_d[n] = 2$ or 3, and $u_d[n] = 0$ otherwise. A complete truth table, an example of which is shown in Fig. 17, can be constructed by applying this procedure to every row of $\mathbf{A_e}$ and $\mathbf{A_o}$.

Note that the rows in both $\mathbf{A_e}$ and $\mathbf{A_o}$ of (223) alternate between two types of vectors: vectors whose odd-indexed elements are zero, referred to as even-entries vectors,

and vectors whose even-indexed elements are zero, referred to as odd-entries vectors. This is a consequence of (222) and holds for all valid state transition matrices.

State transition matrices such as those in (223) were used in [13] to describe the combinatorial logic block in first-order $s_d[n]$ sequence generators. For such $s_d[n]$ sequence generators, the state transition matrices define the pmf of $t_d[n]$ conditioned on $t_d[n-1]$ and a parity sequence. In contrast, the state transition matrices in second-order $s_d[n]$ sequence generators define the pmf of $u_d[n]$ conditioned on $u_d[n-1]$ and the parity sequence $o_d[n]$, as described by (220) and (221). Therefore, if the same state transition matrices are used to describe the combinatorial logic block of a first and a second-order $s_d[n]$ sequence generator, and if the parity sequences of both generators are equal, $t_d[n]$ in the first-order $s_d[n]$ sequence generator and $u_d[n]$ in the second-order $s_d[n]$ sequence generator are statistically equivalent. Furthermore, since $t_d[n]$ and $u_d[n]$ are defined as the running sums of $s_d[n]$ and $t_d[n]$, respectively, $s_d[n]$ in the first-order $s_d[n]$ sequence generator and $t_d[n]$ in the second-order $s_d[n]$ sequence generator are statistically equivalent as well.

For any positive integer h, a sequence $x[n]$ is said to be *immune to spurious tones up to order h* if $x^p[n]$ for $p = 1, 2, \ldots, h$ are free of spurious tones. In [13], conditions are presented on the state transition matrices of a first-order successive requantizer, i.e. a successive requantizer which uses first-order $s_d[n]$ sequence generators, that make $t_d[n]$ and $s_d[n]$ immune to spurious tones up to orders h_1 and h_2, respectively, for each d, where h_1 and h_2 are positive integers which do not depend on the parity sequences of the $s_d[n]$ sequence generators. It is also shown in [13] that such conditions make $t[n]$ and $s[n]$

immune to spurious tones up to orders h_1 and h_2, respectively. Therefore, in a second-order successive requantizer, such conditions make $u_d[n]$ and $t_d[n]$ immune to spurious tones up to orders h_1 and h_2, respectively, for each d. Additionally, as can be verified with identical reasoning to that used in [13] for the first-order successive requantizer, they make

$$u[n] = \sum_{k=0}^{n} t[k] \tag{224}$$

and $t[n]$ immune to spurious tones up to orders h_1 and h_2, respectively. For example, it was proven in [13] that, in a first-order successive requantizer, state transition matrices (223) make $s[n]$ immune to spurious tones up to order 5. Therefore, in a second-order successive requantizer, these state transition matrices make $t[n]$ immune to spurious tones up to order 5. Fig. 18 shows plots of simulated power spectra of $t[n]$ as generated with a second-order successive requantizer that implements the state transition matrices in (223) and of the running sum of the quantization noise of a dithered second-order $\Delta\Sigma$ modulator, $t_{DS}[n]$, before and after the application of fourth and fifth-order nonlinear distortion. As expected, the simulated power spectra of $t^4[n]$ and $t^5[n]$ show no visible spurious tones, whereas those of $t^4_{DS}[n]$ and $t^5_{DS}[n]$ do.

Fig. 18 also shows that $t[n]$ has significantly higher low-frequency power spectrum content than $t_{DS}[n]$. One of the contributions of this paper is to reduce this content by modifying $\mathbf{A_e}$ and $\mathbf{A_o}$ subject to $t[n]$ maintaining a minimum desired order of immunity to spurious tones.

It follows from Theorem 2 and Lemmas 3 and 6 in [13] and the parallels of first and second-order successive requantizers described above that sufficient conditions to make $t[n]$ immune to spurious tones up to order h_t, where h_t is a positive integer, are that

C1) $\mathbf{A_e}$ and $\mathbf{A_o}$ are centrosymmetric[15] with all their odd-entries row vectors containing at least $1 + \lfloor (N_u + 1)/2 \rfloor$ nonzero entries and all their even-entries row vectors containing at least $1 + \lfloor N_u/2 \rfloor$ nonzero entries (where $\lfloor x \rfloor$ denotes the greatest integer that is less than or equal to x), and that

C2) For each positive even integer $p \le h_t$

$$\mathbf{A_e T_e t}^{(p)} = \mathbf{A_e T_o t}^{(p)} = \mathbf{A_o T_e t}^{(p)} = \mathbf{A_o T_o t}^{(p)} = c_p \mathbf{1}_{2N_u+1}, \tag{225}$$

where c_p is a constant,

$$\mathbf{T_x}(i, j) = \begin{cases} \mathbf{A_x}(i, j + i - 2N_u - 1), & \text{if } 2N_u + 2 - i \le j \le 4N_u + 2 - i, \\ 0, & \text{if } j \le 2N_u + 1 - i, j \ge 4N_u + 3 - i \end{cases} \tag{226}$$

for **x** = **e** or **o**,

$$\mathbf{t}^{(p)} = \left((2N_u)^p \quad (2N_u - 1)^p \quad \ldots \quad (-2N_u)^p \right)^T, \tag{227}$$

and $\mathbf{1}_{2N_u+1}$ is a length-$(2N_u + 1)$ vector whose elements are all 1.

For example, if $\mathbf{A_e}$ and $\mathbf{A_o}$ are given by (223), $\mathbf{T_e}$ and $\mathbf{T_o}$, computed using (226), are given by

[15] An NxN centrosymmetric matrix $\mathbf{A}$ is a matrix for which $\mathbf{A}(i, j) = \mathbf{A}(N + 1 - i, N + 1 - j)$ for all i, j.

$$\mathbf{T_e} = \begin{pmatrix} 0 & 0 & 0 & 0 & 1/4 & 0 & 3/4 & 0 & 0 \\ 0 & 0 & 0 & 0 & 5/8 & 0 & 3/8 & 0 & 0 \\ 0 & 0 & 1/8 & 0 & 3/4 & 0 & 1/8 & 0 & 0 \\ 0 & 0 & 3/8 & 0 & 5/8 & 0 & 0 & 0 & 0 \\ 0 & 0 & 3/4 & 0 & 1/4 & 0 & 0 & 0 & 0 \end{pmatrix},$$

$$\mathbf{T_o} = \begin{pmatrix} 0 & 0 & 0 & 0 & 0 & 3/4 & 0 & 1/4 & 0 \\ 0 & 0 & 0 & 3/16 & 0 & 3/4 & 0 & 1/16 & 0 \\ 0 & 0 & 0 & 1/2 & 0 & 1/2 & 0 & 0 & 0 \\ 0 & 1/16 & 0 & 3/4 & 0 & 3/16 & 0 & 0 & 0 \\ 0 & 1/4 & 0 & 3/4 & 0 & 0 & 0 & 0 & 0 \end{pmatrix}. \quad (228)$$

The above conditions hold regardless of how the successive requantizer is initialized.

As explained above, the entries in $\mathbf{A_e}$ and $\mathbf{A_o}$ are constrained to be of the form $k / 2^b$, where $k \in \{0, 1, \ldots, 2^b\}$ and b is the number of bits used to represent each $r_d[n]$. This implies that there is a finite number of matrices $\mathbf{A_e}$ and $\mathbf{A_o}$ which satisfy conditions **C1** and **C2** for each N_u and h_t. As justified in the Appendix, the low-frequency quantization noise can be reduced by choosing the $\mathbf{A_e}$ and $\mathbf{A_o}$ matrices that minimize

$$\lim_{H\to\infty} \sum_{m=-H}^{H} \sum_{i=1}^{2N_u+1} \left(\mathbf{A}^{|m|}\mathbf{u}\right)(i) \cdot \mathbf{u}(i) \cdot \left(\lim_{k\to\infty} \mathbf{A}^k\right)(1,i), \quad (229)$$

where

$$\mathbf{A} = \left(\mathbf{A_e} + \mathbf{A_o}\right)/2, \quad (230)$$

subject to the constraint that $\mathbf{A}$ be primitive, i.e. that there exists a positive integer n such that the entries of $\mathbf{A}^n$ are all greater than zero. Because $\mathbf{A}$ is stochastic, a necessary and sufficient condition for $\mathbf{A}$ to be primitive is that all entries of $\mathbf{A}^{4N_u+1}$ are greater than zero [17]. In this paper, a computer program was written which cycles through all $\mathbf{A_e}$ and $\mathbf{A_o}$

matrices that satisfy conditions **C1** and **C2** for $N_u = 2$ and $h_t = 3$ and picks those which minimize (229), where the limits in (229) are approximated with a suitable number of terms (i.e. a number high enough that increasing it has no visible effect on the simulated power spectrum of $t[n]$). To keep hardware implementation requirements modest, $r_d[n]$ was restricted to values that can be represented with 10 bits, so the entries in $\mathbf{A_e}$ and $\mathbf{A_o}$ are restricted to be of the form $k / 1024$, where $k \in \{0, \ldots, 1024\}$. Note, however, that larger values of N_u and h_t might require $r_d[n]$ to be represented with more than 10 bits. The resulting state transition matrices are

$$\mathbf{A_e} = \begin{pmatrix} 0 & 0 & 333/512 & 0 & 179/512 \\ 0 & 7/128 & 0 & 121/128 & 0 \\ 179/1024 & 0 & 333/512 & 0 & 179/1024 \\ 0 & 121/128 & 0 & 7/128 & 0 \\ 179/512 & 0 & 333/512 & 0 & 0 \end{pmatrix},$$
$$\mathbf{A_o} = \begin{pmatrix} 0 & 7/1024 & 0 & 1017/1024 & 0 \\ 1/512 & 0 & 333/512 & 0 & 89/256 \\ 0 & 1/2 & 0 & 1/2 & 0 \\ 89/256 & 0 & 333/512 & 0 & 1/512 \\ 0 & 1017/1024 & 0 & 7/1024 & 0 \end{pmatrix}. \quad (231)$$

An example combinatorial logic block truth table of a second-order $s_d[n]$ sequence generator that implements these state transition matrices is shown in Fig. 19.

Fig. 20 shows the simulated power spectrum of $t[n]$ from a 20-bit input second-order successive requantizer that implements the state transition matrices in (231). Given that $u_d[n]$ is the double running sum of $s_d[n]$ and is bounded by $N_u = 2$, $s_d[n]$ is bounded by $N_s = 8$. Therefore, as explained in the previous section, for inputs restricted as in (216) , this successive requantizer's output ranges from –8 to 7. For comparison, the figure also

shows the simulated power spectrum of the running sum of the quantization noise of a dithered second-order ΔΣ modulator, $t_{DS}[n]$. At low frequencies, the simulated power spectrum of $t[n]$ is only approximately 1.5 dB above that of $t_{DS}[n]$. At high frequencies the power spectrum of $t[n]$ is higher than that of $t_{DS}[n]$, but as explained shortly this difference negligibly affects phase noise in typical fractional-*N* PLL designs. The range covered by $t[n]$ is (–4, 4), which is higher than that covered by $t_{DS}[n]$. However, $t_{DS}[n]$ is only immune to spurious tones up to order 1, whereas $t[n]$ is immune to spurious tones up to order 3. Additionally, as can be seen in the figure, $t_{DS}[n]$ contains an integrated white noise component due to the ΔΣ modulator's dither, whereas $t[n]$ does not.

To evaluate the feasibility of using this successive requantizer in a PLL, an event-driven PLL simulator was written in C to compare the power spectrum of the PLL phase error when using the second-order successive requantizer against when using a dithered second-order ΔΣ modulator as the PLL's digital quantizer. The simulator models the PLL shown in Fig. 21 which consists of a phase-frequency detector (PFD), a charge pump (CP) with nominal branch currents of 1 mA, a third-order loop filter with component values of C_1 = 67 pF, R_1 = 8.67 kΩ, C_2 = 2.02 nF, R_2 = 8.67 kΩ, and C_3 = 67 pF, a voltage-controlled oscillator (VCO) with a gain of 5 MHz/V, two digital quantizers–a second-order ΔΣ modulator and the second-order successive requantizer described above–with an input, α, of -2^{-11}, and a multi-modulus frequency divider with a modulus of 137 plus the output of one of the digital quantizers [4]. The PLL has a reference frequency f_{ref} of 26 MHz, an output frequency f_{out} of 3.56 GHz, a bandwidth of 45 kHz, and a phase margin of 55°. The circuit noise sources modeled in the simulation are $1/f^2$ noise from the VCO

(–125 dBc/Hz at 1 MHz) and white noise from the reference oscillator (–150 dBc/Hz). The only non-ideality modeled is a 1% mismatch between the charge pump branch currents, which introduces nonlinear distortion.

Fig. 22 shows the simulated power spectrum of the phase error generated using each digital quantizer. As the figure shows, compared to the ΔΣ modulator, the successive requantizer results in significantly lower-power fractional spurious tones in the PLL's phase error: it reduces the largest fractional spurious tone power by 17 dB. The figure also shows that the successive requantizer introduces slightly higher in-band phase noise than the ΔΣ modulator. This is because the low-frequency portion of the nonlinearly distorted quantization noise power of the successive requantizer is slightly higher than that of the ΔΣ modulator. The noise penalty in a real PLL, however, is usually not significant, as $1 / f$ noise dominates the phase noise power spectrum at low frequencies. Due to the relatively low bandwidth of the PLL and the third-order loop filter (both of which are typical design choices for analog fractional-N PLLs), the phase noise contributed by the digital quantizer is not dominant at high frequencies, so the higher high-frequency quantization noise from the successive requantizer does not significantly affect the PLL's phase noise performance compared to the ΔΣ modulator. Therefore, in typical fractional-N PLLs, spurious tones can be reduced significantly by using a successive requantizer at the expense of a slight increase in phase noise power.

A digital implementation of the second-order successive requantizer in 65nm CMOS technology with K = 16 quantization blocks has 1500 digital gates, occupies an area of 6000 μm^2, and has an average power consumption of 100 μW. In contrast, a 16-

bit input, second-order ΔΣ modulator implementation in the same technology has 120 digital gates, occupies an area of 1000 μm^2, and has an average power consumption of 20 μW. Given that the digital quantizer's area and average power consumption represent a small portion of the total area and average power consumption of typical fractional-*N* PLLs, the larger area and higher power consumption of the successive requantizer are not significant in practice.

IV. SECOND-ORDER SUCCESSIVE REQUANTIZERS WITH REDUCED QUANTIZATION NOISE AT LOW-FREQUENCIES

The successive requantizer examples in the previous section highlight a design tradeoff between low-frequency quantization noise power and immunity to spurious tones: the successive requantizer that implements the state transition matrices in (231) has lower immunity to spurious tones (h_t = 3) than that which implements the state transition matrices in (223) (h_t = 5), but it has lower quantization noise power at low frequencies. This motivates finding state transition matrices for which h_t = 1 to reduce the low-frequency quantization noise power further. As can be verified with the proof of Lemma 3 and Theorem 1 in [13] and from the parallels of first and second-order successive requantizers, if $\mathbf{A_e}$ and $\mathbf{A_o}$ are 3×3 centrosymmetric state transition matrices with five and four non-zero elements, respectively, then $t[n]$ is free of spurious tones. Suppose that $\mathbf{A_e}$ and $\mathbf{A_o}$ satisfy the above condition and that their entries are of the form k / 1024, where $k \in \{0, 1, \ldots, 1024\}$, as in the previous section. Then, the low-frequency

quantization noise can be reduced by choosing the $\mathbf{A_e}$ and $\mathbf{A_o}$ matrices that minimize (229) [16]. A computer program was written which cycles through all $\mathbf{A_e}$ and $\mathbf{A_o}$ satisfying the above conditions and picks those which minimize (229), where the limits in (229) are approximated with a suitable number of terms as in the previous section. The resulting state transition matrices are

$$\mathbf{A_e} = \begin{pmatrix} \frac{1}{1024} & 0 & \frac{1023}{1024} \\ 0 & 1 & 0 \\ \frac{1023}{1024} & 0 & \frac{1}{1024} \end{pmatrix}, \mathbf{A_o} = \begin{pmatrix} 0 & 1 & 0 \\ \frac{1}{2} & 0 & \frac{1}{2} \\ 0 & 1 & 0 \end{pmatrix}. \tag{232}$$

As can be verified from simulation, $t^2[n]$ has spurious tones, so $h_t = 1$.

Fig. 23 shows the simulated power spectrum of $t[n]$ from a 20-bit input second-order successive requantizer which implements the state transition matrices in (232) and of the running sum of the quantization noise of a dithered second-order ΔΣ modulator, $t_{DS}[n]$. As seen in the figure, the power spectrum of $t[n]$ is lower by approximately 2 dB than that of $t_{DS}[n]$ at low frequencies. However, the range of $t[n]$ is (–2, 2), which is double to that of $t_{DS}[n]$. Additionally, as in the previous section, $t_{DS}[n]$ contains an integrated white noise component due to the ΔΣ modulator's dither, whereas $t[n]$ does not.

Fig. 24 shows the simulated power spectrum of the phase error of a PLL when using a second-order ΔΣ modulator and when using the second-order successive

[16] The same low-frequency quantization noise reduction method from the previous section can be used because, as can be verified, all results derived in the Appendix hold if condition **C1** is replaced by the above conditions for $N_u = 1$ $\mathbf{A_e}$ and $\mathbf{A_o}$ state transition matrices.

requantizer which implements the state transition matrices in (232). The PLL is identical to that described in Section III but with its reference and VCO noise sources turned off to show the quantization noise contribution to the PLL phase error at all frequencies. It also has perfectly-matched charge pump branch currents, as opposed to the modeled PLL in Section III. This allows comparison of the digital quantizers' contribution to the PLL phase noise in the ideal case in which nonlinearly distorted versions of the quantization noise do not corrupt the low-frequency portion of the PLL phase noise, as in the PLL phase noise PSD shown in Fig. 22b. As seen in Fig. 24 and as predicted by Fig. 23, the PLL phase noise at frequencies below 5 MHz is lower when the successive requantizer is used.

V. THIRD-ORDER SUCCESSIVE REQUANTIZERS WITH REDUCED QUANTIZATION NOISE AT LOW FREQUENCIES

The $s_d[n]$ sequence generator in the successive requantizer can be modified to produce higher-order highpass shaped quantization noise by applying more difference operations to the combinatorial logic block output and by adding logic to ensure $x_d[n]$ and $s_d[n]$ have equal parity for all n. For example, a third-order successive requantizer can be implemented with the $s_d[n]$ sequence generator from Fig. 25. The combinatorial logic block can be described by state transition matrices $\mathbf{A_e}$ and $\mathbf{A_o}$ as before, but since its output is now $v_d[n]$–defined as the triple running sum of $s_d[n]$–instead of $u_d[n]$, where $v_d[n] \in \{N_v, N_v - 1, \ldots, -N_v\}$ for some positive integer N_v, $\mathbf{A_e}$ and $\mathbf{A_o}$ are now defined by

$$\begin{aligned}\mathbf{A_e}(i,j) &= \Pr(v_d[n] = \mathbf{v}(j) \mid v_d[n-1] = \mathbf{v}(i), o_d[n] = 0),\\ \mathbf{A_o}(i,j) &= \Pr(v_d[n] = \mathbf{v}(j) \mid v_d[n-1] = \mathbf{v}(i), o_d[n] = 1),\end{aligned} \tag{233}$$

where

$$\mathbf{v} = \begin{pmatrix} N_v & (N_v - 1) & \ldots & -N_v \end{pmatrix}^T, \tag{234}$$

in analogy to (220) and (221). Reasoning similar to that from (208) to (212) can be used to verify that, for $x_d[n]$ and $s_d[n]$ to have equal parity, the combinatorial logic block must generate $v_d[n]$ such that $v_d[n] - v_d[n-1]$ and $o_d[n]$ have equal parity, where $o_d[n]$ is generated as in Fig. 25.

Fig. 26 shows the simulated power spectrum of the $t[n]$ of a third-order successive requantizer that implements the state transition matrices in (232) and of the running sum of the quantization noise of a dithered third-order ΔΣ modulator, $t_{DS}[n]$. The power spectrum of $t[n]$ is lower than that of $t_{DS}[n]$ by approximately 1 to 2 dB at low frequencies, but the range of $t[n]$ is (–4, 4), which is double that of $t_{DS}[n]$. Fig. 27a shows the simulated power spectrum of the phase error of a PLL when using the third-order ΔΣ modulator and when using the third-order successive requantizer. The PLL modeled is that shown in Fig. 21, where the charge pump (CP) has branch currents of 500 μA, the loop filter has component values of C_1 = 3.7 pF, R_1 = 26 kΩ, C_2 = 112 pF, R_2 = 26 kΩ, and C_3 = 3.7 pF, the voltage-controlled oscillator (VCO) has a gain of 5 MHz/V, the input to the digital quantizers, α, is -2^{-11}, the reference frequency f_{ref} is 26 MHz, the output frequency f_{out} is 3.56 GHz, and the PLL bandwidth is 85 kHz. As seen in the figure, the successive requantizer contributes more low-frequency phase noise than the ΔΣ modulator. This is due to the inherent nonlinear behavior of the PLL and shows that, at low frequencies, the

power of nonlinearly distorted versions of the quantization noise running sum of the successive requantizer is higher than that of the ΔΣ modulator. At frequencies from 400 kHz to 4 MHz the phase noise is lower by 0.5 to 1.5 dB when the successive requantizer is used, whereas at higher frequencies the ΔΣ modulator results in lower phase noise. The worse low-frequency behavior of the successive requantizer when used in a PLL is not an issue in practice, as low-frequency phase noise is typically dominated by reference, charge pump, and VCO noise. Fig. 27b shows the same phase noise simulation but with $1/f^2$ noise from the VCO (–127 dBc/Hz at 1 MHz) and white noise from the reference oscillator (–150 dBc/Hz). As seen in the figure, when these circuit noise sources are included, the phase noise performance when using either digital quantizer is similar at frequencies below 400 kHz. Therefore, in this PLL using a successive requantizer improves PLL spot noise from 400 kHz to 4 MHz at the detriment of PLL spot noise at higher frequencies.

VI. CONCLUSION

Second and third-order successive requantizers that can replace the commonly-used ΔΣ modulator in fractional-*N* PLLs to improve PLL phase error performance have been presented. Specifically, a second-order successive requantizer has been presented which can drastically improve spurious tone performance when used in typical fractional-*N* PLLs by producing quantization noise that is free of spurious tones even when subjected to the PLL's nonlinear distortion. A phase noise simulation of one such PLL

shows a 17 dB power reduction in the largest fractional spurious tone when the digital quantizer is implemented as the second-order successive requantizer instead of as a second-order ΔΣ modulator while maintaining similar phase noise performance. Additionally, second and third-order successive requantizers have been presented which produce lower-power low-frequency quantization noise compared to their ΔΣ modulator counterparts. These successive requantizers are not optimized for nonlinearity-induced spurious tone reduction, but are rather intended for PLLs requiring low phase noise at low or mid frequencies.

APPENDIX

This Appendix contains the derivation of the expression in (229) used to reduce the low-frequency power spectrum content of $t[n]$. The derivation is based on three assumptions: that condition **C1** from Section III holds, that each $o_d[n]$ takes on the values 0 and 1 with equal probability, and that **A** is primitive. The first assumption is a sufficient condition for $t[n]$ to be immune to spurious tones up to at least order one, as explained in Section III. The second assumption is based on the unpredictability of $o_d[n]$ for most quantization blocks. An exact expression for the pmf of $o_d[n]$ conditioned on the $x_0[n]$ and the $r_d[n]$ sequences is hard to find. However, as proven in Section III of [7], each $o_d[n]$ is a deterministic function of $\{x_0[m], m = 0, 1, \ldots, n\}$ and $\{r_k[m], k = 0, 1, \ldots, d-1, m = 0, 1, \ldots, n\}$, which motivates modeling it as being uniformly distributed. Simulations support the validity of this model for most values of d. The third assumption has been

empirically found to hold for most matrices $\mathbf{A_e}$ and $\mathbf{A_o}$ satisfying condition **C1**, so it does not significantly limit the utility of (229). An additional assumption in the derivation is that each sequence $x[n]$ in the successive requantizer is such that $x[n] = 0$ for all $n \leq 0$. This assumption is not necessary to obtain (229) but is reasonable and simplifies the derivation.

The power spectrum of $t[n]$ can be estimated with the expected value of the L-length periodogram of $t[n]$,

$$I_{t,L}(\omega) = \frac{1}{L}\left|\sum_{n=0}^{L-1} t[n]e^{-j\omega n}\right|^2 \tag{235}$$

[7], [18]. It follows from (205) and (206) that this expected value can be written as

$$E\left\{I_{t,L}(\omega)\right\} = E\left\{\frac{1}{L}\left|\sum_{n=0}^{L-1}\left(\sum_{d=0}^{K-1} 2^{d-K}\left(u_d[n]-u_d[n-1]\right)\right)e^{-j\omega n}\right|^2\right\}. \tag{236}$$

Therefore, $E\left\{I_{t,L}(\omega)\right\}$ can be expanded as a finite sum of terms of the form

$$c_{a,b,n,m,L}E\left\{u_a[n]u_b[m]\right\}, \tag{237}$$

where, without loss of generality, $a \geq b$, $a, b \in \{0, 1, \ldots, K-1\}$, $n, m \in \{0, 1, \ldots, L-1\}$, and $c_{a,b,n,m,L}$ is a constant. Using the law of total expectation, the expectation in (237) can be written as

$$E\left\{u_a[n]u_b[m]\right\} = E\left\{u_b[m]E\left\{u_a[n]\,|\,u_b[m]\right\}\right\}. \tag{238}$$

The inner expectation in (238) can be conditioned on additional variables as long as the outer expectation in (238) is computed over all possible values of those variables. Thus, (238) can be rewritten as

$$E\{u_a[n]u_b[m]\} = E\{u_b[m]E\{u_a[n]\,|\,u_b[m],u_a[0],u_b[0], o_a[k],o_b[k];k=1,2,...,\max\{n,m\}\}\}. \tag{239}$$

In Section III of [7], it is proven that in a first-order $s_d[n]$ sequence generator $t_d[n]$ conditioned on $t_d[0]$, $o_d[1]$, $o_d[2]$, …, $o_d[n]$ is a deterministic function of $r_d[0]$, $r_d[1]$, …, $r_d[n]$ for each $n > 0$. It follows from the parallels of first and second-order $s_d[n]$ sequence generators explained in Section III of this paper that in a second-order $s_d[n]$ sequence generator $u_d[n]$ conditioned on $u_d[0]$, $o_d[1]$, $o_d[2]$, …, $o_d[n]$ is a deterministic function of $r_d[0]$, $r_d[1]$, …, $r_d[n]$. It follows from this, from the derivation in [7] proving that $o_d[n]$ is a deterministic function of $x_0[n]$ and $\{r_k[m], k = 0, 1, \ldots, d-1, m = 0, 1, \ldots, n\}$, and from the independence of the $r_d[n]$ sequences that, for $a \neq b$, (239) can be written as

$$E\{u_a[n]u_b[m]\} = E\{u_b[m]E\{u_a[n]\,|\,u_a[0], o_a[k];k=1,2,...,n\}\}. \tag{240}$$

Lemma 3 and equation (9) in [13] imply that in a first-order $s_d[n]$ sequence generator

$$E\{t_a[n]\,|\,t_a[0]=0,o_a[k];k=1,2,...,n\}=0 \tag{241}$$

for each $a \in \{0, 1, \ldots, K-1\}$. Therefore, in a second-order $s_d[n]$ sequences generator

$$E\{u_a[n]\,|\,u_a[0]=0,o_a[k];k=1,2,...,n\}=0 \tag{242}$$

for each $a \in \{0, 1, \ldots, K-1\}$. Since $u_a[0] = 0$, it follows that the right side of (240) is zero[17]. Therefore,

[17] If $u_a[0] \neq 0$ it can be shown that the right side of (240) approaches zero as $n \to \infty$, which allows obtaining (229) but requires a longer derivation.

$$E\{u_a[n]u_b[m]\} = 0 \text{ when } a \neq b, \tag{243}$$

so (236) can be rewritten as

$$E\{I_{t,L}(\omega)\} = \sum_{d=0}^{K-1} 2^{d-K} E\left\{\frac{1}{L}\left|\sum_{n=0}^{L-1}(u_d[n]-u_d[n-1])e^{-j\omega n}\right|^2\right\}. \tag{244}$$

This shows that $E\{I_{t,L}(\omega)\}$ can be reduced by reducing the expected value of the L-length periodogram of $t_d[n]$,

$$I_{t_d,L}(\omega) = \frac{1}{L}\left|\sum_{n=0}^{L-1}(u_d[n]-u_d[n-1])e^{-j\omega n}\right|^2, \tag{245}$$

for each $d \in \{0, 1, \ldots, K-1\}$.

Equation (245) can be rewritten as

$$I_{t_d,L}(\omega) = \frac{1}{L}\left|(1-e^{-j\omega})\sum_{n=0}^{L-1}u_d[n]e^{-j\omega n} + u_d[L-1]e^{-j\omega L}\right|^2. \tag{246}$$

Let $I_{u_d,L}(\omega)$ be the L-length periodogram of $u_d[n]$. For any ω such that $I_{u_d,L}(\omega) \neq 0$, (246) can be rewritten as

$$I_{t_d,L}(\omega) = I_{u_d,L}(\omega)\left(\left|1-e^{-j\omega}\right|^2 + B(\omega, L)\right), \tag{247}$$

where

$$B(\omega, L) = \frac{1}{L}\frac{2u_d[L-1]\mathrm{Re}\left\{(1-e^{-j\omega})e^{j\omega L}\sum_{n=0}^{L-1}u_d[n]e^{-j\omega n}\right\} + {u_d}^2[L-1]}{I_{u_d,L}(\omega)} \tag{248}$$

Using the proof of Theorem 1 in [7], Lemma 3 and Theorem 1 in [13] prove that in a first-order $s_d[n]$ sequence generator where condition **C1** holds, $I_{t_d,L}(\omega)$ is bounded

in probability for all $L \geq 1$ and $0 < |\omega| \leq \pi$. Moreover, the proof of Lemma 3 in [13] shows that the constant C_{t^1} in equation (29) of the proof of Theorem 1 in [7] equals 0, which implies that $J_{2,2}$ in equation (30) of [7] equals 0 when $p = 1$. It follows from this and from the rest of the proof of Theorem 1 in [7] that in a first-order $s_d[n]$ sequence generator $I_{t_d,L}(\omega)$ is uniformly bounded in probability for all $L \geq 1$ and $0 \leq |\omega| \leq \pi$. This implies that in the second-order $s_d[n]$ sequence generator $I_{u_d,L}(\omega)$ is uniformly bounded in probability for all $L \geq 1$ and $0 \leq |\omega| \leq \pi$.

The above implies that

$$\lim_{L\to\infty} \frac{1}{L} \sum_{n=0}^{L-1} u_d[n] e^{-j\omega n} = 0 \tag{249}$$

for all $0 \leq \omega \leq \pi$ almost surely. This and the fact that $u_d[n]$ is bounded for all n imply that

$$\lim_{L\to\infty} B(\omega, L) = 0 \tag{250}$$

almost surely, so it follows from (247) that for large enough values of L and for each $\omega \neq 0$ for which $E\{I_{u_d,L}(\omega)\} \neq 0$, $E\{I_{t_d,L}(\omega)\}$ can be reduced by reducing $E\{I_{u_d,L}(\omega)\}$. Additionally, the continuity of the L-length periodogram and the fact that $I_{u_d,L}(\omega)$ is uniformly bounded for all $L \geq 1$ and all $0 \leq |\omega| \leq \pi$ implies that the low-frequency power spectrum content of $u_d[n]$ can be reduced by reducing $E\{I_{u_d,L}(0)\}$.

It can be shown that

$$I_{u_d,L}(\omega) = \sum_{m=-(L-1)}^{L-1} R_{u_d,L}[m] c_L[m] e^{-j\omega n} \ , \tag{251}$$

where

$$R_{u_d,L}[m]=\begin{cases}\dfrac{1}{L-|m|}\displaystyle\sum_{n=0}^{L-1-|m|}u_d[n]u_d[n+|m|], & |m|\le L-1,\\ 0, & \text{otherwise}\end{cases} \tag{252}$$

and

$$c_L[m]=\begin{cases}\dfrac{L-|m|}{L}, & |m|\le L-1,\\ 0, & \text{otherwise.}\end{cases} \tag{253}$$

By assumption, $o_d[n]$ takes on the values 0 and 1 with equal probability, and as proven in [7], $o_d[n]$ is independent of $r_d[n]$, so the pmf of $u_d[n]$, as described by $\mathbf{A_e}$ and $\mathbf{A_o}$ in (220) , depends only on $u_d[n-1]$ and not on n. This implies $u_d[n]$ is stationary. Therefore, it follows from (252) that

$$E\left\{R_{u_d,L}[m]\right\}=R_{u_d}[m], \tag{254}$$

where

$$R_{u_d}[m]=E\left\{u_d[n]u_d[n+m]\right\} \tag{255}$$

is the autocorrelation of $u_d[n]$. It follows from the proof of Theorem 1 in [13] and the parallels between the first and second-order $s_d[n]$ sequence generators that $R_{u_d}[m]$ decreases exponentially with $|m|$. This, with (251), (253), and (254), implies that

$$\begin{aligned}\lim_{L\to\infty}E\left\{I_{u_d,L}(0)\right\}&=\lim_{L\to\infty}\sum_{m=-(L-1)}^{L-1}R_{u_d}[m]c_L[m]\\&=\lim_{L\to\infty}\sum_{m=-(L-1)}^{L-1}R_{u_d}[m].\end{aligned} \tag{256}$$

As proven in [7], the sequence whose pmf is described by $\mathbf{A_e}$ and $\mathbf{A_o}$ is a Markov process, and $\mathbf{A_e}$ and $\mathbf{A_o}$ are its state transition matrices conditioned on the value of $o_d[n]$

at each n. In the second-order successive requantizer, this Markov process is $u_d[n]$, as shown in (220). By assumption, $o_d[n]$ takes on the values 0 and 1 with equal probability, so the state transition matrix of $u_d[n]$ is given by $\mathbf{A}$ as defined in (230). This implies that

$$\mathbf{A}(N_u + 1 - i, N_u + 1 - u) = \Pr(u_d[n] = u \,|\, u_d[u-1] = i) \tag{257}$$

for all $i, u \in \{-N_u, \ldots, N_u\}$. Because $\mathbf{A}$ is primitive,

$$\lim_{k\to\infty} \mathbf{A}^k \tag{258}$$

exists and

$$\left(\lim_{k\to\infty} \mathbf{A}^k\right)\left(N_u + 1 - i, N_u + 1 - u\right) = \Pr\left(u_d[n] = u\right) \tag{259}$$

for all $i, u \in \{-N_u, \ldots, N_u\}$ [19] (the left side of (259) should be interpreted as the $(N_u + 1 - i)$th row, $(N_u + 1 - u)$th column entry of the matrix inside the first parentheses). Additionally, using identical reasoning to that in [13] to derive equation (94) in that paper, it follows from (221) and (257) that

$$\left(\mathbf{A}^{|m|}\mathbf{u}\right)\left(N_u + 1 - u\right) = E\left\{u_d[n+m] \,|\, u_d[n] = u\right\} \tag{260}$$

for all $u \in \{-N_u, \ldots, N_u\}$.

Using (255) and the law of total expectation, $R_{u_d}[m]$ can be evaluated as

$$\begin{aligned} R_{u_d}[m] &= \sum_{u=-N_u}^{N_u} E\left\{u_d[n]u_d[n+m] \,|\, u_d[n] = u\right\} \cdot \Pr\left(u_d[n] = u\right) \\ &= \sum_{u=-N_u}^{N_u} E\left\{u_d[n+m] \,|\, u_d[n] = u\right\} \cdot u \cdot \Pr\left(u_d[n] = u\right). \end{aligned} \tag{261}$$

With (221), (259), and (260), (261) can be rewritten as

$$R_{u_d}[m] = \sum_{u=-N_u}^{N_u} \left(\mathbf{A}^{|m|}\mathbf{u}\right)\left(N_u+1-u\right)\cdot\mathbf{u}(N_u+1-u)\cdot \left(\lim_{k\to\infty}\mathbf{A}^k\right)\left(1, N_u+1-u\right) \tag{262}$$
$$= \sum_{i=1}^{2N_u+1} \left(\mathbf{A}^{|m|}\mathbf{u}\right)(i)\cdot\mathbf{u}(i)\cdot\left(\lim_{k\to\infty}\mathbf{A}^k\right)(1,i).$$

With (256), this implies that

$$\lim_{L\to\infty} E\left\{I_{u_d,L}(0)\right\} = \sum_{m=-\infty}^{\infty}\sum_{i=1}^{2N_u+1}\left(\mathbf{A}^{|m|}\mathbf{u}\right)(i)\cdot\mathbf{u}(i)\cdot\left(\lim_{k\to\infty}\mathbf{A}^k\right)(1,i) \tag{263}$$

which is the expression in (229).

ACKNOWLEDGEMENTS

The authors would like to thank Professor Peter Kennedy for his helpful comments relating to this work.

Chapter 3, in full, has been submitted for publication to the IEEE Transactions on Circuits and Systems I: Regular Papers. E. Familier, I. Galton, 2016. The dissertation author is the primary investigator and author of this paper. Professor Ian Galton supervised the research which forms the basis for this paper.

FIGURES

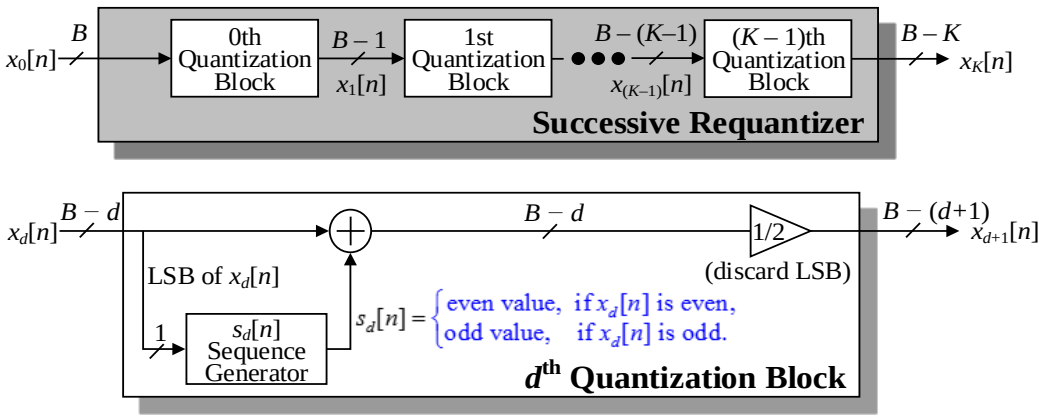

Figure 14: High-level diagram of a successive requantizer.

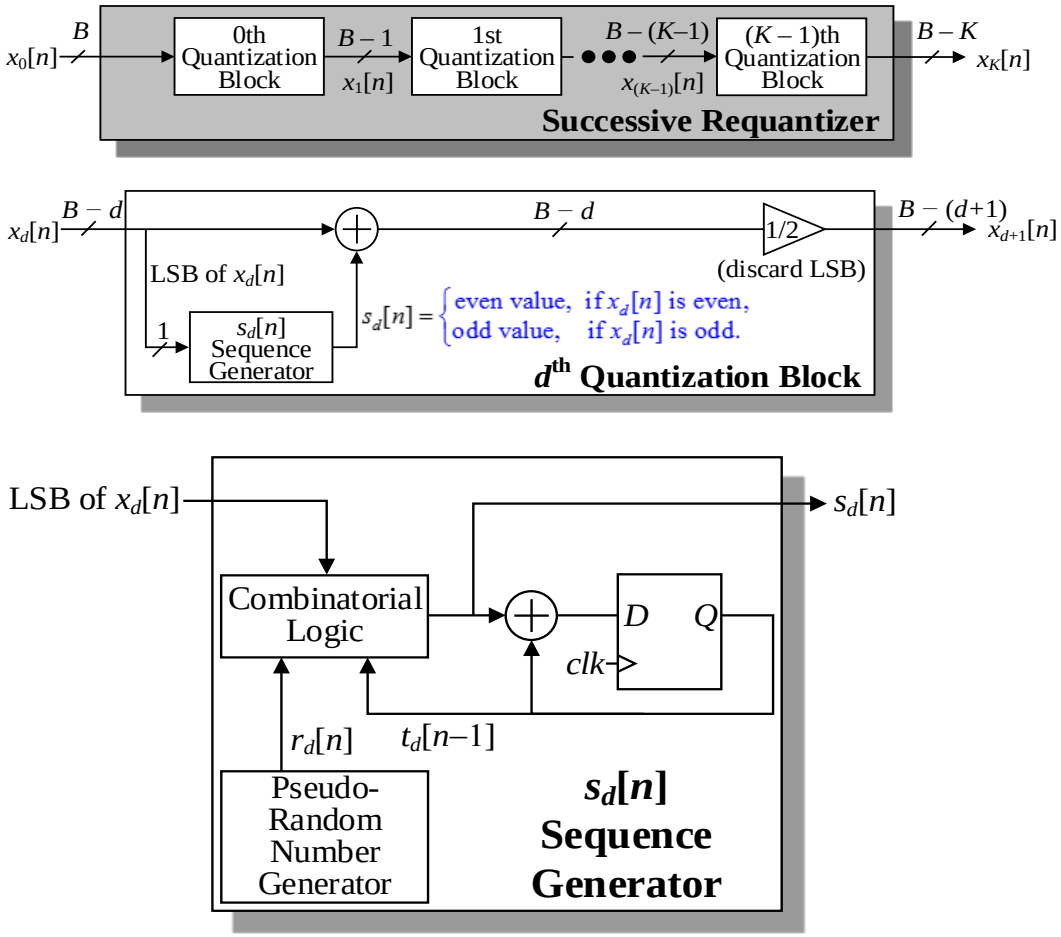

Figure 15: Block diagram of a first-order $s_d[n]$ sequence generator.

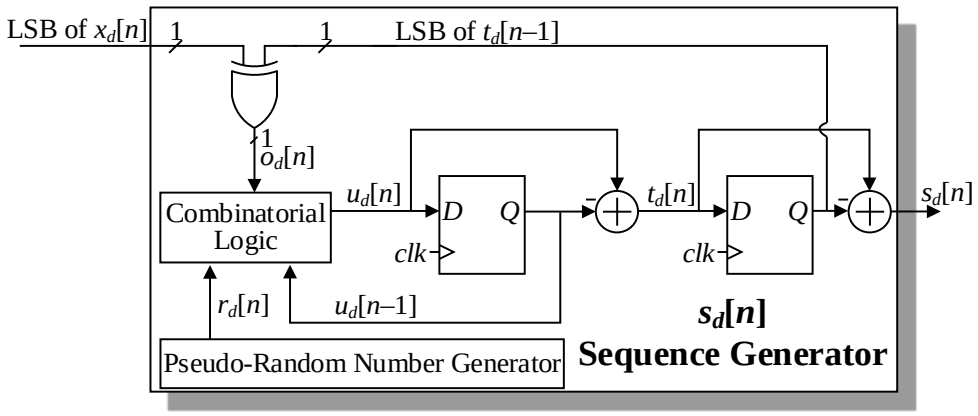

Figure 16: Block diagram of a second-order $s_d[n]$ sequence generator.

$o_d[n] = 0$		
$u_d[n-1]$	$r_d[n]$	$u_d[n]$
−2	≥ 0 and ≤ 3	−2
−2	≤ -1 or ≥ 4	0
−1	≤ -1 or ≥ 6	−1
−1	≥ 0 and ≤ 5	1
0	0 or 1	−2
0	≤ -1 or ≥ 4	0
0	2 or 3	2
1	≥ 0 and ≤ 5	−1
1	≤ -1 or ≥ 6	1
2	≤ -1 or ≥ 4	0
2	≥ 0 and ≤ 3	2

$o_d[n] = 1$		
$u_d[n-1]$	$r_d[n]$	$u_d[n]$
−2	≤ -1 or ≥ 4	−1
−2	≥ 0 and ≤ 3	1
−1	≥ 1 and ≤ 3	−2
−1	≤ -1 or ≥ 4	0
−1	0	2
0	≥ 0	−1
0	≤ -1	1
1	0	−2
1	≤ -1 or ≥ 4	0
1	≥ 1 and ≤ 3	2
2	≥ 0 and ≤ 3	−1
2	≤ -1 or ≥ 4	1

Figure 17: Example truth table for the combinatorial logic block described by the state transition matrices in (223), with $r_d[n] \in \{-8, -7, \ldots, 7\}$.

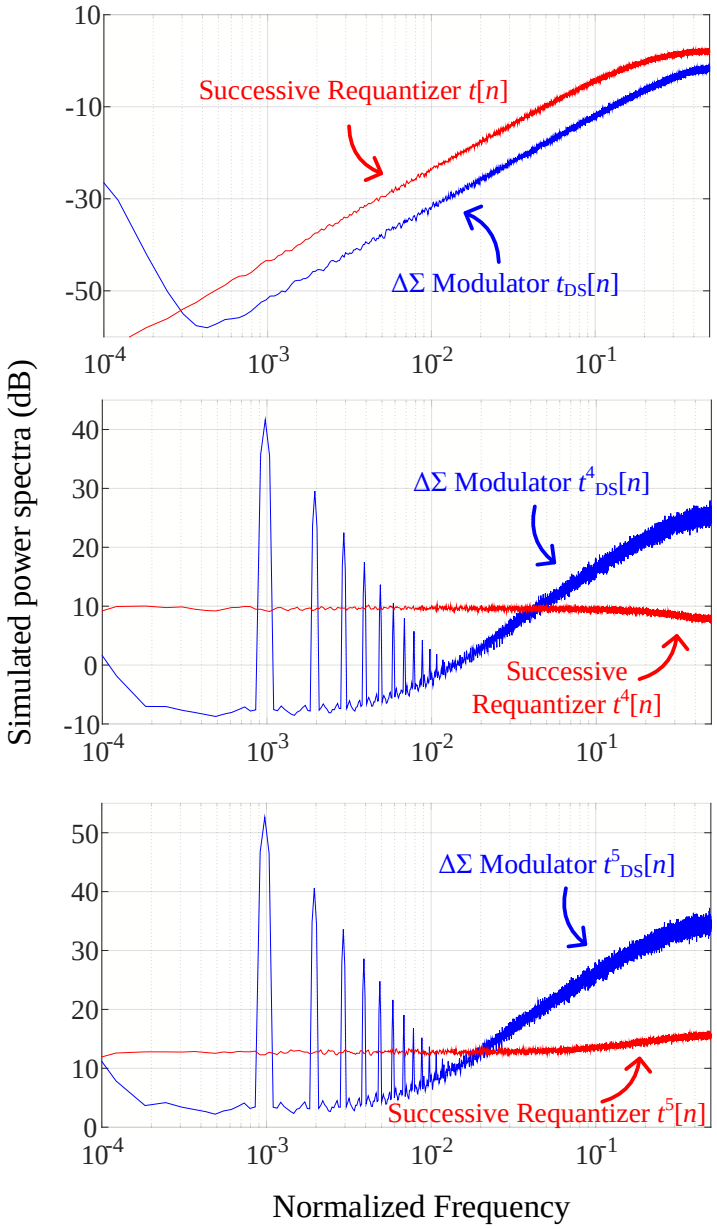

Figure 18: Simulated power spectra of the running sum of the quantization noise of a second-order successive requantizer that implements the state transition matrices in (223) and a second-order ΔΣ modulator before and after the application of fourth and fifth-order nonlinear distortion.

$o_d[n] = 0$		
$u_d[n-1]$	$r_d[n]$	$u_d[n]$
−2	≥ −512 and ≤ 153	0
−2	≥ 154	2
−1	≥ 0 and ≤ 55	−1
−1	≤ −1 or ≥ 56	1
0	≥ 0 and ≤ 178	−2
0	≤ −1 or ≥ 358	0
0	≥ 179 and ≤ 357	2
1	≤ −1 or ≥ 56	−1
1	≥ 0 and ≤ 55	1
2	≥ 154	−2
2	≥ −512 and ≤ 153	0

$o_d[n] = 1$		
$u_d[n-1]$	$r_d[n]$	$u_d[n]$
−2	≥ 0 and ≤ 6	−1
−2	≤ −1 or ≥ 7	1
−1	−512 or −511	−2
−1	≥ −510 and ≤ 155	0
−1	≥ 156	2
0	≥ 0	−1
0	≤ −1	1
1	≥ 156	−2
1	≥ −510 and ≤ 155	0
1	−512 or −511	2
2	≤ −1 or ≥ 7	−1
2	≥ 0 and ≤ 6	1

Figure 19: Example truth table for the combinatorial logic block described by the state transition matrices in (231), with $r_d[n] \in \{-512, -511, \ldots, 511\}$.

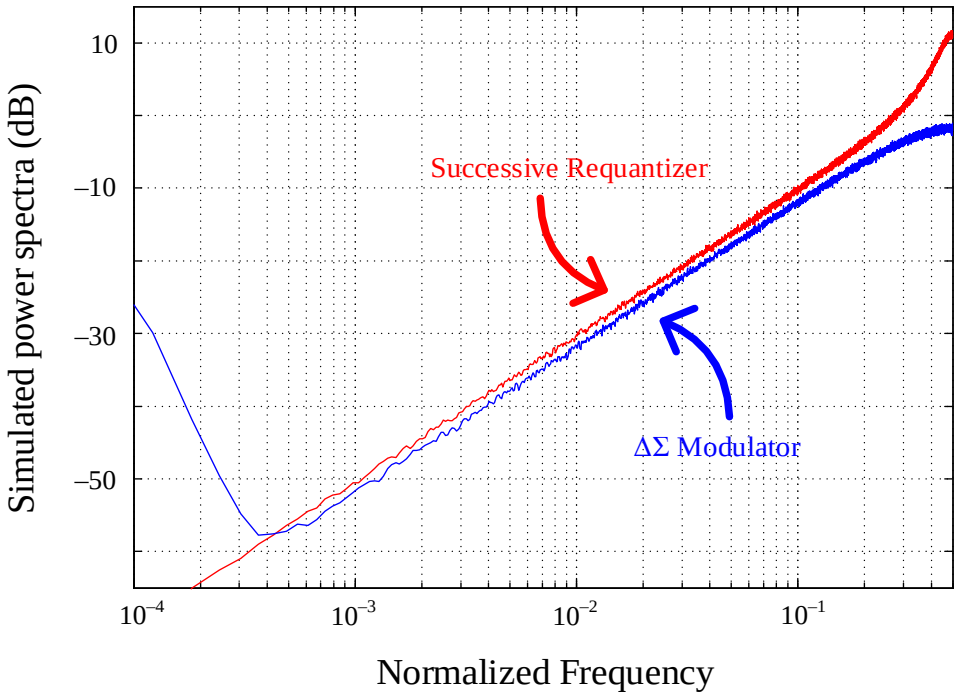

Figure 20: Simulated power spectra of the running sum of the quantization noise of a second-order successive requantizer that implements the state transition matrices in (231) and of a second-order ΔΣ modulator.

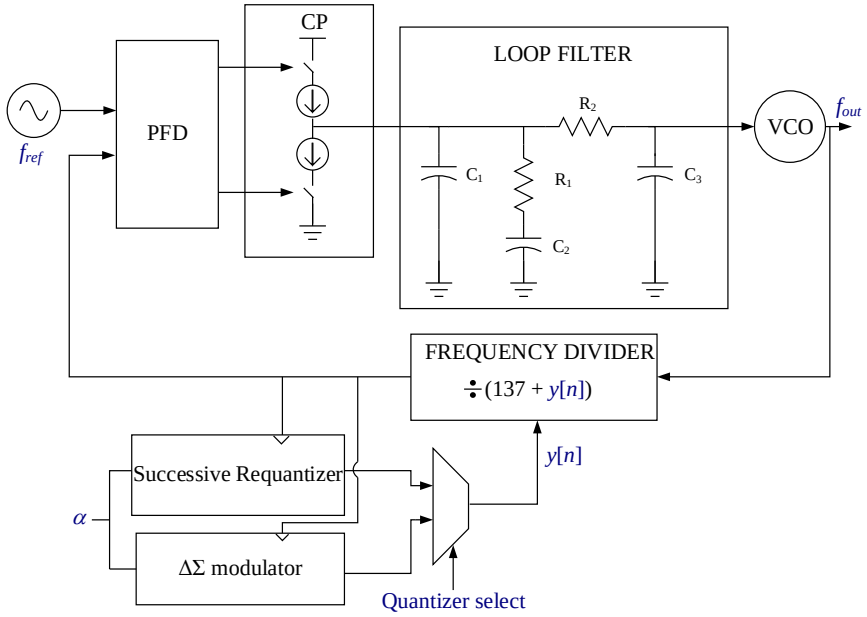

Figure 21: Block diagram of the PLL used in phase error simulations.

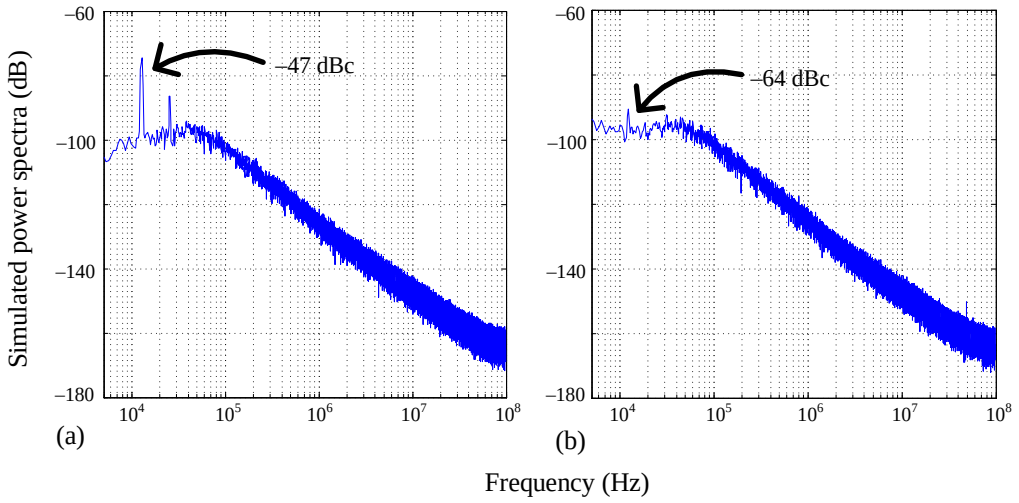

Figure 22: Simulated power spectra of the phase error of a 3.56 GHz output frequency, 45 kHz bandwidth PLL when its digital quantizer is implemented as (a) a second-order

ΔΣ modulator and (b) a second-order successive requantizer that implements the state transition matrices in (231).

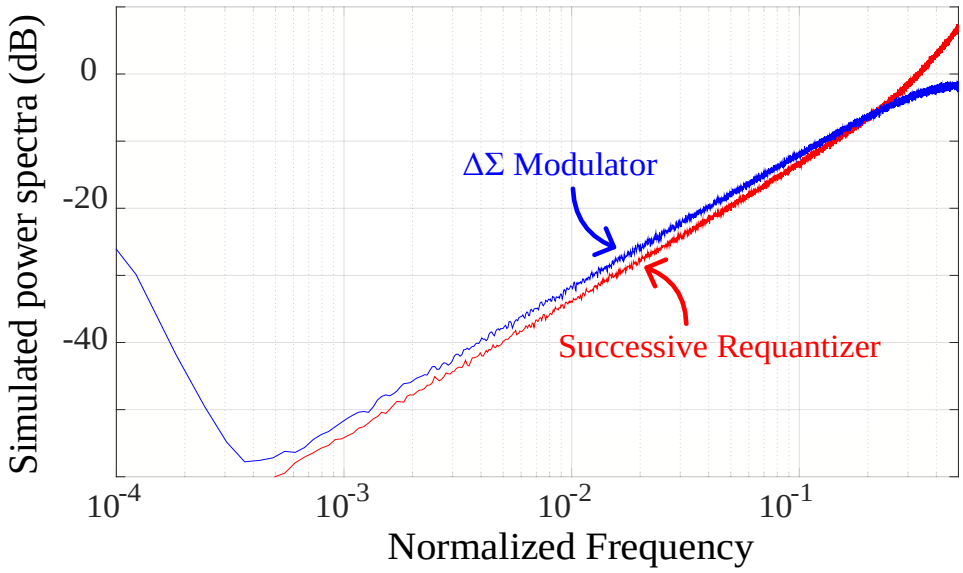

Figure 23: Simulated power spectra of the running sum of the quantization noise of a second-order successive requantizer that implements the state transition matrices in (232) and a second-order ΔΣ modulator.

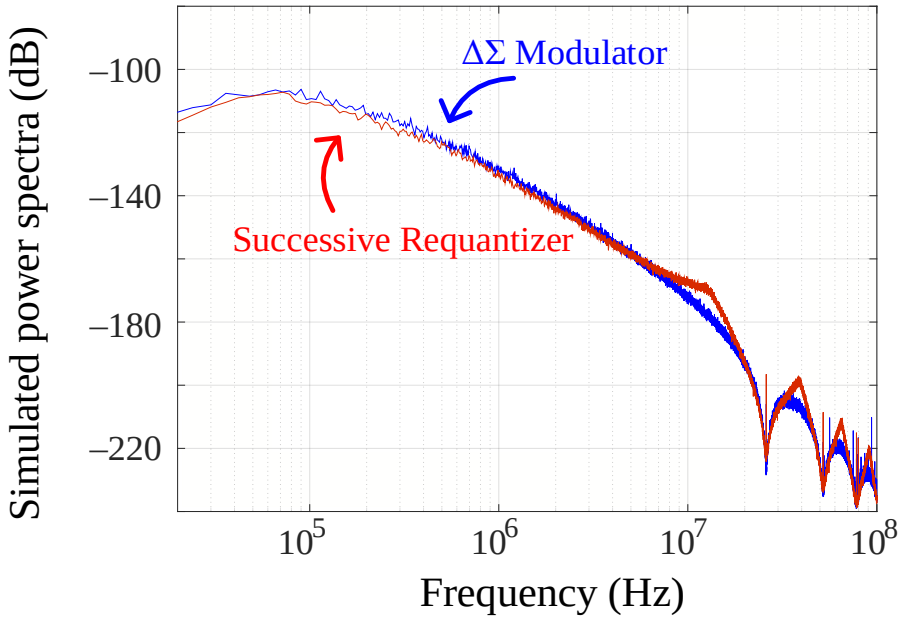

Figure 24: Simulated power spectra of the phase error of a 3.56 GHz output frequency, 45 kHz bandwidth PLL when its digital quantizer is implemented as a second-order ΔΣ modulator and a second-order successive requantizer that implements the state transition matrices in (232).

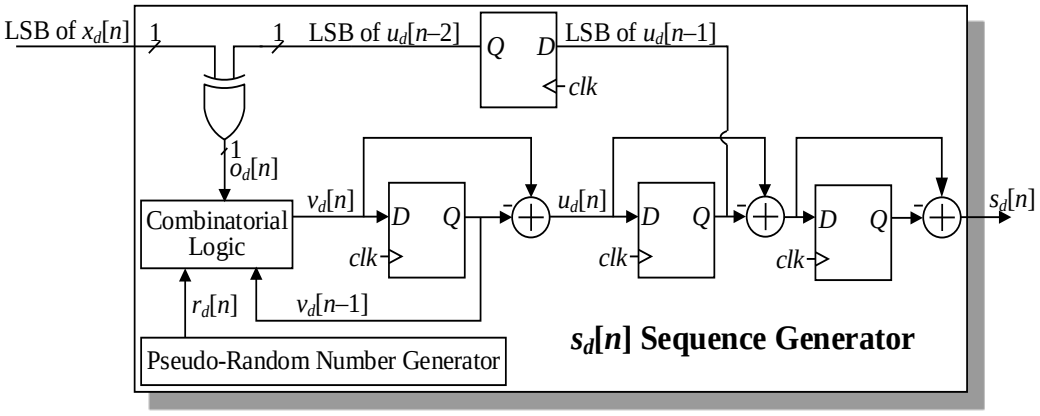

Figure 25: Block diagram of a third-order $s_d[n]$ sequence generator.

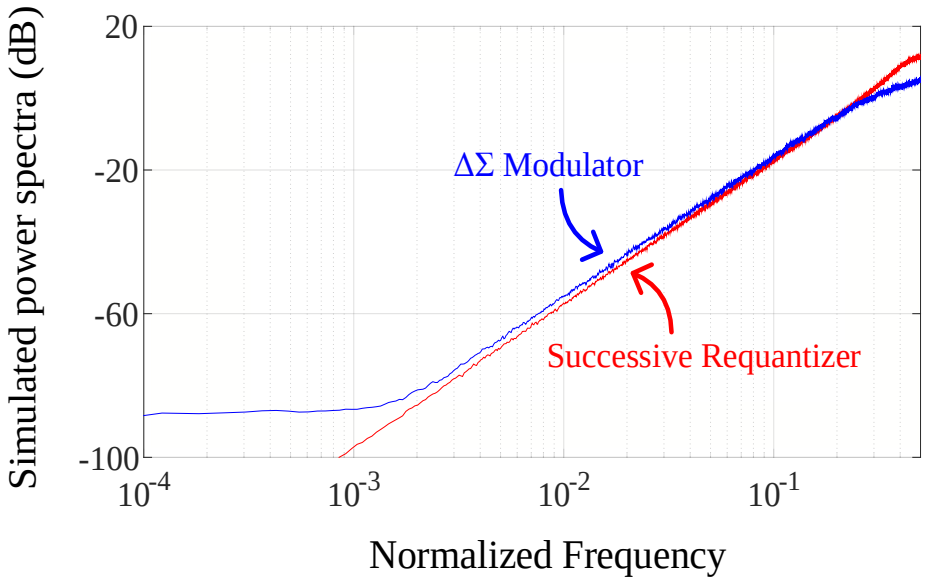

Figure 26: Simulated power spectra of the running sum of the quantization noise of a third-order successive requantizer that implements the state transition matrices in (232) and a third-order ΔΣ modulator.

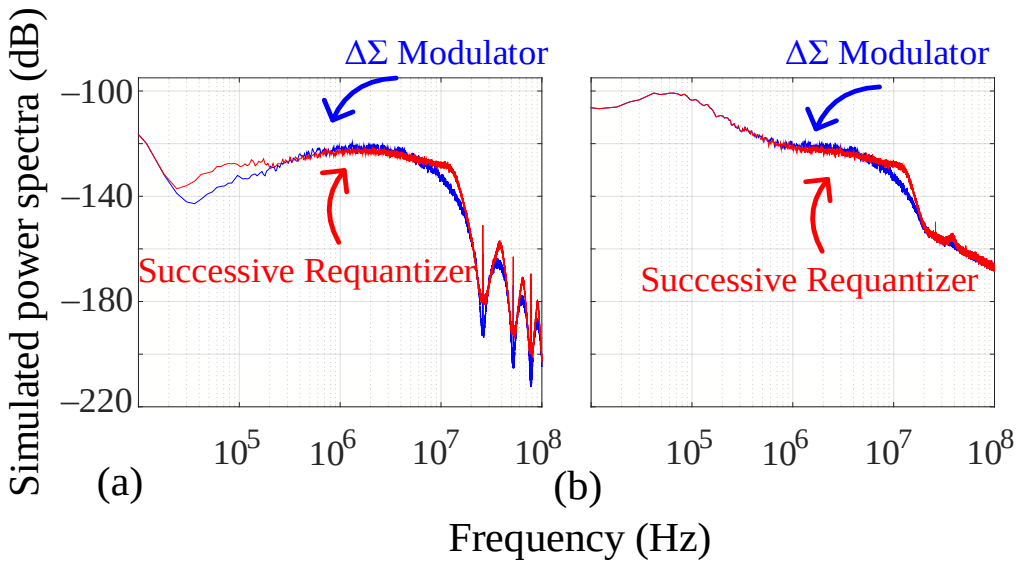

Figure 27: Simulated power spectra of the phase error of a 3.56 GHz output frequency, 85 kHz bandwidth PLL when its digital quantizer is implemented as a third-order ΔΣ modulator and a third-order successive requantizer that implements the state transition matrices in (232) when (a) there are no circuit noise sources modeled and when (b) reference and VCO noise are modeled.

REFERENCES

1. B. Miller, B. Conley, "A multiple modulator fractional divider," *Annual IEEE Symposium on Frequency Control*, vol. 44, pp. 559-568, Mar. 1990.

2. B. Miller, B. Conley, "A multiple modulator fractional divider," *IEEE Transactions on Instrumentation and Measurement*, vol. 40, no. 3, pp. 578-583, Jun. 1991

3. T. A. Riley, M. A. Copeland, T. A. Kwasniewski, "Delta-Sigma modulation in fractional-*N* frequency synthesis," *IEEE Journal of Solid-State Circuits*, vol. 28, no. 5, pp. 553-559, May 1993.

4. B. Razavi, Phase-Locking in High-Performance Systems: From Devices to Architectures, Wiley-Interscience, 2003.

5. B. De Muer, M. Steyaert, "A CMOS monolithic ΔΣ-controlled fractional-*N* frequency synthesizer for DCS-1800," *IEEE J. Solid-State Circuits*, vol. 37, no. 7, pp.835, 844, Jul. 2002.

6. S. Pamarti, L. Jansson, I. Galton, "A wideband 2.4 GHz ΔΣ fractional-*N* PLL with 1 Mb/s in-loop modulation," *IEEE J. Solid-State Circuits*, vol. 39, no. 1, pp. 49-62, Jan. 2004.

7. A. Swaminathan, A. Panigada, E. Masry, I. Galton, "A digital requantizer with shaped requantization noise that remains well behaved after nonlinear distortion," *IEEE Transactions on Signal Processing*, vol. 55, no. 11, pp. 5382-5394, Nov. 2007.

8. K. J. Wang, A. Swaminathan, I. Galton, "Spurious tone suppression techniques applied to a wide-bandwidth 2.4 GHz fractional-*N* PLL," *IEEE Journal of Solid-State Circuits*, vol. 43, issue 12, pp. 2787-2797, Dec. 2008.

9. H. Jian, Z. Xu, Y. Wu, F. Chang, "A compact 0.8-6 GHz fractional-*N* PLL with binary-weighted D/A differentiator and offset-frequency Δ-Σ modulator for noise and spurs cancellation," in *Proc. Symp. VLSI Circuits*, Jun. 16-18, 2009, pp. 186-187.

10. P. Su, S. Pamarti, "Mismatch shaping techniques to linearize charge pump errors in fractional-*N* PLLs," *IEEE Trans. Circuits Syst. I, Reg. Papers*, vol. 57, no. 6, pp. 1221-1230, Jun. 2010.

11. K. Hosseini, B. Fitzgibbon, M. P. Kennedy, "Observations concerning the generation of spurious tones in digital Delta-Sigma modulators followed by a

memoryless nonlinearity," *IEEE Trans. Circuits Syst. II, Exp. Briefs*, vol. 58, no. 11, pp. 714-718, Nov. 2011.

12. E. Familier, I. Galton, "A fundamental limitation of DC-free quantization noise with respect to nonlinearity-induced spurious tones," *IEEE Transactions on Signal Processing*, vol. 61, no, 16, Aug. 2013.

13. E. Familier, C. Venerus, I. Galton, "A class of quantizers with DC-free quantization noise and optimal immunity to nonlinearity-induced spurious tones," *IEEE Transactions on Signal Processing*, vol. 61, no, 17, Sep. 2013.

14. Z. Li, H. Mo, M. P. Kennedy, "Comparative spur performance of a fractional-*N* frequency synthesizer with a nested MASH-SQ3 divider controller in the presence of memoryless piecewise-linear and polynomial nonlinearities," *ISSC/CIICT* 2014, June 26-27, 2014, pp. 374-379.

15. M. P. Kennedy, H. Mo, Z. Li, G. Hu, P. Scognamiglio, E. Napoli, "The noise and spur delusion in fractional-*N* frequency synthesizer design," *ISCAS* 2015, May 24-27, pp. 2577-2580.

16. E. Fogleman, I. Galton, W. Huff, H. Jensen, "A 3.3-V single-poly CMOS audio ADC delta-sigma modulator with 98-dB peak SINAD and 105-dB peak SFDR," *IEEE Journal of Solid-State Circuits*, vol. 35, no. 3, Mar. 2000.

17. P. Perkins, "A theorem on regular matrices," *Pacific Journal of Mathematics*, vol. 11, no. 4, pp. 1529-1533, 1961.

18. A. V. Oppenheim, R. W. Schafer, J. R. Buck, *Discrete-Time Signal Processing*, 2nd. Ed. Englewood Cliffs, NJ, USA: Prentice-Hall, 1999.

19. A. Papoulis and S. U. Pillai, *Probability, Random Variables and Stochastic Processes*, Fourth Ed. New York, NY, USA: McGraw-Hill, 2002.

CHAPTER 4

A 3.35 GHZ FRACTIONAL-*N* PLL USING A NEW CLASS OF DIGITAL QUANTIZERS AND A LINEARITY-ENHANCEMENT TIMING SCHEME FOR SPURIOUS TONE MITIGATION

Abstract—This paper presents a 3.35 GHz fractional-*N* PLL optimized for fractional spurious tone mitigation. The PLL features a new class of second and third-order digital quantizers which replace the commonly-used second and third-order delta-sigma modulators to lower fractional spurious tones or lower PLL phase noise. It uses a new timing scheme, enabled by a modified frequency divider and a new phase and frequency detector, by which the PLL's charge pump response is greatly linearized without resorting to high power consumption circuit linearization techniques. The PLL has a 48 kHz bandwidth, uses a 26 MHz reference, dissipates 19.52 mW from 1.0 / 1.2 V supplies, and has an active area of 0.34 mm^2. Its worst-case in-band spurious tone and reference tone are –72 dBc and –79 dBc, respectively, and its phase noise is –87.5, –99, and –126 dBc / Hz at offsets of 10 kHz, 100 kHz, and 1 MHz, respectively.

This work was supported by the National Science Foundation and by IC fabrication provided by STMicroelectronics via their membership in the UCSD Center for Wireless Communications.
The authors are with the Department of Electrical and Computer Engineering, University of California at San Diego, La Jolla, CA 92093-0407 USA (e-mail: eythanfc@gmail.com).

I. INTRODUCTION

Fractional-*N* phase-locked loops (PLLs) are widely used in communication systems to down-convert and up-convert received and transmitted signals [1-2]. The goal of such PLLs is to generate a periodic output. In practice, however, non-idealities result in a deviation of the output from its ideal phase by a signal called *phase error*. The phase error can be decomposed into a stochastic component called *phase noise* and a periodic component which consists of *spurious tones*. The maximum power of both components is severely limited in relevant frequency bands by modern communication standards.

Fractional-*N* PLLs use coarse digital quantizers to control their output frequency [3-5]. Typically, the quantizer is implemented with a delta-sigma (ΔΣ) modulator, which generates highpass shaped, spurious tone-free quantization noise. The quantization noise ideally contributes a term proportional to a lowpass filtered version of its running sum to the PLL phase error. However, due to non-idealities in the PLL architecture and circuits, both the quantization noise and the quantization noise running sum are subjected to nonlinear distortion, a process which inevitably introduces spurious tones in the PLL phase error [6-17].

One technique to mitigate these spurious tones is to linearize key PLL circuits like the charge pump, but conventional designs usually achieve this at the expense of increased power consumption. Another technique is to replace the ΔΣ modulator with a digital quantizer that is better behaved in terms of nonlinearity-induced spurious tones [8, 9, 14, 17].

In [9], a new type of digital quantizer called the successive requantizer was implemented in a PLL for this purpose. In PLLs, the nonlinearities to which the quantization noise and its running sum are subjected are usually well-modeled by truncated memoryless power series [8, 9]. Therefore, the successive requantizer was designed to generate quantization noise $s[n]$ with the property that $s^p[n]$ for p = 1, 2, 3, 4, and 5 are free of spurious tones and such that the quantization noise running sum $t[n]$ has the property that $t^p[n]$ for p = 1, 2, and 3 are free of spurious tones. The PLL achieved record-setting spurious tone performance. However, the successive requantizer quantization noise was only first-order highpass shaped, so a phase noise cancelling technique was implemented to avoid an otherwise-significant quantization noise contribution to the PLL phase noise at low frequencies.

This work presents a 3.35 GHz PLL using a new generation of successive requantizers which produce second and third-order highpass shaped quantization noise to avoid this issue [17]. The successive requantizers are used as second and third-order ΔΣ modulator replacements to improve either PLL spurious tone performance or lower PLL phase noise. In particular, a second-order successive requantizer is implemented which achieves state-of-the-art fractional spurious tone performance at the expense of a slight PLL phase noise increase compared to a second-order ΔΣ modulator, and second and third-order successive requantizers are implemented which achieve good spurious tone performance and lower PLL phase noise compared to their ΔΣ modulator counterparts.

The work also presents a new PLL timing scheme, enabled by a modified frequency divider and a new phase and frequency detector, to improve PLL linearity and

reduce spurious tones further. The scheme allows linearizing the PLL charge pump response without resorting to high power consumption circuit linearization techniques.

II. HIGH-LEVEL ARCHITECTURE AND FUNCTIONALITY

A. Spurious Tone Generation in Fractional-*N* PLLs

The goal of a fractional-*N* PLL is to produce a periodic output with frequency $f_{\mathrm{PLL}} = f_{ref}(N + \alpha)$, where f_{ref} is the frequency of a reference oscillator, N is an integer, and $|\alpha| < 1$. A high-level diagram of a typical fractional-*N* PLL is shown in Fig. 28. It contains a phase and frequency detector (PFD), a charge pump, a lowpass loop filter, a voltage-controlled oscillator (VCO), a frequency divider, and a coarse digital quantizer which introduces DC-free quantization noise. The divider outputs a two-level signal with rising edges separated ($N + y[n]$) VCO periods on the nth reference period, where $y[n]$ is an integer-valued sequence generated by the digital quantizer. During the nth reference period, the PFD and charge pump output a current pulse with a width and polarity equal to the magnitude and sign, respectively, of the nth rising edge time of the divider minus that of the reference. The lowpass loop filter receives the charge pump current pulses and drives the VCO, whose output instantaneous frequency differs from its center frequency by an amount proportional to the loop filter's output voltage deviation from its center value. The PLL's feedback loop acts so as to zero the average charge pump output current, which sets the PLL average output frequency to f_{ref} time the average of ($N + y[n]$). The sequence $y[n]$ is generated to equal α on average and can be written as

$$y[n] = \alpha + s[n], \tag{264}$$

where $s[n]$ is the quantization noise.

The PLL output can be written as

$$v_{out}(t) = g(2\pi f_{ref}(N+\alpha)t + \theta(t)), \tag{265}$$

where $g(t)$ is a 2π-periodic function and $\theta(t)$ is the phase error of the PLL resulting from noise, including quantization noise [18]. As explained in the introduction, the phase error consists of phase noise and spurious tones. Typically, the most significant types of spurious tones are reference spurious tones, i.e. tones located at multiples of f_{ref}, and fractional spurious tones, i.e. tones located at multiples of αf_{ref}[19]. Depending on the value of α, fractional spurious tones may be located within the PLL's loop bandwidth, where they are not attenuated by the PLL's lowpass filtering.

Two mechanisms have been identified for the generation of fractional spurious tones [9]. The first mechanism is the parasitic coupling between VCO and reference lines. For example, intermodulation of the nth harmonic of the reference with the VCO produces a component with a frequency of $(N+\alpha)f_{ref} - Nf_{ref} = \alpha f_{ref}$. The coupling is usually most significant in the PFD and charge pump, as these circuits process signals aligned with both the VCO and the reference edges. The second mechanism is the nonlinear distortion of the quantization noise $s[n]$ and its running sum

$$t[n] = \sum_{k=0}^{n} s[k]. \tag{266}$$

[19] In the PLL output spectrum, reference and fractional spurious tones are located at offsets of multiples of f_{ref} and αf_{ref}, respectively.

As explained in the introduction, the nonlinearities in a PLL are usually well-modeled by truncated memoryless power series. This implies that the PLL phase error contains versions not only of $t[n]$ but of $s^p[n]$ and $t^p[n]$ for integers $p > 1$. Typically, the digital quantizer is implemented with a second or third-order ΔΣ modulator, i.e. a ΔΣ modulator with second or third-order highpass shaped quantization noise, respectively. Adding dither to the ΔΣ modulator ensures $s[n]$ and $t[n]$ are free of spurious tones. However, it does not ensure $s^p[n]$ or $t^p[n]$ are free of spurious tones for integers $p > 1$ [8, 9]. This sensitivity makes ΔΣ modulators poorly-behaved with respect to nonlinearity-induced spurious tones.

The PLL's nonlinearities can be attributed to both architectural and circuit non-idealities. An example of the former is the variation in the turn-on and turn-off times of the charge pump branch currents from reference period to reference period, as seen in the timing diagram of the PLL from Fig. 28. An example of the latter is the nonlinear response of the charge pump, which is typically the most dominant nonlinearity contributor in the PLL.

Nonlinear distortion of $s[n]$ can be mostly avoided by resynchronizing the divider output edges with those of the VCO [1]. Therefore, this work focuses on techniques to mitigate spurious tones due to nonlinear distortion of $t[n]$. The first technique is to use a second or third-order successive requantizer instead of a ΔΣ modulator. The successive requantizers can be optimized for low nonlinearity-induced spurious tones or low PLL phase noise. The second technique is to use a new PLL timing scheme to linearize the charge pump response. This is enabled by a modified frequency divider and a new PFD,

and results in significant spurious tones mitigation without the need for high power consumption circuit linearization techniques. The techniques are described in detail in the following two sub-sections.

B. Second and Third-Order Successive Requantizers

The PLL's digital quantizer can be switched between a second-order ΔΣ modulator, a third-order ΔΣ modulator, a low-spurs, second-order successive requantizer, a low-noise, second-order successive requantizer, and a low-noise, third-order successive requantizer. A high-level diagram of the successive requantizer, common to the three successive requantizers used, is shown in Fig. 29 [8]. Its sequences are all integer-valued and represented in two's complement format. It processes a 20-bit constant input sequence $x_0[n] = 2^{16}\alpha$ through 16 serially-connected quantization blocks and outputs a 4-bit output sequence $y[n]$. The dth quantization block, for each $d = 0, 1, \ldots, 15$, divides its input, $x_d[n]$, by two and quantizes the result by one bit such that its output sequence has the form

$$x_{d+1}[n] = \frac{x_d[n] + s_d[n]}{2}, \tag{267}$$

where $s_d[n]$ / 2 can be viewed as quantization noise. The $s_d[n]$ *sequence generator* generates $s_d[n]$ to have the same parity as $x_d[n]$ for all n (otherwise $x_{d+1}[n]$ would not be integer-valued) and with a small enough magnitude that $x_{d+1}[n]$ can be represented with one less bit than $x_d[n]$.

It can be shown that the quantization noise of the successive requantizer and its running sum can be written as

$$s[n] = \sum_{d=0}^{15} 2^{d-16} s_d[n] \tag{268}$$

and

$$t[n] = \sum_{d=0}^{15} 2^{d-16} t_d[n], \tag{269}$$

respectively, where

$$t_d[n] = \sum_{k=0}^{n} s_d[n] \tag{270}$$

for each d [8].

A second-order $s_d[n]$ sequence generator, i.e. one for which $s_d[n]$ is second-order highpass shaped, is shown in Fig. 30 [17]. It contains a pseudo-random number generator that outputs a sequence of 10-bit independent, identically and uniformly distributed pseudo-random variables $r_d[n]$, two difference blocks, and a combinatorial logic block that generates a bounded sequence $u_d[n]$ as a function of the lowest significant bit (LSB) of $x_d[n]$, $t_d[n-1]$, $u_d[n-1]$, and $r_d[n]$. The first difference block takes $u_d[n]$ and outputs $t_d[n]$, so

$$t_d[n] = u_d[n] - u_d[n-1]. \tag{271}$$

The second difference block takes $t_d[n]$ and outputs $s_d[n]$, so $s_d[n] = t_d[n] - t_d[n-1]$. Therefore, $s_d[n]$ is the result of differencing $u_d[n]$ twice.

It can be shown that if there exists a positive integer h_t such that $t_d^p[n]$ is free of spurious tones for $p = 1, 2, \ldots, h_t$ then $t^p[n]$ is free of spurious tones for $p = 1, 2, \ldots, h_t$ [14, 17]. Additionally, (269) implies that the PSD of $t[n]$ is determined by the PSD of the $t_d[n]$ sequences. Therefore, $t[n]$ inherits the noise and the nonlinearity-induced spurious

tone behavior of the $t_d[n]$ sequences. This, with (271), imply that the combinatorial logic block, which outputs $u_d[n]$, determines the statistical properties of $t[n]$.

The low-spurs and low-noise, second-order successive requantizers differ by their combinatorial logic block. That of the low-spurs version is described by the truth table in Fig. 31 and is designed to make $t[n]$, $t^2[n]$, and $t^3[n]$ free of spurious tones. This is done by ensuring that the autocorrelation functions of $t_d[n]$, $t_d{}^2[n]$, and $t_d{}^3[n]$ each converge to a constant asymptotically as their time spread increases [8, 14, 17]. The downside of this quantizer is its higher $t[n]$ PSD content compared to that of a second-order ΔΣ modulator, which results in slightly higher PLL phase noise. Additionally, the range of the quantization noise running sum of this quantizer is (– 8, 7), whereas that of a second-order ΔΣ modulator is (–4, 4). The increased range imposes larger charge pump output swing requirements. The combinatorial logic block of the low-noise, second order successive requantizer is described by the truth table in Fig. 32 with $z_d[n] = u_d[n]$ and is such that $t[n]$ is free of spurious tones. It does not ensure $t^2[n]$ and $t^3[n]$ are free of spurious tones. Rather, it is designed so that the PSD of $t[n]$ is lower than that of a second-order ΔΣ modulator at low and mid frequencies, which results in lower PLL phase noise at those frequencies. This is done by ensuring there is a high probability that $u_d[n]$ has a different sign than $u_d[n-1]$ for all n, which has the effect of displacing quantization noise power from low to high frequencies. As a result, the PSD of $t[n]$ of this quantizer is higher than that of a second-order ΔΣ modulator at high frequencies. In typical PLLs, high frequency quantization noise is heavily attenuated by the loop filter, so the quantization

noise contribution of this quantizer to the PLL phase noise is usually lower than that of a second-order ΔΣ modulator.

Fig. 33 shows the PSD of the quantization noise running sum of the low-spurs and low-noise, second-order successive requantizers and of a second-order ΔΣ modulator. The plot shows that at low and mid frequencies, the low-noise, second-order successive requantizer contributes the least amount of noise, followed by the second-order ΔΣ modulator. Fig. 34 shows the PSD of a nonlinearly-distorted version of the quantization noise running sum $t[n]$ given by

$$m[n] = 0.15t^3[n] + 0.32t^2[n] + 0.99t[n] - 0.23 \tag{272}$$

for the three second-order digital quantizers. The nonlinearity in (272) is representative of the strong nonlinear behavior a typical PLL might impose on $t[n]$ [8]. As seen in the figure, distorting the quantization noise running sum of the second-order ΔΣ modulator results in spurious tones. The same is true for the low-noise, second order successive requantizer, but the spurious tones generated are lower, although seemingly higher in quantity. As expected, the distorted quantization noise running sum of the low-spurs, second-order successive requantizers is free of spurious tones.

A third-order $s_d[n]$ sequence generator, i.e. one for which $s_d[n]$ is third-order highpass shaped, is shown in Fig. 35 [17]. It contains a pseudo-random number generator that outputs a sequence of 10-bit independent, identically and uniformly distributed pseudo-random variables $r_d[n]$ like in the second-order case, three difference blocks, and a combinatorial logic block that generates a bounded sequence $v_d[n]$ as a function of the lowest significant bit (LSB) of $x_d[n]$, $u_d[n-2]$, $v_d[n-1]$, and $r_d[n]$, where $u_d[n] = v_d[n] -$

$v_d[n-1]$ for all n. Reasoning similar to that used for the second-order $s_d[n]$ sequence generator shows that the statistical properties of $t[n]$ are determined by the output sequence of the combinatorial logic block.

The truth table of the combinatorial logic block of the low-noise, third-order successive requantizer is the same as that of the low-noise, second-order successive requantizer shown in Fig. 32 with $z_d[n] = v_d[n]$. Like its second-order counterpart, the low-noise, third-order successive requantizer is such that $t[n]$ is free of spurious tones, but does not ensure $t^2[n]$ and $t^3[n]$ are free of spurious tones. Rather, it is designed to make the PSD of $t[n]$ lower at low and mid frequencies than a third-order $\Delta\Sigma$ modulator at the expense of higher high frequency content.

Fig. 36 shows the PSD of the quantization noise running sum of the low-noise, third-order successive requantizer and of the third-order $\Delta\Sigma$ modulator. Fig. 37 shows the PSD of the nonlinearly-distorted version of the quantization noise running sum given by (272) for both third-order digital quantizers. As seen in the figures, the low-noise, third-order successive requantizer achieves lower quantization noise running sum at low and mid frequencies than the third-order $\Delta\Sigma$ modulator unless it is subjected to strong nonlinearities.

C. Proposed PLL with Linearity-Enhancement Timing Scheme

The PFD response can be linearized by forcing the PLL to lock at a phase offset, so that the reference and divider rising edge times are separated by a constant time on average every reference period. In [9], this was done by adding an offset pulse generator (OPG), which is an additional charge pump branch with a nominal current equal to that

of the upper charge pump branch but which is turned on on the reference rising edge and stays on for a fixed amount of time T_{OC}. With the OPG, the PLL's feedback loop adjusts the divider rising edges so that they arrive on average T_{OC} after the reference rising edges. As a result, the lower charge pump branch and the OPG are turned on at the same time but turned off at different times every reference period. This is problematic for linearity. Ideally, as the divider's rising edge time, which controls the turn-off time of the lower charge pump branch, is linearly varied with respect to the reference's rising edge time, the total amount of charge supplied by the charge pump during the reference period varies linearly. In practice, turning off one of the charge pump branch currents results in a transient that couples into the other branch's bias nodes via parasitic capacitances and modulates its current. Consider the charge $Q(t)$ supplied by the OPG and the lower charge pump branch during a reference period, as depicted in Fig. 38. The plots of Fig. 38a) show the current contributed by the OPG, $I_u(t)$, and by the lower charge pump branch, $I_d(t)$, in the case where the falling edge times of the switch control signal of the OPG, OFFSET, and of the lower charge pump branch, DOWN, are sufficiently separated. As seen in the plots, before t_1 the current sources contribute currents i_1 and i_2, so $Q(t)$ increases with slope $I_c(t) = i_1 + i_2$. At t_1, the OPG is turned off, and the resulting transient modulates $I_d(t)$ until time t_r, when $I_d(t)$ re-settles to i_2. At t_2, the lower charge pump branch is turned off, and between times t_r and t_2, $Q(t)$ increases with slope $I_c(t) = I_2$, whereas between t_1 and t_r, $I_c(t)$ varies between $i_1 + i_2$ and i_2. If t_2 were decreased by a small amount of time Δt, the total charge supplied during the reference period would decrease by $\Delta t \cdot I_c(t_2) = \Delta t \cdot i_2$. However, as illustrated in the plots of Fig. 38b), if Δt is sufficiently large, t_2 occurs before

$I_d(t)$ has time to re-settle to i_2, so the total charge supplied decreases by less than $\Delta t \cdot i_2$. Adding capacitance to the branches' bias nodes can decrease the magnitude of the transient coupling, but it also tends to slow down charge pump settling time, which hurts linearity.

A second problem with the above technique is that the OPG adds extra noise and hurts charge pump linearity by decreasing the charge pump output impedance, even though its only function in the PLL is to separate the reference and divider rising edges.

One solution to the first problem is to make the magnitude of the OPG current lower than that of the lower charge pump branch [19]. However, this solution still suffers from extra noise and charge pump output impedance degradation.

This work proposes adjusting the timing of the PLL to linearize the PFD and charge pump responses and lower the charge pump noise contribution to the PLL phase noise instead of using an OPG. The implemented PLL and its timing diagram are shown in Figs. 39 and 40. The timing is enabled by a new PFD and a modified frequency divider. A sampled loop filter is used to avoid large reference spurs [9]. As shown in the figures, the divider generates two signals for the PFD, v_{div0} and v_{div1}, with rising edges separated by 34 VCO periods. The PFD DOWN and UP signals control the lower and upper charge pump branch currents, respectively, but unlike conventional PLLs, DOWN is high from the rising edge of v_{div0} to the rising edge of v_{ref}, and UP is high from the rising edge of v_{ref} to the rising edge of v_{div1} if the rising edge of v_{ref} is located between the rising edges of v_{div0} and v_{div1} and low otherwise. If the upper and lower charge pump branch currents are equal, the PLL feedback loop acts so as to place the rising edges of v_{ref} in the mid-point

between the rising edges of v_{div0} and v_{div1} (i.e. 17 VCO periods after the rising edge of v_{div0}) on average. This zeros the average charge injected by the charge pump and linearizes the PFD response. Any deviation Δt of the rising edge time of v_{ref} from this mid-point results in a nominal supplied charge of $\Delta t(i_{up} + i_{down})$, where i_{up} and i_{down} are the nominal upper and lower charge pump branch currents, respectively. Therefore, unlike conventional PLLs, both the upper and lower charge pump branch currents contribute to the charge pump gain, so the effective charge pump current equals $i_{cp} = i_{up} + i_{down}$. Since the lower charge pump branch always turns off at the same time the upper charge pump branch turns on, the resulting transients always modulate the charge pump currents equally on every reference period, thereby avoiding the nonlinearity discussed previously. Also, since the charge pump's effective output current is $i_{up} + i_{down}$, each of the charge pump currents can be lower than what they would be in a conventional PLL with the same charge pump gain (e.g. half of what they would be if $i_{up} = i_{down}$). This results in lower thermal and 1 / f noise contributions, although this effect is partially cancelled by the total charge pump on-time being longer than in conventional designs. Finally, the charge pump output impedance is greatly improved, both by the currents being smaller than usual and by the charge pump branches not being on at the same time.

To achieve good linearity, the charge pump currents need to have sufficient time settle. The rising edge time of the reference varies from its average mid-point mostly by the digital quantizer's quantization noise running sum $t[n]$ times the VCO period during the nth reference period, so the minimum settling times of the lower and upper charge pump branch currents are approximately $(17 + \min\{t[n]\})T_{VCO}$ and $(17 - \max\{t[n]\})T_{VCO}$,

respectively, where T_{VCO} is the VCO period. For a second-order ΔΣ modulator these values are both $15T_{VCO}$, while for the low-spurs, second-order successive requantizer they are both $13T_{VCO}$.

The downside of the proposed timing is that the charge pump output needs to handle a larger voltage swing, as illustrated in Fig. 40. The increased output swing forces the charge pump output transistors and the capacitor C_{11} into more nonlinear regions of operation. Nonetheless, extensive simulations and the measurement results presented in Section IV demonstrate that the charge pump linearity can be improved significantly with the proposed timing scheme.

III. IMPLEMENTATION DETAILS

A. Timing

The PLL timing is that shown in Fig. 40. The divider generates two outputs for the PFD: v_{div0} and v_{div1}, the digital clock clk_{dig}, and the sampled loop filter switch control signal v_{sw}.

The divider, shown in Fig. 41, runs on 1.0 V, is built entirely with GP standard cells, and is based on the 2/3 cell multi-modulus divider presented in [20]. It uses six 2/3 cells but includes circuitry to automatically disconnect the last three, two or one cells depending on its modulus. This increases its modulus range from {64, 65, …, 127} (the range of a standard six 2/3 cell design) to {8, 9, …, 127}.

The divider is designed to cycle through eight different moduli: 8, 8, 8, N_0, 12, N_1, 12, and $N + y[n] - 90$, where N_0 and N_1 are integers such that $N_0 + N_1 = 42$, so that the sum of the moduli equals $N + y[n]$. The values of $N + y[n]$ can range from 98 to 217. For a reference frequency f_{ref} of 26 MHz, this implies that the divider can support PLL frequencies from 2.548 GHz to 5.642 GHz. The signal mod_1 is used to clock the four divider outputs before being resynchronized to a VCO edge, as shown in the timing diagram of the figure. The value of N_1 can be programmed via the SPI and represents a tradeoff between the charge pump's PLL phase noise contribution and its linearity: increasing N_1 increases the time between the rising edges of v_{div0} and v_{div1}, time during which the charge pump is on when the PLL is locked. This gives the charge pump branch currents more time to settle at the expense of adding more noise every reference period. All of the IC's measurements were done with the maximum possible value of N_1, 34, to optimize for charge pump linearity. The rising edge of clk_{dig} occurs at the same time as that of v_{sw}, time at which the charge pump is off when the PLL is locked. This avoids digital clocking noise from corrupting the charge pump branch currents via substrate-coupling.

B. PFD

The PFD runs on 1.2 V and is built with LP transistors. As seen in Fig. 42, it outputs the DOWN signal, which is high from the rising edge of v_{div0} to that of v_{ref}, and the UP signal, which is high from the rising edge of v_{ref} to that of v_{div1} if the rising edge time of v_{ref} is located within the time interval from the rising edge time of v_{div0} to that of v_{div1}. The latter is to avoid the PLL from locking when the rising edge of v_{ref} is outside of

the mentioned time interval, as illustrated in the figure. If the PLL were to lock this way, the charge pump would be on for the entire reference period instead of being on only when the sampled loop filter switch is open. Instead, if the rising edge of v_{ref} is located outside of the desired time interval, the UP signal stays low and the PLL's feedback loop acts to lower the VCO's frequency until the rising edge of v_{ref} is placed within the desired time interval. In such a situation, the DOWN signal can cause the charge pump output to be at its minimum voltage for several reference periods before the UP signal starts adjusting the charge pump output.

C. Charge pump and sampled loop filter

The charge pump, shown in Fig. 43, is based on wide-swing cascode currents mirrors, and is biased with an off-chip resistor. It runs on 1.2 V and is built with LP transistors. Its upper and lower branch currents can be independently adjusted in 125 μA steps from 125 μA to 725 μA, so the effective charge pump current i_{cp} ranges from 250 μA to 1500 μA . For the IC measurements, the UP and DOWN currents were each set to 500 μA. Mismatches between the UP and DOWN currents are not a significant concern, as the loop filter is sampled and only receives the total charge pump supplied charge during each reference cycle when the PLL is locked. The design was optimized for low noise to improve PLL phase noise and fast current settling times to improve linearity and, therefore, fractional spurious tone performance.

The sampled loop filter is that shown in Fig. 39. The loop filter switch is the same as that in [9] and was designed for optimal linearity and charge injection minimization with LP transistors. The two loop filter resistors R_1 and R_2 consist of series combinations

of unsilicided *N*+ poly resistors which can be switched on and off via the SPI to adjust their total resistance values. The on-chip loop filter capacitors C_{11}, C_{12}, and C_3 consist of parallel combinations of *N*-well *N*+ poly capacitors and stacked metal capacitors using metal levels two through five which can be switched on and off via the SPI to adjust their total capacitance values. The stacked metal capacitors have less capacitance per volume than the poly capacitors, but they are more linear. For the IC measurements, the loop filter resistors R_1 and R_2 were each set to 8.88 kΩ and the on-chip loop filter capacitors C_{11}, C_{12}, and C_3 were set to 34 pF, 34 pF, and 68 pF, respectively. The 2020 nF capacitor C_2 is implemented with two ceramic X7R 1 nF capacitors and one ceramic NP0 20 pF capacitor. The capacitors' bottom plates are connected to the charge pump's on-chip ground to avoid PLL phase noise from off-chip/on-chip ground node variations.

D. VCO

The VCO is a modified version of the LC-tank DCO core presented in [21]. The main difference is that the VCO uses two differentially-connected accumulator-mode *N*-well MOS varactors instead of the slow and fast FCE banks from [21]. The VCO runs on 1.0 V, has an SPI-controlled output center frequency which ranges from 3.0 GHz to 3.5 GHz, and has a gain k_{VCO} which varies from 4 MHz / V to 6 MHz / V. The relatively low value of k_{VCO} prevents the loop filter resistors from contributing significant PLL phase noise and ensures that the PLL's linearity is limited by the charge pump and C_{11}, as opposed to by the VCO.

E. Digital and SPI

The digital contains the five digital quantizers. The pseudo-random number generators for the successive requantizers and the ΔΣ modulators are implemented with one 201-register modified linear feedback shift register (LFSR) that outputs 160 independent, identically and uniformly distributed random bits every clock period [22]. When using a successive requantizer, each of the sixteen $s_d[n]$ sequence generators uses 10 bits of the LFSR output to form a uniformly distributed random variable which ranges from –512 to 511.

The digital and SPI both use GP transistors and were synthesized and placed-and-routed with the Synopsis Design Compiler and IC Compiler tools. They were synthesized and placed-and-routed separately and each have their own power supply to avoid digital quantizer clocking noise coupling into sensitive PLL nodes via the SPI output lines.

F. Power distribution

The die has six separate power domains: reference, analog feedforward (PFD, charge pump, sampled loop filter), VCO, divider, digital, and SPI. The IC has one global ground provided by a low-impedance metal mesh that covers the active layout wherever possible. The use of a single ground simplifies block-to-block communication as all signals are passed differentially with a ground shield, minimizing inter-supply current [21].

Each supply is heavily filtered with passive *RC* networks occupying any unused layout area. The analog feedforward supply was further sub-divided into three additional *RC*-filtered domains: PFD, charge pump, and sampled loop filter.

IV. MEASUREMENT RESULTS

The IC was fabricated in ST 65 nm single-poly, seven-copper CMOS process, and makes use of the dual-oxide (LP and GP transistors both available) as well as high-resistivity poly process options. Its die in Fig. 44 shows the VCO, divider (DIV), digital (DIG), SPI, loop filter, PFD, charge pump (CP), and reference circuit (XO). Its total area is 1.0 x 1.3 mm^2, and its active area, which includes all decoupling capacitors, is 0.34 mm^2. The IC's area and power breakdowns are given in Table I.

The IC is packaged in a QFN36 package with a ground paddle. Nine copies of the IC were produced. However, a mistake in the SPI design allowed only two of the nine copies of the IC to be tested. The measurement results from the two ICs were consistent, but only the results from one of them are presented, because the other IC had an issue that resulted in its PLL output power being very low.

The test board uses an Abracon ABM8G 26 MHz crystal for the reference oscillator and a TDK HHM1583B1 wideband RF balun to match the differential output buffer to the measurement equipment. Power to all supply domains except for the VCO's was provided by Analog Devices ADP171 voltage regulators with parallel 10 μF X7R ceramic capacitors. The VCO supply was provided by an Agilent E5052B signal source

analyzer's internal power supply, because it was found that the ADP171 regulators do not sufficiently attenuate low-frequency noise. The test board was connected to a motherboard that supplied power and USB communication to a PC.

The phase noise measurements were taken with the Agilent E5052B signal source analyzer, and the spurious tone measurements were taken with an Agilent E4448A spectrum analyzer.

The PLL's phase noise for a 3.35 GHz output with a 16.68 kHz fractional frequency offset when using the low-spurs, second-order successive requantizer is shown in Fig. 45. It is suspected that an output-power-limiting impedance mismatch limits the phase noise floor. By running multiple measurements with different PLL configuration parameters, the phase noise contributions of all the individual blocks were extrapolated to produce the plot shown in Fig. 45. By design, the VCO phase noise dominates the PLL phase noise at all but low frequencies, where the charge pump $1 / f$ noise is dominant.

Fig. 46 compares the measured PLL phase noise when using the five digital quantizers. The figure shows that, for the chosen PLL bandwidth of 48 kHz, the PLL phase noise when using the different digital quantizers differs noticeably only at offset frequencies between 10 kHz and 100 kHz. The low-noise, third-order successive requantizer and third-order ΔΣ modulator contribute the least amount of phase noise, followed by the low-noise, second-order successive requantizer, then the second-order ΔΣ modulator, and finally the low-spurs, second-order successive requantizer.

Fig. 47 shows the PLL output spectrum when using the low-spurs, second-order successive requantizer and when using the second-order ΔΣ modulator, for a fractional

offset of 16.68 kHz. The spectrum demonstrates the nonlinearity-induced spurious tone mitigation properties of the successive requantizer. This measurement was repeated several times for all fractional frequency offsets and the five digital quantizers to produce the plots in Fig. 48. Due to the SPI design mistake mentioned above, it was only possible to set the fractional frequency offset to most, but not all, of the desired values, so the plots contain some measurement gaps. The figure shows that the low-spurs, second-order successive requantizer and low-noise, third-order successive requantizer result in the lowest fractional spurious tones, followed by the third-order ΔΣ modulator, then the low-noise, second-order successive requantizer, and finally the second-order ΔΣ modulator. As seen from Figs. 33, 34, 46, and 48, the low-noise, second-order successive requantizer results in both a lower quantization noise PLL phase noise contribution at low and mid frequencies and lower fractional spurious tones than the second-order ΔΣ modulator, making it an ideal replacement for the second-order ΔΣ modulator in PLLs with sufficiently low bandwidths. As seen in Figs. 36 and 37, the low-noise, third-order successive requantizer can result in a lower or higher quantization noise PLL phase noise contribution depending on the strength of the PLL nonlinearities, and as seen in Figs. 46 and 48, it results in the same quantization noise PLL phase noise contribution and lower fractional spurious tones than the third-order ΔΣ modulator. The low-spurs, second-order successive requantizer results in very low fractional spurious tones-below –72 dBc-although its quantization noise PLL phase noise contribution is slightly higher than that of the second-order delta-sigma modulator.

The reference spurious tone, shown in Fig. 49, is –79 dBc. Due to the asymmetry of the negative and positive offset spurious tones, it is suspected that the origin of the –79 dBc tone is direct coupling. The open-loop VCO phase noise is shown in Fig. 50.

The PLL's measured performance is summarized in Table 2 along with that of the best comparable low fractional spurious tones PLLs published to date.

ACKNOWLEDGEMENTS

The authors are grateful to Kevin Rivas for test support, Colin Weltin-Wu for helpful discussions, Julian Puscar for digital development and support, Professor Gabriel Rebeiz for access to measurement equipment, and STMicroelectronics for IC fabrication and advice.

Chapter 4, in full, is currently being prepared for submission for publication of the material. E. Familier, I. Galton. The dissertation author is the primary investigator and author of this material. Professor Ian Galton supervised the research which forms the basis for this material.

FIGURES

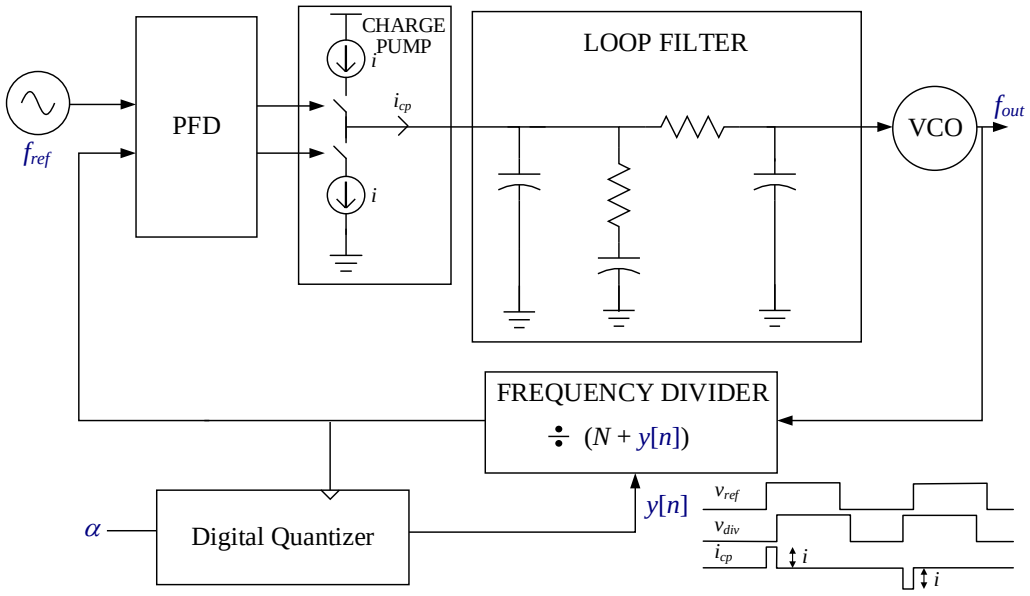

Figure 28: High-level diagram of a typical fractional-*N* PLL.

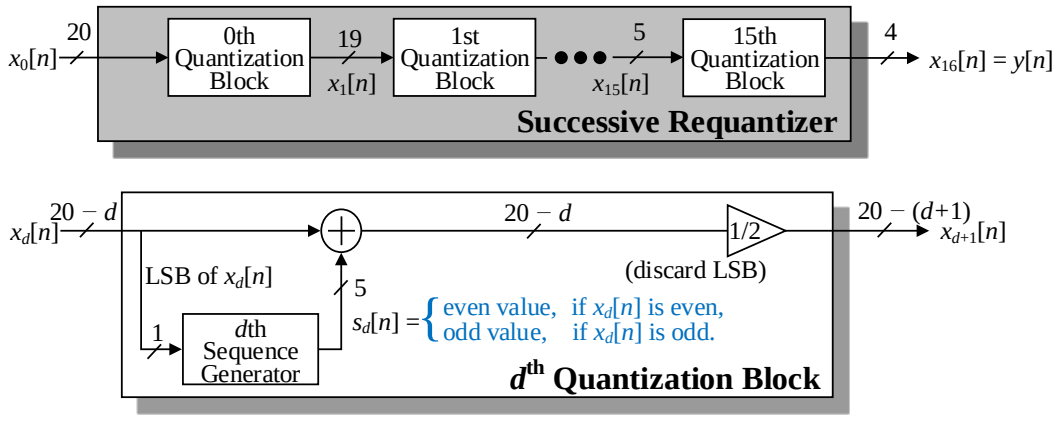

Figure 29: High-level diagram of the successive requantizer.

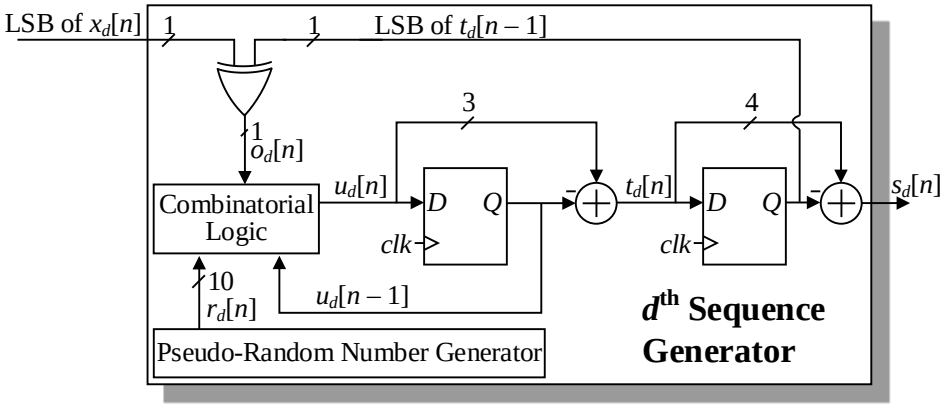

Figure 30: Block diagram of the second-order $s_d[n]$ sequence generator.

$o_d[n] = 0$			$o_d[n] = 1$		
$u_d[n-1]$	$r_d[n]$	$u_d[n]$	$u_d[n-1]$	$r_d[n]$	$u_d[n]$
−2	≥ −512 and ≤ 153	0	−2	≥ 0 and ≤ 6	−1
−2	≥ 154	2	−2	≤ −1 or ≥ 7	1
−1	≥ 0 and ≤ 55	−1	−1	−512 or −511	−2
−1	≤ −1 or ≥ 56	1	−1	≥ −510 and ≤ 155	0
0	≥ 0 and ≤ 178	−2	−1	≥ 156	2
0	≤ −1 or ≥ 358	0	0	≥ 0	−1
0	≥ 179 and ≤ 357	2	0	≤ −1	1
1	≤ −1 or ≥ 56	−1	1	≥ 156	−2
1	≥ 0 and ≤ 55	1	1	≥ −510 and ≤ 155	0
2	≥ 154	−2	1	−512 or −511	2
2	≥ −512 and ≤ 153	0	2	≤ −1 or ≥ 7	−1
			2	≥ 0 and ≤ 6	1

Figure 31: Truth table for the combinatorial logic block of the low-spurs, second-order successive requantizer, where $r_d[n] \in \{-512, -511, \ldots, 511\}$.

$o_d[n] = 0$		
$z_d[n-1]$	$r_d[n]$	$z_d[n]$
−1	= 0	−1
−1	≠ 0	1
0	X	0
1	≠ 0	−1
1	= 0	1

$o_d[n] = 1$		
$z_d[n-1]$	$r_d[n]$	$z_d[n]$
−1	X	0
0	< 0	−1
0	≥ 0	1
1	X	0

Figure 32: Truth table for the combinatorial logic block of the low-noise, second-order and low-noise, third-order successive requantizers, where $r_d[n] \in \{-512, -511, \ldots, 511\}$.

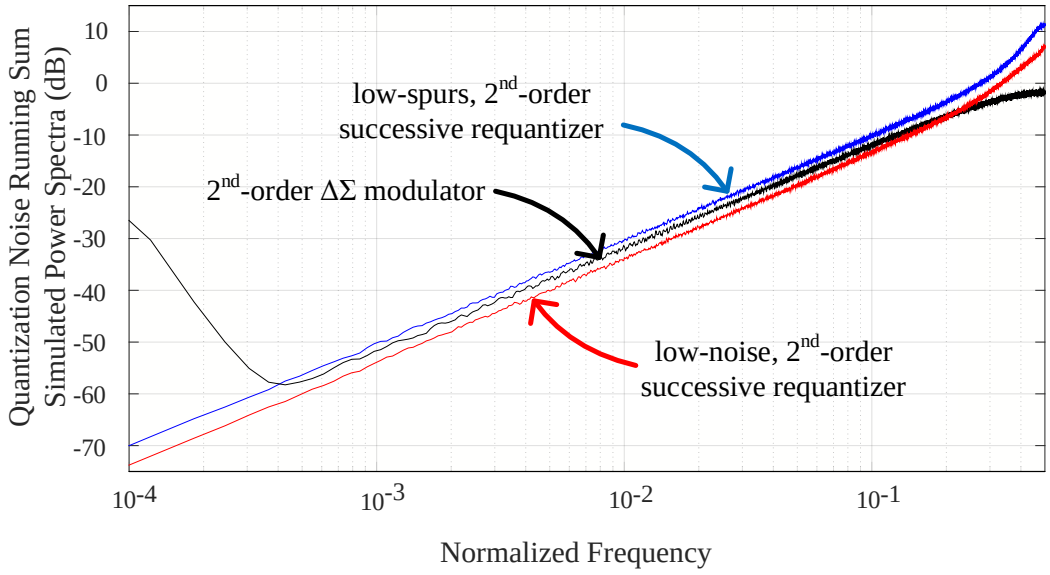

Figure 33: Comparison of the quantization noise running sum PSD of the low-spurs, second-order successive requantizer, the low-noise, second-order successive requantizer, and a second-order ΔΣ modulator.

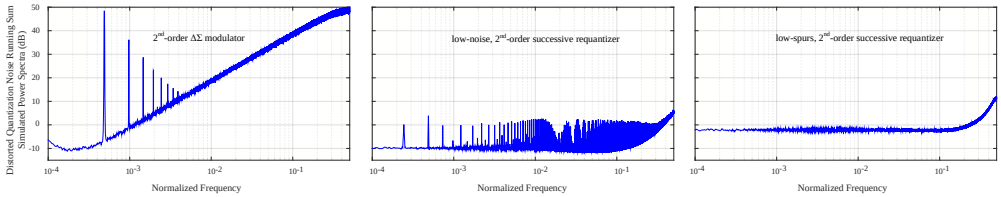

Figure 34: Comparison of a distorted version of the quantization noise running sum PSD of the low-spurs, second-order successive requantizer, the low-noise, second-order successive requantizer, and a second-order ΔΣ modulator.

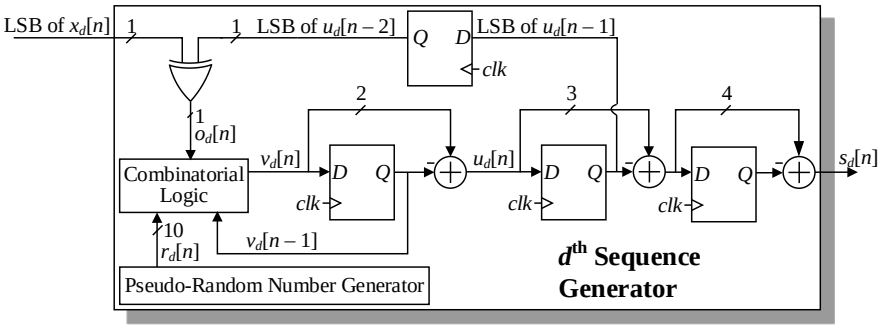

Figure 35: Block diagram of the third-order $s_d[n]$ sequence generator.

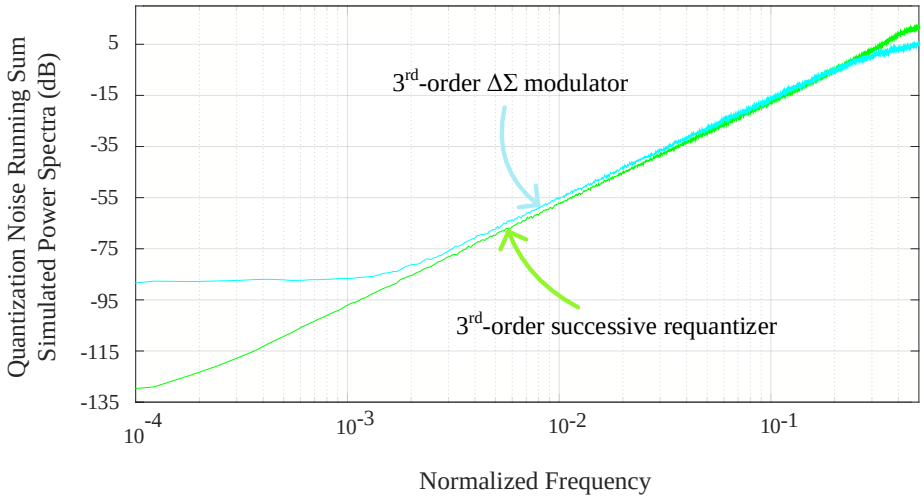

Figure 36: Comparison of the quantization noise running sum PSD of the low-noise, third-order successive requantizer and a third-order ΔΣ modulator.

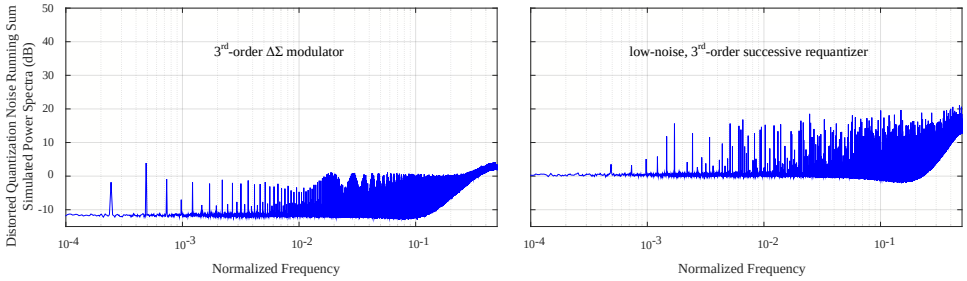

Figure 37: Comparison of a distorted version of the quantization noise running sum PSD of the low-noise, third-order successive requantizer and a third-order ΔΣ modulator.

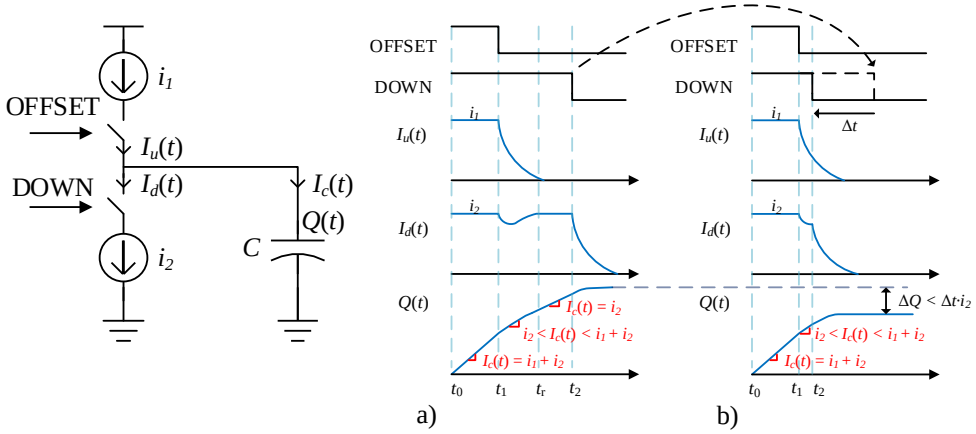

Figure 38: Charge pump nonlinearity example when using an offset pulse generator.

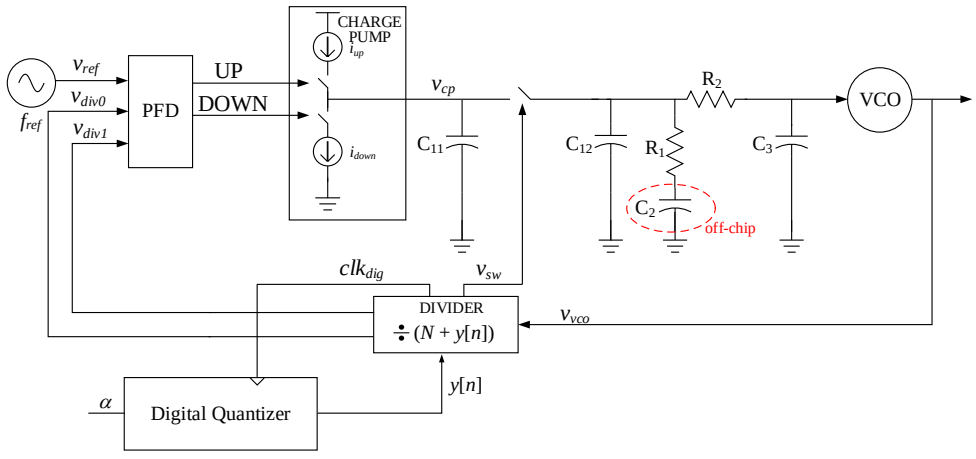

Figure 39: Block diagram of the implemented fractional-*N* PLL.

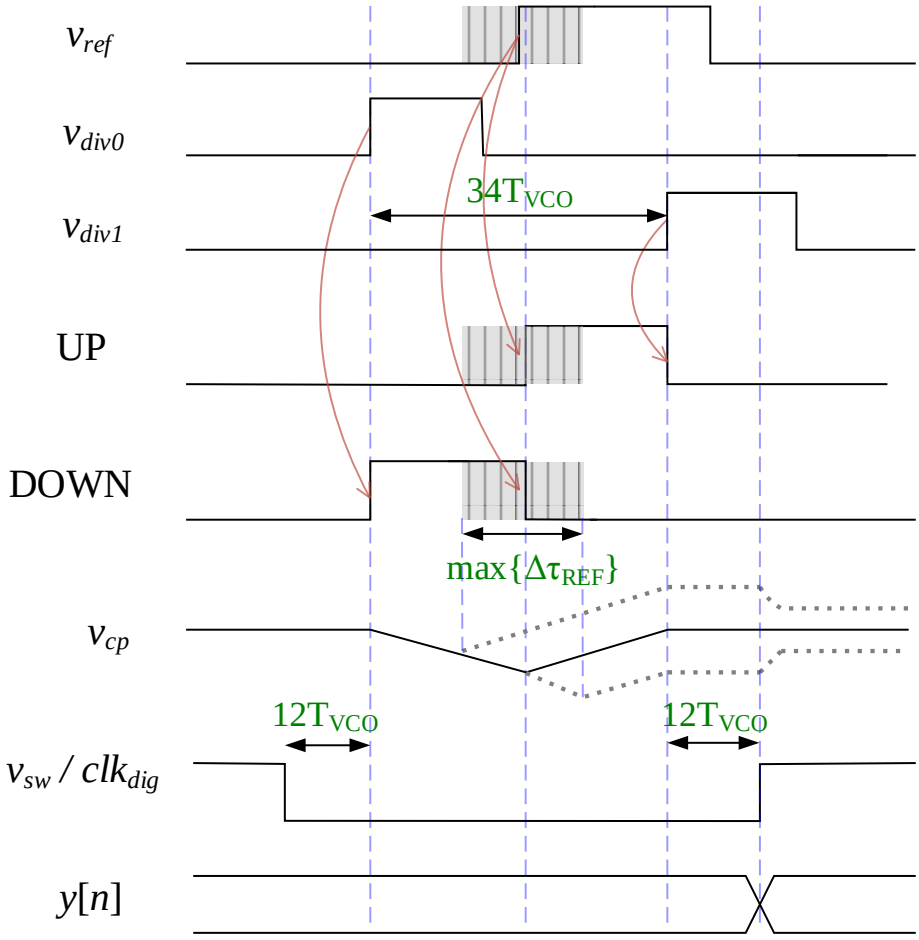

Figure 40: Timing diagram of the implemented fractional-*N* PLL.

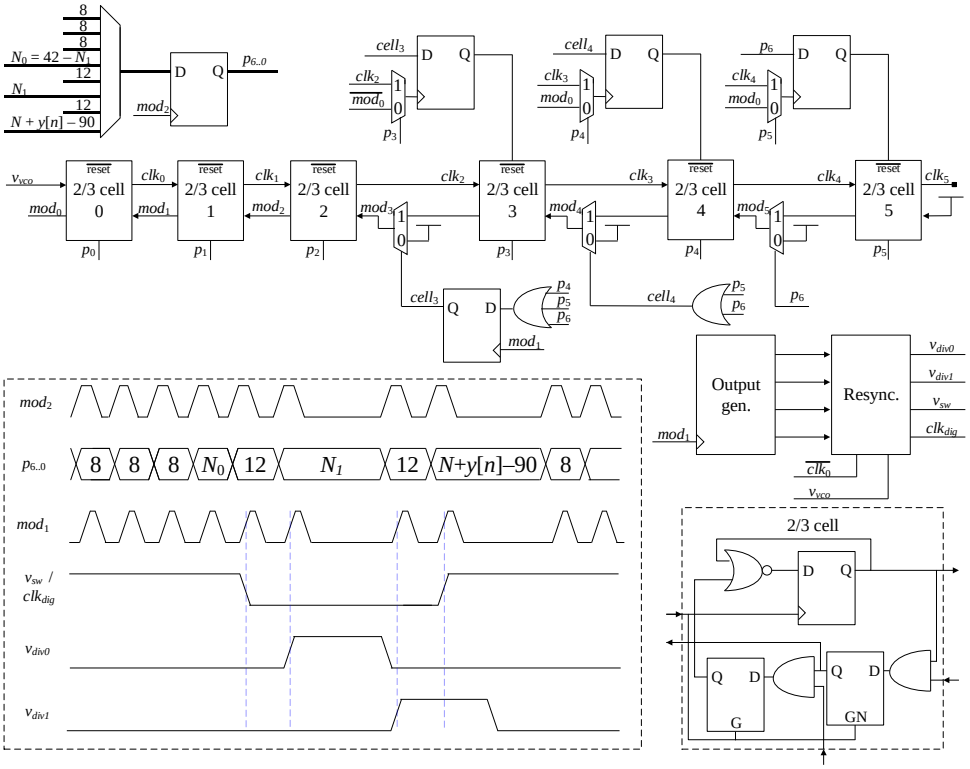

Figure 41: Implemented frequency divider.

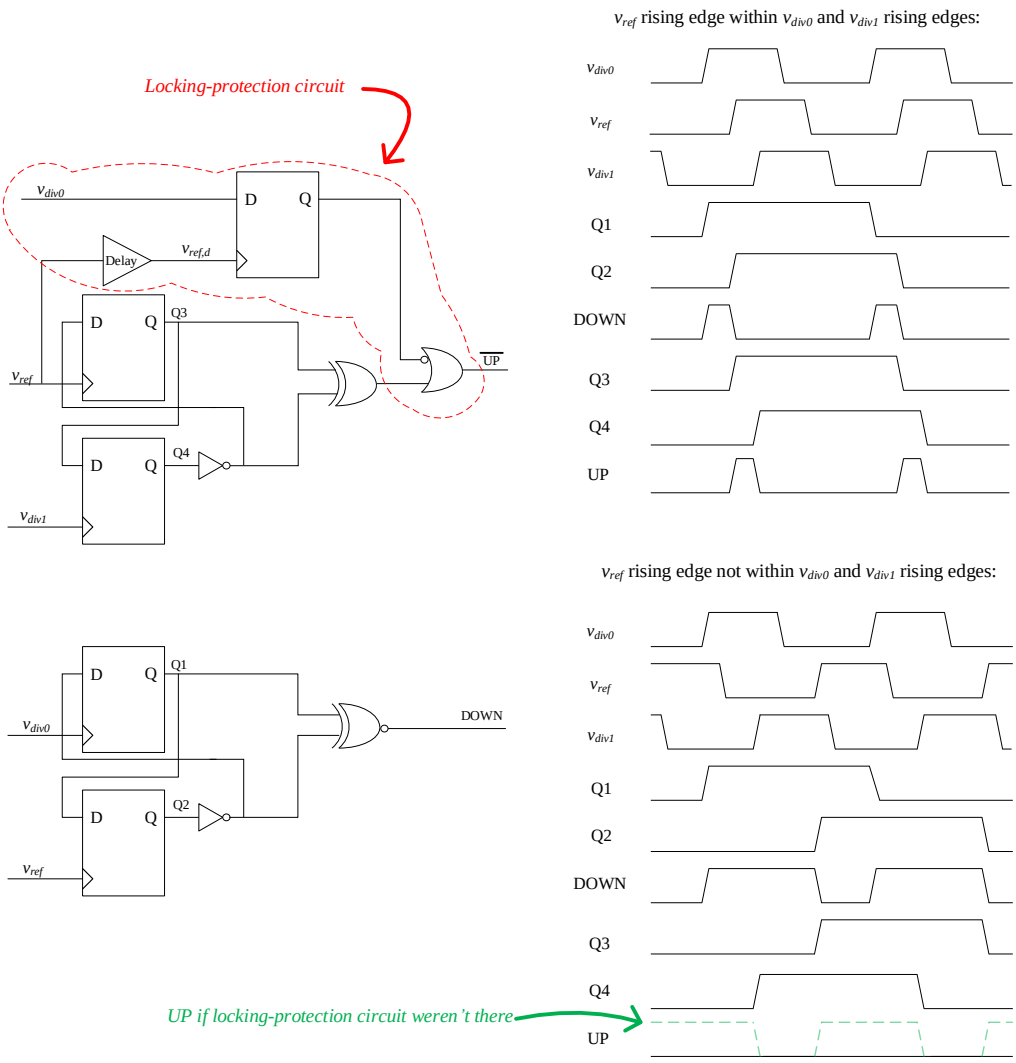

Figure 42: Block and timing diagrams of the PFD.

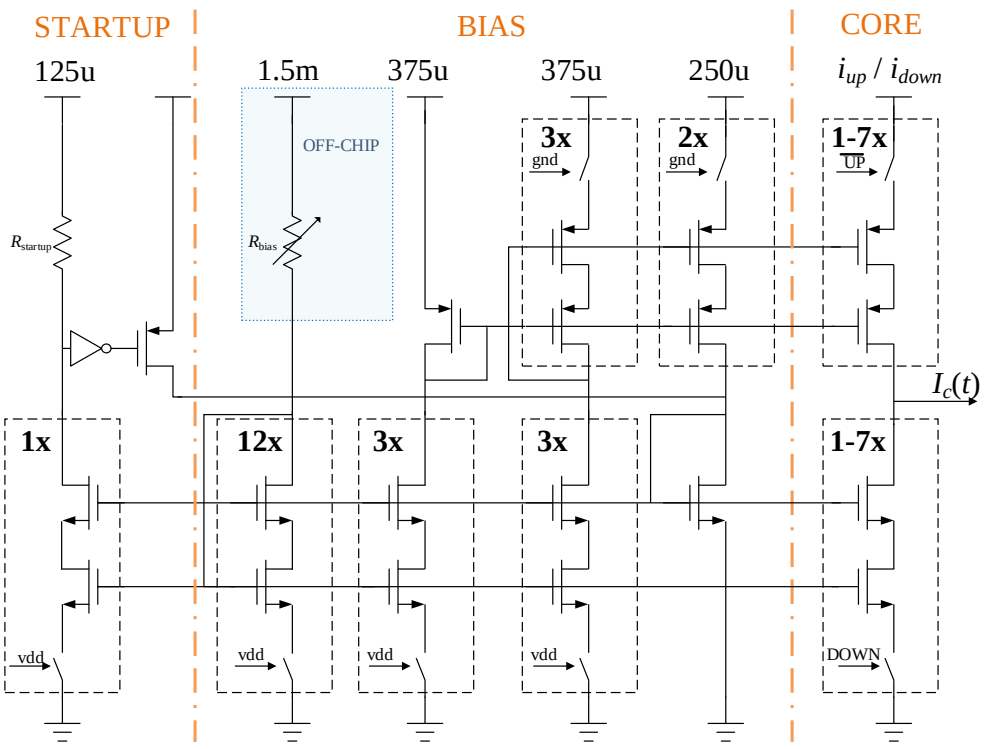

Figure 43: Implemented charge pump.

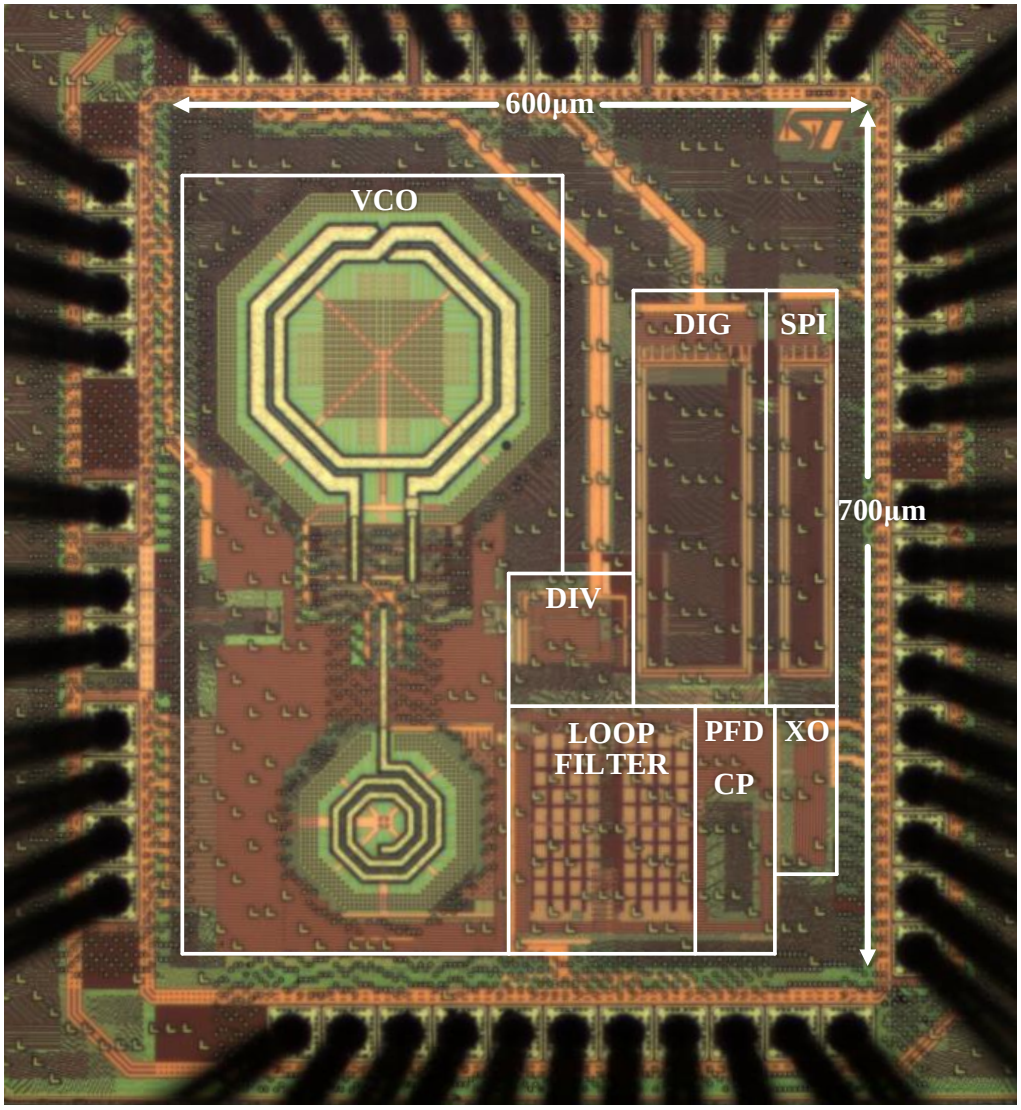

Figure 44: Die photograph.

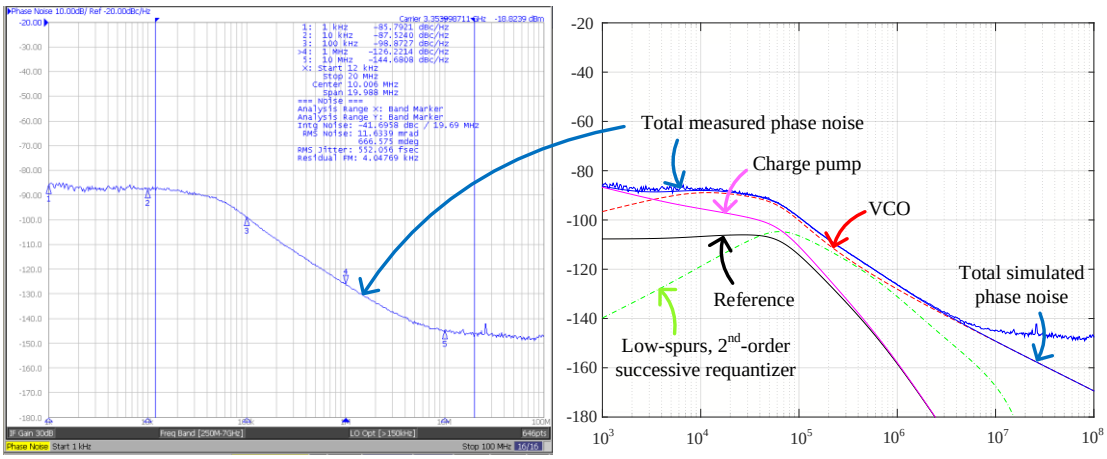

Figure 45: Measured PLL phase noise for a 3.35 GHz output and 16.68 kHz fractional frequency when using the low-spurs, second-order successive requantizer, and estimated phase noise contributions.

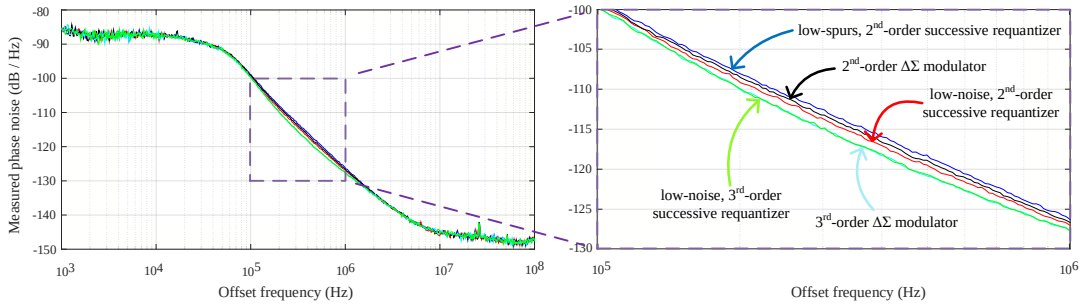

Figure 46: Comparison of the measured PLL phase noise for a 3.35 GHz output and a 16.68 kHz fractional frequency between the five digital quantizers.

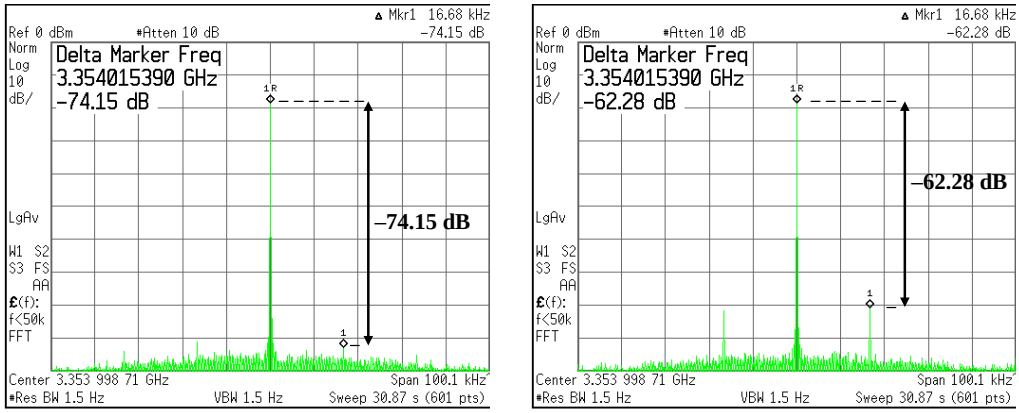

Figure 47: Measured PLL output spectrum showing the worst fractional spurious tone at 16.68 kHz when using a) the low-spurs, second-order successive requantizer and b) a second-order ΔΣ modulator.

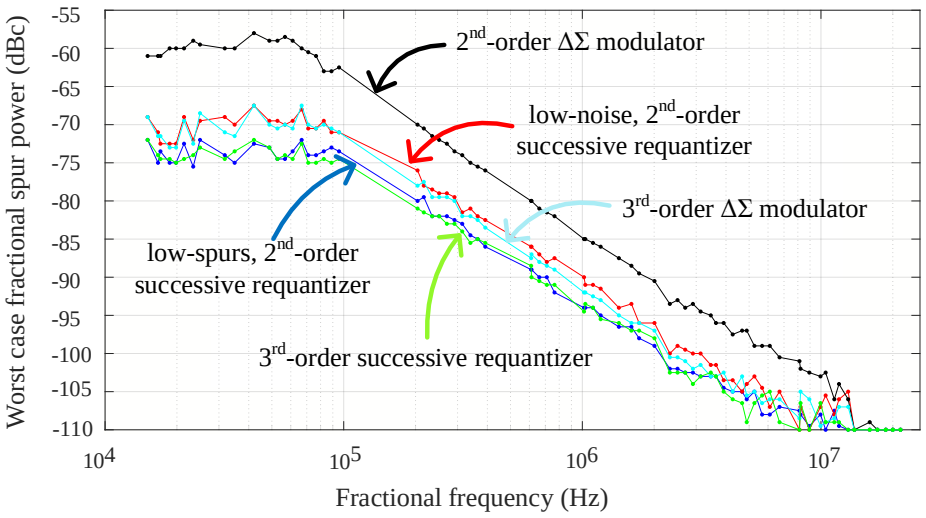

Figure 48: The largest measured fractional spurious tone as a function of the PLL fractional frequency for the five digital quantizers.

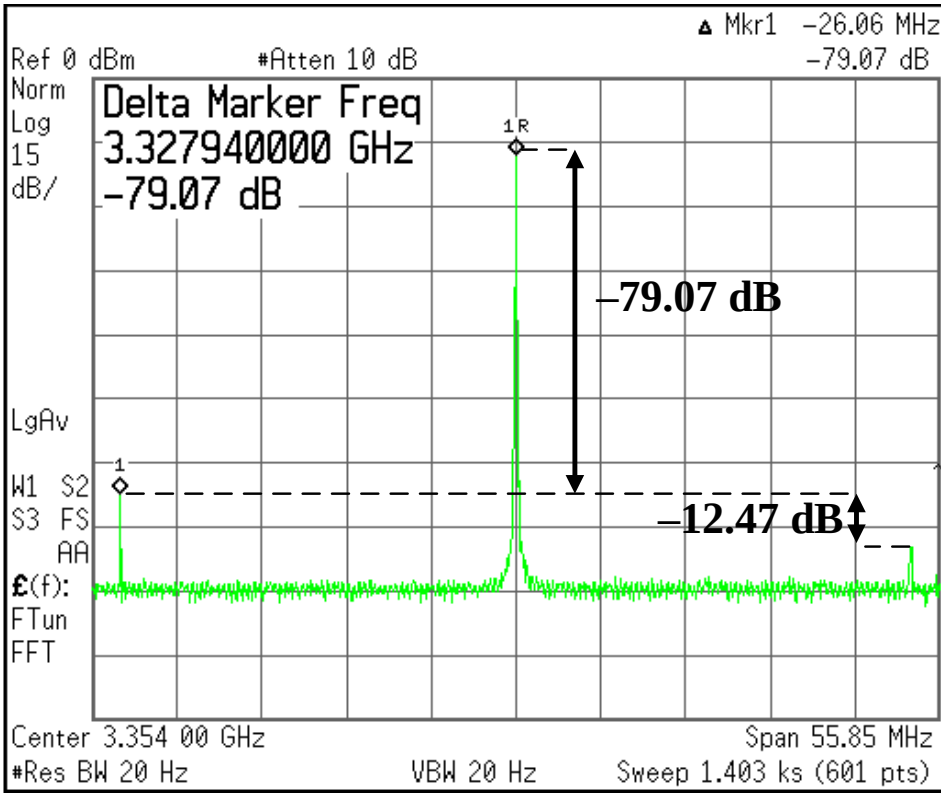

Figure 49: Measured PLL output spectrum showing the reference spur.

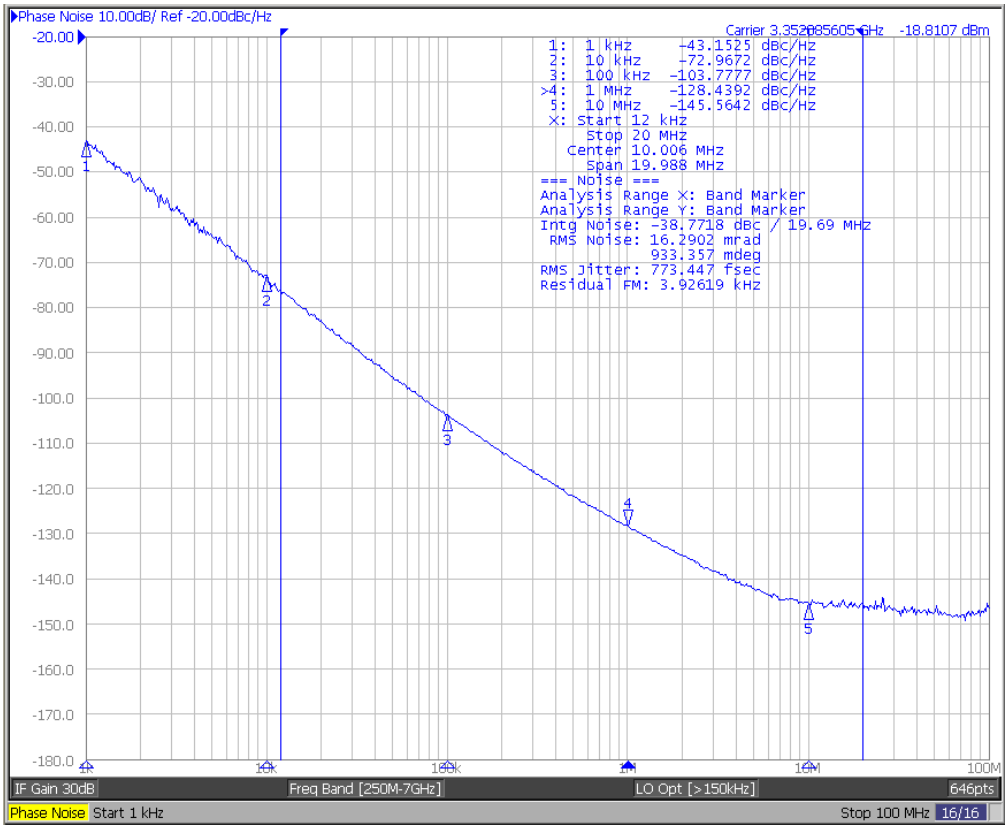

Figure 50: Measured open-loop VCO phase noise.

TABLES

Table 1: Area and power breakdown of the IC.

	Area (mm^2)	**Power (mW)**
VCO and External Buffer	0.21	VCO: 9.64, Buffer: 4.39
Crystal /Reference Circuitry	0.004	0.31
Digital	0.029	1.25
PFD, Charge Pump, Loop Filter	0.046	3.25
Divider	0.007	0.61
SPI	0.017	0.07
Decoupling capacitance	0.028	-
TOTAL	0.341	19.52

Table 2: Performance summary and comparison table.

	[9]	[19]	[23]	[24]	[25]	[26]	[27]	[28]	**This work**
Technology (nm)	180	40	180	40	65	55	65	180	65
Supply (V)	1.2	1.3	1.8	1.0 / 2.0	1.0	1.2	1.0	1.8	1.0 / 1.2
Power Consumption (mW)	66.42	17.5	28	9.1	20.9	36	11.5	46.98	19.52
Area (mm^2)	4.84 (package and die)	0.29	3.4 (PADs included)	0.046 active area	0.77 active area	0.68 core area	0.23	3.24 core area	0.341
Reference Frequency (MHz)	12	26	35	26	30	40	49.15	38	26
PLL Frequency (GHz)	2.4	3.88	2.1	2.002	3.57	5.8	2.68	6.12	3.35
Bandwidth (kHz)	975	250	700	1500	500	500	700	1000	48
In-band Phase Noise (dBc/Hz)	–98 @ 100 kHz	–105 @ 100 kHz	–104 in-band floor	–91 @ 5 kHz	–103 @ 100 kHz	–105 @ 100 kHz	–110.6 @ 100 kHz	–112 @ 300 kHz	–87.5 @10 kHz
Out-of-band Phase Noise (dBc/Hz)	–121 @ 3 MHz	–123 @ 1 MHz	–129 @ 2 MHz	–130 @ 26 MHz	–122 @ 3 MHz	–133 @ 10 MHz	–1318 @ 1 MHz	–130 @ 3 MHz	–126.2 @ 1 MHz
In-band Fractional Spur (dBc)(*)	–64	–65	–60	–70	–73.66(*)	–70	–63.1	–61	–72
Reference Spur (dBc)	–70	–100	Not stated	–87	–117	–94	–60	–78	–79

(*) Only one fractional spurious tone is reported.

REFERENCES

1. B. Razavi (Editor), Phase-Locking in High-Performance Systems: From Devices to Architectures, Wiley-Interscience, 2003.

2. T.H.Lee,*TheDesignofCMOSRadio-FrequencyIntegratedCircuits*, 2nd ed. Cambridge, U.K.: Cambridge Univ. Press, 2003.

3. B. Miller, B. Conley, "A multiple modulator fractional divider," *Annual IEEE Symposium on Frequency Control*, vol. 44, pp. 559-568, March 1990.

4. B. Miller, B. Conley, "A multiple modulator fractional divider," *IEEE Transactions on Instrumentation and Measurement*, vol. 40, no. 3, pp. 578-583, June 1991.

5. T. A. Riley, M. A. Copeland, T. A. Kwasniewski, "Delta-sigma modulation in fractional-*N* frequency synthesis," *IEEE Journal of Solid-State Circuits*, vol. 28, no. 5, pp. 553-559, May 1993.

6. B. De Muer, M. Steyaert, "A CMOS monolithic ΔΣ-controlled fractional-*N* frequency synthesizer for DCS-1800," *IEEE J. Solid-State Circuits*, vol. 37, no. 7, pp.835, 844, Jul. 2002.

7. S. Pamarti, L. Jansson, I. Galton, "A wideband 2.4 GHz ΔΣ fractional-*N* PLL with 1 Mb/s in-loop modulation," *IEEE J. Solid-State Circuits*, vol. 39, no. 1, pp. 49-62, Jan. 2004.

8. A. Swaminathan, A. Panigada, E. Masry, I. Galton, "A digital requantizer with shaped requantization noise that remains well behaved after nonlinear distortion," *IEEE Transactions on Signal Processing*, vol. 55, no. 11, pp. 5382-5394, Nov. 2007.

9. K. J. Wang, A. Swaminathan, I. Galton, "Spurious tone suppression techniques applied to a wide-bandwidth 2.4 GHz fractional-*N* PLL," *IEEE Journal of Solid-State Circuits*, vol. 43, issue 12, pp. 2787-2797, Dec. 2008.

10. H. Jian, Z. Xu, Y. Wu, F. Chang, "A compact 0.8-6 GHz fractional-*N* PLL with binary-weighted D/A differentiator and offset-frequency Δ-Σ modulator for noise and spurs cancellation," in *Proc. Symp. VLSI Circuits*, Jun. 16-18, 2009, pp. 186-187.

11. P. Su, S. Pamarti, "Mismatch shaping techniques to linearize charge pump errors in fractional-*N* PLLs," *IEEE Trans. Circuits Syst. I, Reg. Papers*, vol. 57, no. 6, pp. 1221-1230, Jun. 2010.

12. K. Hosseini, B. Fitzgibbon, M. P. Kennedy, "Observations concerning the generation of spurious tones in digital Delta-Sigma modulators followed by a memoryless nonlinearity," *IEEE Trans. Circuits Syst. II, Exp. Briefs*, vol. 58, no. 11, pp. 714-718, Nov. 2011.

13. E. Familier, I. Galton, "A fundamental limitation of DC-free quantization noise with respect to nonlinearity-induced spurious tones," *IEEE Transactions on Signal Processing*, vol. 61, no, 16, Aug. 2013.

14. E. Familier, C. Venerus, I. Galton, "A class of quantizers with DC-free quantization noise and optimal immunity to nonlinearity-induced spurious tones," *IEEE Transactions on Signal Processing*, vol. 61, no, 17, Sep. 2013.

15. Z. Li, H. Mo, M. P. Kennedy, "Comparative spur performance of a fractional-*N* frequency synthesizer with a nested MASH-SQ3 divider controller in the presence of memoryless piecewise-linear and polynomial nonlinearities," *ISSC/CIICT* 2014, June 26-27, 2014, pp. 374-379.

16. M. P. Kennedy, H. Mo, Z. Li, G. Hu, P. Scognamiglio, E. Napoli, "The noise and spur delusion in fractional-*N* frequency synthesizer design," *ISCAS* 2015, May 24-27, pp. 2577-2580.

17. E. Familier, I. Galton, "Second and Third-Order Noise Shaping Digital Quantizers for Low Phase Noise and Nonlinearity-Induced Spurious Tones in Fractional-*N* PLLs," *IEEE Trans. Circuits Syst. I, Reg. Papers*, accepted for publication.

18. A. Hajimiri and T. H. Lee, "A general theory of phase noise in electrical oscillators," *IEEE J. Solid-State Circuits*, vol. 33, no. 2, pp. 179–194, Feb. 1998.

19. Y. L. Hsueh, L. C. Cho, C. H. Shen, Y. C. Tsai, T. C. Chueh, T. Y. Chang, J. L. Hsu, J. H. C. Zhan, "A 0.29mm^2 Frequency Synthesizer in 40nm CMOS with 0.19ps$_{rms}$ Jitter and <-100dBc Reference Spur for 802.11ac," *2014 IEEE International Solid-State Circuits Conference Digest of Technical Papers*, 2014.

20. C. S. Vaucher, I. Ferencic, M. Locher, S. Sedvallson, U. Voegeli, Z. Wang, "A family of low-power truly modular programmable dividers in standard 0.35-um CMOS technology," *IEEE Journal of Solid-State Circuits*, vol. 35, no. 7, pp. 1039-1045, July 2000.

21. C. Weltin-Wu, G. Zhao, I. Galton, "A 3.5 GHz Digital Fractional-*N* PLL Frequency Synthesizer Based on Ring Oscillator Frequency-to-Digital Conversion," *IEEE Journal of Solid-State Circuits*, vol. 50, no. 12, pp. 2988–3002, Dec. 2015.

22. E. Fogleman, I. Galton, W. Huff, H. Jensen, "A 3.3-V single-poly CMOS audio

ADC delta-sigma modulator with 98-dB peak SINAD and 105-dB peak SFDR," *IEEE Journal of Solid-State Circuits*, vol. 35, no. 3, Mar. 2000.

23. E. Temporiti, G. Albasini, I. Bietti, R. Castello, M. Colombo, "A 700 kHz Bandwidth ΔΣ Fractional Synthesizer with Spurs Compensation and Linearization Techniques for WCDMA Applications", *IEEE J. Solid-State Circuits*, vol. 39, no. 9, September 2004.

24. C. F. Liang, P. Y. Wang, "A wideband fractional-N ring PLL using a near-ground pre-distorted switched-capacitor loop filter," *2015 IEEE International Solid-State Circuits Conference Digest of Technical Papers*, 2015.

25. C. R. Ho, M. S. W. Chen, "A Digital PLL with Feedforward Multi-Tone Spur Cancelation Loop Achieving <-73dBc Fractional Spur and <-110dBc Reference Spur in 65nm CMOS," *2016 IEEE International Solid-State Circuits Conference Digest of Technical Papers*, 2016.

26. W. Yao, L. Lin, B. Nissim, H. Arora, T, Cho, "A Low Spur Fractional-*N* Digital PLL for 802.11 a/b/g/n/ac with 0.19 ps_{rms} Jitter," *2011 Symposium on VLSI Circuits Digest of Technical Papers*, 2011.

27. Z. Z. Chen, Y. H. Wang, J. Shin, Y. Zhao, S. A. Mirhaj, Y. C. Kuan, H. N. Chen, C. P. Jou, M. H. Tsai, F. L. Hsueh, M. C. F. Chang, "A Sub-Sampling All-Digital Fractional-N Frequency Synthesizer with -111dBc/Hz In-Band Phase Noise and an FOM of -242dB," *2015 IEEE International Solid-State Circuits Conference Digest of Technical Papers*, 2015.

28. H. Hedayati, W. Khalil, and B. Bakkaloglu, "A 1 MHz Bandwidth, 6 GHz 0.18 μm CMOS Type-I ΔΣ Fractional-*N* Synthesizer for WiMAX Applications," *IEEE Journal of Solid-State Circuits*, vol. 44, no. 12, December 2009.